Computer Simulation and Visualisation of Complex Systems: Arcs and Hot Gas Flow in Auto-expansion Circuit Breakers

UNIVERSITY OF LIVERPOOL

Thesis submitted in accordance with the requirements of the University of Liverpool for the degree of Doctor in Philosophy by

Toh Ming Wong

March 2008

Department of Electrical Engineering and Electronics
The University of Liverpool

To my parents...

Acknowledgements

This thesis is the product of many hours of hard toil, and would never have been possible without the support of those around me. First of all, I would especially like to thank Professor M.T.C. Fang for providing me the opportunity to study here and without whom none of this would have been possible. He is an extremely kind and helpful person and a great source of knowledge, encouragement and wisdom. My deepest appreciation must be addressed to my supervisor, Dr. J.D. Yan, for his tremendous help, continuous guidance and support, good advice and sincere friendship. Chinese proverbs said 'one day teacher, forever friend'!

Special appreciation goes to Dr X.Y. Ye, Dr M. Claessens and J. Abrahamsson from ABB Ltd. for all the collaboration, discussions, great source of data, generation and exchange of ideas, and their friendliness.

A very special thanks must be addressed to Dr C.D. Hill, for his enormous support and care. Thanks also to my colleagues/friends from the University, flatmates, church brothers and sisters as well as friends from my home country for all their friendship, encouragement and/or prayers.

Special acknowledgement must be addressed to the Lee Foundation, Malaysia and ABB, Switzerland for the financial support. Thanks also to Professor H.T. Chuah from Multimedia University, Malaysia for his support to pursue my degree in the UK.

Last but not the least, my deepest gratitude is specially addressed to my dad and mum, brothers and sister, who have been so loving all the time.

Thank God, I've made it!

Summary

Auto-expansion circuit breakers (also known as the self-blast circuit breakers) are an advanced generation of high voltage switchgear. This type of circuit breaker uses the arc's energy to generate a high pressure source in the expansion volume (also known as the heating chamber) to create the required thermal and aerodynamic conditions for interrupting the circuit at a current zero. Ablation of the arc confining nozzle at high current is the main mechanism for pressurisation of the expansion volume. The operation of such a breaker is extremely complex and its performance depends on the whole arcing history as well as a number of geometrical factors characterising the geometry of the interrupter. It is a complex system with inter-related mechanical parts (moving pistons, valves, ablating nozzles, and moving contact) and physical processes (radiation, thermodynamics, aerodynamics, turbulence and ablation of solid materials). The relationship between all the constituent parts and physical processes gives rise to the collective behaviour of the whole system.

Computer simulation of the arcing process in such a breaker has been carried out in the present work. Because of the very high power level encountered in such a breaker the arc interacts intensely with its surroundings. The objective of the work is to establish a computer model to simulate the whole arcing process, validate the model and then perform an extensive analysis of system behaviour to extract useful information for the optimisation design of such devices.

The history of circuit breaker development, fundamental aspects related to the operation of high voltage circuit breakers, and history of computer modelling of switching arcs are first reviewed in chapter 1, which provides an overall background picture for the present work. The mathematical description of the important physical processes is then given in chapter 2 which includes the governing equations for arc flow, the modelling of radiation and turbulence, the calculation of nozzle ablation, and the

computation of electrical and magnetic fields for Lorentz force and Ohmic heating.

The temperature and pressure encountered in computer simulation of the auto-expansion circuit breaker arc covers a wide range, from 300K to possibly 40,000K and from atmospheric pressure to 100 bar. The material and transport properties of the mixture of the working gas and ablated nozzle vapour are highly non-linear functions of plasma parameters. Thus a robust computational fluid dynamics (CFD) solver is essential. In the present work, a commercial CFD package, *PHOENICS*, is used for the simulation. The practically important issues, such as the implementation of the arc model with input of material properties into the solver, the specification of initial and boundary conditions, the approximate of the circuit breaker geometry, and choice of time step and control of convergence, are discussed in chapter 3.

In the operation of an ABB auto-expansion circuit breaker, there are a number of mechanical parts that move with time during an operation process. The operation of over pressure valves, with one of them attached to the moving piston, has to be correctly modelled. This is detailed in chapter 4 where validation of the numerical methods is provided by comparing the prediction with analytical results from isentropic compression and also with measurement from ABB. Results show that the proposed numerical scheme can satisfactorily model the valve operation and the piston movement. Typical results of the gas flow in such a circuit breaker without the presence of an arc (no-load operation) are presented and discussed.

In chapter 5 the operation of the ABB breaker under specified arcing current is then simulated for almost a whole arcing period. Results indicate that Lorentz force has a profound effect on the flow field as well as the arc shape. Detailed energy and mass balance calculation is performed for the arcing space and also for the expansion volume, which clearly shows the importance of radiation transfer, convection at different nozzle exits and the change of energy and mass storage at different instants in the arcing process. It is also shown that the pressurisation of the expansion volume is due to the influx of thermal energy, not the mass influx. The predicted arc voltage overally agrees with the test results within 15% for all three cases simulated with different breaker geometry. The predicted pressure at current zero is within 10% of the test results. On the whole the prediction is considered satisfactory in consideration of the approximations that have been introduced in the geometry and radiation model.

It has been found that for the auto-expansion circuit breaker the pressure in the arcing space can fluctuate rapidly in the period shortly before the thermal recovery period. Pressure fluctuation with several bars around the current zero period results in a scatter of thermal interruption and dielectric recovery performances. Large pressure variation is therefore not desirable. Optimisation of design parameters is necessary in order to avoid pressure variation and to ensure maximum pressure and lowest temperature possible in the arcing volume. A systematic study of the mechanisms responsible for the pressure fluctuation is therefore carried out in chapter 6. It has been found that the evolution of pressure and temperature fields in the arcing space around current zero depend on the supply rate of gas from the expansion volume and the exhaustion rate at the nozzle exits. Thus, an optimum design is directly linked with the design of the expansion volume and the link channel between the arcing space and the expansion volume. A systematic study of the influence of various design parameters is also carried out to identify the most influencing parameter, which is the dimension of the channel link. Based on the knowledge and understanding derived from this study a new design has been simulated which produces very promising result in smoothing the pressure fluctuation in the arcing space. Pressure and temperature fields at current zero depend on the whole arcing history as well as the contact movement which determines the gas exhaust passage. Arcing processes with different arcing time (altogether three cases with different arcing times) are finally performed to assess the efficiency of the new design. In all cases it has been shown that with the addition of a buffer volume the pressure smoothly changes in the period approaching the final current zero.

In summary, the three objectives stated in chapter 1 have all been achieved by the work presented in chapters 2 to 6. Nevertheless, there are still several aspects of the model that need to be improved. This is discussed in the final chapter.

Contents

List of Figures

List of Tables

List of Symbols and Abbreviations

SF_6	Sulphur Hexafluoride	4
$PTFE$	Polytetrafluorethylene	7
R	Resistance	12
k	Constant	12
Q	Heat content	12
Q_0	Heat content at steady state	12
t	Time	12
τ	Time constant	12
E	Electric Field	12
I	Current	12
P_0	Energy loss at steady state	12
r	Radius	12
k	Thermal conductivity	12
T	Temperature	12
σ	Electrical conductivity	12
$RRRV$	Rate of rise of recovery voltage	15
ρ	Gas density	21
ϕ	Dependent variable	21
w	Axial velocity component	21
v	Radial velocity component	21
c_m	PTFE mass concentration	21
Γ	Diffusion coefficient	21
S_ϕ	Source term for dependent variable	21
h	Enthalpy	21
P	Pressure	21

Chapter 1

Introduction

I loved the feeling of beginning at the beginning
and going through to the end.
– Natalie Wood

1.1 Complex Systems and Modern Industrial Devices

With the increasing use of modern technologies including those related to materials, surface treatment, embedded micro-processor and intelligent communication and remote monitoring, industrial devices have a trend to become more complex in their design and configuration. A complex system is a system built up with many simple systems/parts which interact and are interrelated or interdependent to each other. The relationship between all constituent parts gives rise to the collective behaviour of the whole system. A complex system is therefore difficult to understand because the behaviour of the whole can only be understood from the behaviours of the parts; and the behaviour of the parts depends on the behaviours of the whole through interaction. A good example would be the system under investigation in this thesis, which is the modern auto-expansion circuit breaker used in power transmission networks as a connecting/switching point. The operational principles of this type of devices will be given later on in detail.

The physical phenomena which occur during the operation of an auto-expansion circuit breaker involves aerodynamics (high speed flow, possible shock waves), electromagnetism (electric field, magnetic field and Lorentz force acting on a conducting medium), thermodynamics (high pressure gas with varying pressure, temperature and mass concentration of vapour in a gas mixture), plasma physics (ionisation of gases by strong electric field, Ohmic heating and radiation), surface ablation (nozzle

surface caused by strong arc radiation), and turbulence (contributing to arc cooling and momentum exchange).

To adequately model the behaviour and performance of this type of circuit breaker, a clear understanding of the principles and mechanisms of the involved phenomena is essential. Based on this understanding, we then need to construct mathematical models to represent them in a package of modelling software. System integration is also an important issue in modelling the complex system. For example, an over pressure valve mounted on a moving piston can only be modelled by considering the collective effects of the opening-closing action of valve holes and also the translational motion of the valve body in a transient flow field. To verify the results from modelling it is necessary to compare the results with known analytic solutions for well specified cases, such as when the valve is permanently closed while the piston moves in a closed cylinder. Experimental results also play an important role in the verification process of the model since approximation of the real situation is often necessary to make the problem attackable. By comparing with measurements (with well defined experimental error) we can obtain critical information as regards how realistic the model's performance is.

Arc modelling has evolved in the past eighty years from a very simple mathematical description [2] to advanced computer codes [3, 4, 5, 6] including much detail of the important physical phenomena. With the latter model we can hopefully answer questions directly from circuit breaker designers about the optimum design of the product. This is because with the above mentioned auto-expansion circuit breaker the performance of the device depends on many design parameters and also depends on the history of the operation cycle. With these interlinked mechanisms operating concurrently, it is not an easy job for a breaker designer to answer, without relying on costly and time consuming tests, the question that what the trend of the performance would be if a design parameter is changed. Computer modelling of circuit breakers could greatly reduce the number of costly tests necessary to achieve an optimum design of the breaker.

The work presented in this thesis is an attempt to develop PC based models for the auto-expansion circuit breaker - a typical complex system in this field. The operation of the various key elements and models will be described in relevant chapters. The collective performance of the system will then be modelled by integrating with the

arc model and results verified using analytic solutions and test results obtained by ABB. In the rest of this chapter, the history of circuit breaker development will be briefly reviewed to give the reader a continued picture of the technologies employed in different periods and the models developed to add the understanding of these circuit breakers. The major findings and novelty from the study will also be outlined at the end of this chapter.

1.2 History of Circuit Breaker Development

Circuit breakers are essential for electrical power networks since they act as both a connection point and also an insulating point. They possess two stable conditions which are 'close' and 'open'. In the former, the two main electrical contacts (electrodes) are in good mechanical contact therefore having ideally zero yet in reality a very small impedance. In the latter state, the two contacts are separated by insulating medium such as high pressure gas or vacuum thus having ideally an infinite yet in reality an extremely high impedance. Circuit breakers are required to carry out its duty of switching between the above two stable states in a short duration (tens of milli-second) under both normal and abnormal (disastrous short circuit) conditions. In this section we only focus on the interruption of alternating current, which is relevant to the theme of this research.

1.2.1 The function and interrupting principles of high-voltage circuit breakers

Circuit breakers are essential for electrical power networks control such as switching in power transmission and distribution. Circuit breakers are designed to carry out its function by controlling current which may flow in the circuit of which it constitutes a part of the conductor system, under both normal and abnormal conditions. These breakers must be able to change from either condition to the other when instructed (*e.g.* open to close/ close to open), at a rate of change of impedance which is compatible with the parameters of the circuit being controlled. In alternating-current circuits, the impedance may change quickly from zero to infinity without generating overvoltages. Should rapid change of impedance occur less than a few microseconds around

a current zero, disastrous overvoltages may be generated. Current zero is where the alternating current arc either re-ignites or is extinguished.

There are two requirements in interrupting alternating currents. The first one is to increase arc plasma resistance in the region around a natural current zero so that any possible subsequent current flow is suppressed and finally interrupted. The other is to ensure that the dielectric strength (measured by the so-called breakdown voltage) in the contact gap (normally the space that the plasma left after extinction) increases faster than the electrical stress imposed by the network reaction so eventual electrical insulation is achieved. All circuit breakers are therefore designed to optimise their response to these requirements, using a wide variety of arc control configurations based on parameters such as liquid, gas, pressure, vacuum, turbulence, arc, nozzle ablation and contact movement.

The arc is therefore an essential element in current interrupting processes. The thermodynamics and physical properties of the arc are of great interest for physicists, circuit-breaker designers and analysts. The arc often appears to have the power of self preservation which leads to challenges in design. Power arcs evade deionisation systems by swerving, by striking out in new and unexpected directions, and by reigniting after they appear to have been successfully interrupted.

Nevertheless, the properties of the arc can also be manipulated to extinguish itself. The arc plasma has no upper limit in current carrying capacity. It is resilient and can be stretched. Its resistance can be increased by either increasing its length or by confinement. The mobility of the arc can also be advantageously used to impose its own magnetic field to react on the arc plasma itself, in order to promote high-speed controlled movement of the arc.

The development of circuit breakers dates from the construction of special short-circuit test plants about 1925, after the development of the cathode ray oscillograph, which made possible controlled in association with accurate measurement of performance, not previously attainable with the ad hoc and sometimes spectacular arrangement customary before that time, using production turbogenerators and test beds on the open shop floor [7]. In the later stage, more sophisticated approach for arc extinction have been developed using air, oil, compressed air, SF_6 gas and vacuum as interrupting medium and a brief history of some of this background is given as the

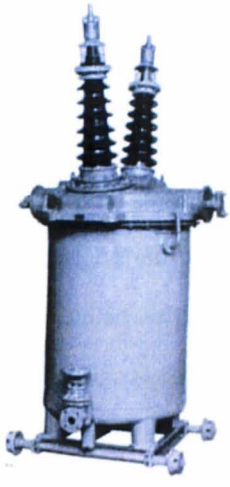

Figure 1.1: Outdoor single pole oil circuit breaker from 1923, with voltage 100kV and current 350A

following.

1.2.2 Types of circuit breaker

Historically the most successful arc interrupting system in the earlier years was undoubtedly the oil circuit breaker [8], due to the high availability of insulation which is one of the key parameters of high-voltage circuit breakers development [9, 7, 10, 11]. Oil molecules dissociate under high temperature of arc, and produce hydrogen. The high pressure hydrogen gas bubbles created by arc energy are therefore advantageously used to confine, compress and cool the arc. The arc is then extinguished at current zero. Oil circuit breakers have proved a very successful circuit interrupting technology with voltage ratings per break between 3.3kV to 33kV for the bulk oil design and 11kV to 170kV for minimum oil design [9]. There are a number of disadvantages of using oil as quenching media in circuit breakers. Flammability and high maintenance cost are two such disadvantages. Research has been done from now and then to search for better types of circuit breakers as a replacement [12]. Figure 1.1 shows an example of an oil circuit breaker in use.

In 1926, Sorensen [13] developed the world first vacuum circuit breaker. Vacuum circuit breakers appear to be the simplest type of circuit breaker. When the contacts in a vacuum interrupter are separated, the current to be interrupted initiates a metal vapour arc discharge and flows through the plasma until the next current zero. The arc

is supported by ionised metal vapour derived from the contacts instead of by ionised gas compared to other types of breakers. The arc is then extinguished and the conductive metal vapour condenses on the metal surfaces within a matter of micro seconds. As a result the dielectric strength in the breaker builds up very rapidly. Vacuum circuit breakers are maintenance free and consistent in interrupting current. They are mainly used for voltage distribution up to approximately 36kV [7]. Vacuum circuit breakers have minimal arcing and the arc quenches in a very small contact gap (from less than 2 to 3mm). In high voltage applications, practical voltage for one vacuum interrupter was limited to 84kV or 100kV [14], because the dielectric insulation level of the vacuum gap is more or less saturated. Therefore, a connection of two or more high voltage vacuum interrupters was investigated around end of 1970s [14] in order to raise the voltage ratings [10]. Vacuum circuit breakers at 132kV are therefore available in service in some outdoor stations [9]. The properties of a vacuum interrupter depend largely on the material and form of the contacts. At the moment it is accepted that an oxygen free copper chromium alloy is the best material for high voltage circuit breakers. In this alloy, chromium is distributed through copper in the form of fine grains. This material combines good arc extinguishing characteristic with a reduced tendency to contact welding and low chopping current when switching inductive current. Much research was conducted before vacuum circuit breakers became a commercially viable and mass produced product [15, 16, 17, 18, 19, 20]. The research was mainly concerned with vacuum technology and contact materials.

Air-break circuit breakers were first developed by Slepian at Westinghouse in 1929 [7]. The arc is extinguished by magnetically forcing the arc into a chute where the arc is lengthened and cooled. Arc resistance is thus increased and considerable energy is released, which leads to favourable conditions for arc extinction at current zero. For current interruption at voltage levels higher than 15kV [11], air-break circuit breakers demand an arc chute of formidable size and were replaced in 1930's by air-blast circuit breakers. It was developed experimentally by the British Electrical Research Association and was put into production in Germany and Switzerland [7]. The switching arc is confined and cooled by the high speed air flow through an insulating nozzle. Air-blast circuit breakers provide high speed operation, having short and consistent arcing and total breaking time, require minimum maintenance and are suitable for

frequent switching duties. Nevertheless, the drawbacks are the relatively high cost of compressor and dryer systems. Research work for air-break circuit breakers has been continued till late 1980s [21, 22, 23, 24, 25]. However, these two types of circuit breakers are not sustainable in the market since they are bulky and cumbersome.

The discovery of sulphur hexafluoride by Henri Moissan in 1900 [26] fascinated man with its interesting and unusual properties. In 1937 it was discovered that sulphur hexafluoride possesses a much higher dielectric strength than air [27], a fact that led to a new generation of sulphur hexafluoride (SF_6)-blast circuit breakers. The first patent on the use of SF_6 as an interrupting medium was filed in Germany in 1938 by Vitaly Grosse (AEG) and independently later in Westinghouse, USA by Lingal et. al. in 1953 [28]. The first generation of SF_6 circuit breakers were puffer type circuit breakers. During the opening operation, the gas contained inside a part of the circuit breaker is compressed by moving a cylinder supporting the contact system or by a piston which forces the SF_6 through the interrupting nozzle, further extinguishing the arc near the current zero period. The nozzles of these circuit breakers are usually made up of Teflon/Polytetrafluorethylene (PTFE) . PTFE is mechanically strong, capable of resisting relatively high temperature and has the property of vapourising when exposed to high levels of radiation.

The great success of SF_6 switchgear originates in the excellent properties of SF_6 gas as dielectric medium because of its electron attachment and also as thermally arc quenching medium for reasons not completely understood. The superb insulating and dielectric performance of SF_6 is due to its electron affinity/electronegativity. SF_6 is an efficient electron scavenger, capturing and attaching electrons [29]. The relative dielectric constant for SF_6 is 1.002 and SF_6 has no dipole moment thus its dielectric constant does not vary with frequency. Its high dielectric strength helps to reduce the size of breakers, and the SF_6 dissociation products rapidly recombine after the source of arcing is removed [30]. However, despite their good interruption capability, conventional SF_6 puffer-type breakers have a disadvantage which becomes more pronounced under the current economic constraints. The mechanical compression to the pressure required for arc quenching requires considerable mechanical operating input energy. Circuit breaker design as well as the construction of substations depend on the mechanical energy requirements. High compression forces imply high reaction forces

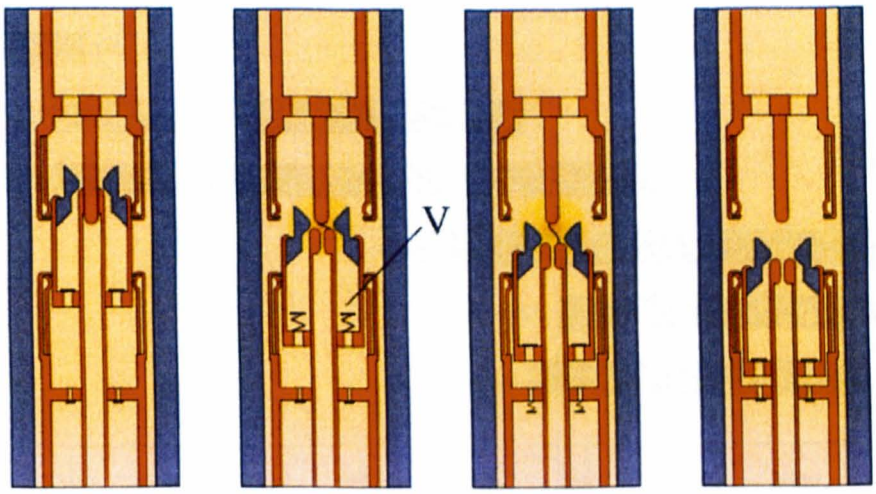

Figure 1.2: Diagram showing the operation of an SF_6 self-blast circuit breaker.

which need a rigid construction of the breakers support structure and a large effort for its foundation. A new generation of SF_6 circuit breakers, the so called pressure chamber principle [31] or the self-blast circuit breakers (figure 1.2) have therefore been developed, which make use of the arc energy itself for the pressure build-up. From left to right, the first subfigure shows the closed position of contacts. The second subfigure shows contact separation and the formation of the arc. V indicates the volume where the high pressure gas in stored. The third subfigure shows a stabilised arc. The final subfigure shows the contact gap when fully open and the arc is distinguised. During the last ten years puffer circuit breakers have been widely replaced by SF_6 self-blast circuit breakers due to reduced driving forces and improved maintainability [32].

Figure 1.3 shows a brief historical summary of major types of breakers used from approximately 1920 to the present day. This diagram reflects the changes in breaker technology as well as the ever increasingly demand on the interruption capacity of the breakers.

1.2.3 Development and maintenance cost of circuit breakers

Design and construction of high-voltage circuit breakers are in several ways a mature technology. The majority of the high voltage circuit breakers being installed today are the SF_6 puffer type, and their reliability is very good. With the increasing demand on the short-circuit interruption capability, the development cost based on trial and error

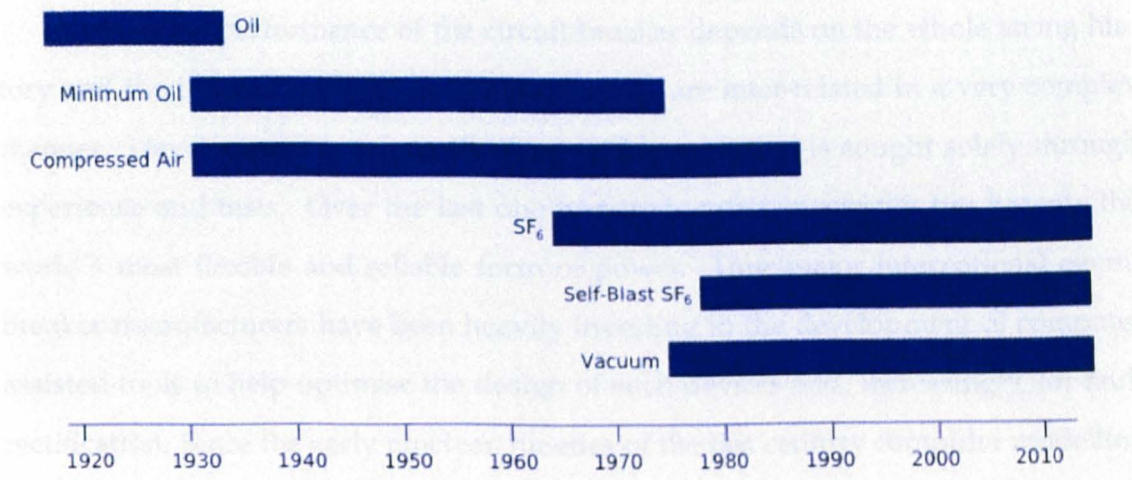

Figure 1.3: Major types of power circuit breakers.

is extremely high. SF6 puffer breakers were introduced in the Norwegian power grid in the mid-seventies, and a considerable number of these breakers were installed in the following years. The manufacturers usually specify a periodic maintenance program, which in most cases includes a complete overhaul every 10 or 15 years. This work has been going on for a few years now, and some conclusions can be drawn with regard to the condition of these circuit-breakers and the need for maintenance.

In general, the breakers are found to be in excellent condition after more than ten years of service and up to $500 - 600$ operations. Only minor irregularities that do not influence the circuit-breakers' operating ability have been disclosed. In particular, the arcing chamber and the contacts are virtually like new.

These overhauls, where the entire circuit-breaker is dissembled, are however, time-consuming and expensive. A general rule is that the maintenance costs are between one third and one half of the price of a new breaker, and the utilities are questioning the economic justification of such a comprehensive maintenance program on a 10 or 15 year old circuit-breaker. Moreover, it is well-known that the dismantling and reassembly itself may introduce defects. On the other hand, there is not yet a good recommendation as to how long the contacts and other important parts of the circuit breaker should remain in operation uninspected. This is also a matter of discussion, in particular considering that these breakers are likely to be in service for decades to come. Earlier, the rapid increase in demand for electric power in many cases led to a

replacement of 10 – 20 years old components, which are still in excellent condition.

In short, the performance of the circuit breaker depends on the whole arcing history and the influences of the design parameters are inter-related in a very complex manner. Development is too costly if an optimum design is sought solely through experience and tests. Over the last one hundreds years, electricity has become the world's most flexible and reliable form of power. Thus major international circuit breaker manufacturers have been heavily investing in the development of computer assisted tools to help optimise the design of such devices and, increasingly, for fault rectification. Since the early nineteen nineties of the last century computer modelling of the switching arcs in SF_6 breakers has advanced at a rapid pace [33]. The ever increasing computer power of a PC at an affordable price, the improved understanding of the basic physical processes and the availability of robust algorithms have made computer simulation of circuit-breaker optimisation an essential tool for breaker designers.

1.3 The Collision Dominated Plasma

The plasma state is frequently referred to as the fourth state of matter in the sequence of solid, liquid, gas and plasma. This classification as a state of matter is justified by the fact that more than 99 % of the known universe is in the plasma state. A typical example is the sun, whose interior temperatures exceed 10^7K. The high energy content of a plasma compared to that of solids, liquids, or ordinary gases lends itself to a number of important applications [34].

An electric arc consists of a plasma column, the temperature for which lies between about 4000K to 40000K. At these high temperatures all materials are in the gaseous phase and complicated molecules are more or less decomposed into molecular fragments and atoms, some of which are ionised into electrons and ions. These electrical charges make it possible for an electric current to flow through the plasma, if a sufficient voltage gradient is present. In the arc column and the electrode fall regions complicated processes such as excitation, ionisation, recombination by impact, diffusion, light emission and absorption take place. The decisive factors governing the existence and the behaviour of the arc are the balance of the energy between en-

ergy input (usually Ohmic heating) and the energy dissipation processes (*e.g.* thermal conduction, convection or radiation cooling).

Arcs in high voltage circuit breakers are known as collision dominated plasmas. At pressures at or above atmospheric pressure, collisions between particles are sufficient to make plasma behave like a single fluid [35] where electrons are locked with heavy particles to move together. Due to the very frequent collisions between particles, all the particle species inside a high pressure arc attain a single temperature, thus high pressure arcs are also known as thermal plasmas or arcs [34, 35]. The properties of a thermal plasma arc uniquely determined by two thermodynamic variables (usually temperature and pressure). The conducting state of an arc is determined by its temperature. To quench an arc is to find means to reduce the temperature to a value where electrical conductivity is negligible.

1.4 Review of Arc Modelling

Although the arc was already used as a switching element in a simple knife-switch as early as in 1800's, little research towards understanding the physical processes inside an arc was done before the World War II. The discovery of nuclear fusion and its potential application in energy generation triggered intense research activities in basic plasma physics immediately after the war [36]. Arc modelling started as early as in the 1930s but breakthrough was gained in the 1970s when the radiation characteristics of SF_6 were calculated from fundamental theory [1]. Since then rapid progress has been made up until the present day. In the following sections a brief review will be conducted of models at various stages.

1.4.1 Early simple arc models

The first model was probably proposed by Slepian [2] for arcs in high voltage switchgear. The model states that successful interruption is achieved whenever the rate at which the dielectric strength of the gap increases faster than the rate at which the reapplied system voltage increases.

The first mathematical description of a dynamic arc was given in 1939 by Cassie [37], who assumed constant and uniform temperature in the arc column. The diam-

eter of the arc responds proportionally to the variation of the electric current. This is an approximation of radiation dominated high current arc with a top-hat style radial temperature profile. Since there is no description of variation of physical quantities inside the arc column, this type of model is commonly referred to as the black box model.

In 1943, Mayr [38] proposed a model for low current arc. Different from Cassie's assumption on high current arcs, he assumed that the arc radius and the energy loss per unit length of arc remain constant. This is similar to a turbulence cooled thin arc column with steep radial temperature gradient. By relating the resistance of the arc to its heat content (or temperature) through an exponential function, $R = k\exp(-Q/Q_0)$ with Q being the heat content, Q_0 is the heat content at a steady state, R the arc's resistance, and k the constant. Mayr expressed the energy conservation equation in a differential form

$$R\frac{d}{dt}\left(\frac{1}{R}\right) = \frac{1}{\tau}\left[\frac{EI}{P_0} - 1\right] \tag{1.1}$$

where P_0 is the energy loss at the steady state and $\tau = Q_0/P_0$ is the time constant. E is the electric field and I the current. The models of Cassie and Mayr are only for extreme cases in circuit interruption arcs. Browne [39, 40] in 1948 started to combine these two descriptions to form a more general description of the arc dynamics. However, due to the very black box nature of the model, its applicability is restricted to situations where sufficient amount of experimental results are available to derive the model parameters.

Elenbaas [41] in 1946 first initiated the work to describe the arc's behaviour in terms of its thermal and electrical properties based on energy conservation. He assumed a uniform, cylindrical arc column maintained by a direct current, for which the energy loss is solely due to thermal conduction. The conservation equation (also known as Elenbaas equation) is then given by

$$\frac{1}{r}\frac{d}{dr}\left(rk\frac{dT}{dr}\right) + \sigma E^2 = 0 \tag{1.2}$$

where r is the arc radius, k is the thermal conductivity, T the temperature, σ the electrical conductivity, and E the axial electrical field. Equation 1.2 is obviously oversimplified in that some of the important processes such as radiation and convection are

not present, thus limiting its validity to arcs with negligible axial variation and radiation energy loss. Subsequent applications of Elenbaas' equation by Frind [42] and Phillips [43] to transient wall stabilised arcs established for the first time how arc's time constant is related to the gas properties and the system dimension.

1.4.2 Arc model based on integral method

Followed by the rapid advance of plasma theory, vigorous development of the integral method of arc analysis occurred in the late sixties and early seventies last century. Arc conservation equations were also well-known. However, the solution of these conservation equations was still a formidable task as the computers were not powerful enough. Due to the complexity of the conservation equations and lack of efficient numerical method for highly non-linear partial differential equations, the integral approach was therefore generally adopted.

A series of seven papers on arc modelling were published by Swanson and Roidt between 1970 to 1977 [44, 45, 46, 47, 48, 49, 50], which, together with the work of Topham [51], marked a turning point in gas blast arc modelling. The similarity between an axially blown arc and a hot boundary layer was clearly recognised and used to simplify the arc conservation equations. However, their starting conservation equation for energy [44] is generally not correct, as pointed out by Fang [52]. The treatment of the terms in the radially integrated energy equation was not physically justified.

In 1975, Lowke and his co-workers proposed another integral model [53, 54, 55, 56, 57, 58]. Lowke and Ludwig [54] developed an arc model for convection stabilised arcs to a certain current range. Tuma and Lowke [53] applied this model to analyse the data of Hermann *et al* [59]. El-Akkari and Tuma [60] later extended this model to transient arcs.

During the similar period of time, a group of workers in BBC (Brown Boveri) in Switzerland were engaged in an extensive experimental and theoretical investigation on arcs in gas flow [61, 59, 62, 63, 64, 65]. Temperature, pressure distribution and the electric field of a gas blast arc were accurately measured for the first time. Arc was demonstrated to be turbulent. A two-zone model including turbulent enhanced momentum and heat transfer was successfully employed for a 2kA dc nitrogen arc [63]. However, research by Lowke [54] and Zhang *et al* [66] has caused lots of controversy

where their results showed good agreement between theory and experiments for 2kA dc nitrogen arc without introducing turbulence at all. A similar arc model neglecting the axial variation of thermodynamic quantities has been introduced to study the arc behaviour for current zero period [64].

Compared with all previous integral models, the integral equations for the arc together with its external flow were formulated rigorously and in a very general form by Fang et. al. [67, 68, 69]. Cowley's simplified model [67] of arc analysis, the boundary layer integral method, was taken in that the arc conservation equations in general form, together with the external flow equations were powerfully formulated. Chan *et al* [70, 68, 69] extended this formulation to include an energy equation for arc column. In short, the Liverpool-Cambridge arc model has been widely used to investigate the effects of nozzle ablation, particularly at the end of the last century [71, 72, 73, 74, 75, 76, 77, 78].

1.4.3 Arc model based on full differential equations

Despite low computational costs and adaptability of empirical information into the model, the integral method suffers from limited success especially for current zero period due to difficulties in correlating the shape factors with an arc characteristic quantity. The basic idea of the differential approach is to solve the conservation equations for mass, momentum and energy with appropriate initial and boundary conditions of the physical domain. Simplifications and approximations must be made due to the complexity of some of the physical mechanisms in switching arcs such as radiation transfer, turbulent mixing and electrode sheath interaction. Thus various models were devised for different arcing situations.

Maeker [79], in the 1950s, marked the beginning of quantitative investigation of arcs by invented wall stabilised arc. Then for a few decades arc modelling based on the differential method was hindered by the difficulties in accounting satisfactory internal energy transport of radiation. Lowke and Liebermann [80] have marked great contribution by using net radiation emission coefficient on the axis of a top hat temperature profile of a wall stabilised arc that can be used for high accuracy of temperature profile prediction. Zhang *et al* [66] extended this method to include a net radiation reabsorption layer. The adaption of such a radiation transport model has been proven

very successful in predicting arc temperature, the electric as well as aerodynamic characteristics [66, 81].

Research development in the differential method was remarkably significant in the 1980s. Ragaller *et al* [82] at Brown Boveri Electric Company (BBC) proposed a model in 1982 for predicting the dielectric recovery of a gas blast arc after current zero. Strong turbulent energy exchange must be introduced in the model in order to bring the numerical prediction closer to the measured dielectric recovery characteristics [83]. Mitchell *et al* [84] investigated the dielectric behaviour after current zero assuming laminar flow. Radiation from the high temperature arc column is assumed to be fully absorbed in a single layer of one-cell thickness of arc edge. Although Mitchell *et al* [84] argued that the energy loss by convection and laminar thermal conduction is sufficient to cool the residual plasma under the same conditions as in [83], their results of radial temperature profiles are clearly similar to those of Hermann and Ragaller based on laminar flow for the period up to 200$^-$s after current zero. Results of the steady state SF_6 arc at 1200kA and 3.6 bar suggested that the net emission coefficient by Liebermann and Lowke [1] should be increased by a factor of four. At the same time, Lowke and Lee [85] investigated the thermal process of a gas blast circuit breaker for transient case, from a steady state 2kA before current zero. The predicted rate of rise of recovery voltage, *RRRV* (for both nitrogen and SF_6) in laminar showed one order of magnitude than that given by Hermann and Ragaller [65]. The first published attempt of gas blast arc modelling based on arc conservation equations in full differential form was due to Lee *et al* [86]. However, their energy equation is not correct where the expansion cooling term is not included. This term can account for 25% of the power input in a supersonic nozzle. In their work also radiation absorption is not properly accounted for, and results for numerical accuracy is not known.

Fang and his co-workers [87, 88, 89] at the University of Liverpool have been at the forefront of gas blast arc modelling since 1980's. Reasonable prediction of thermal interruption capability for nitrogen arcs has been shown [87], but not for SF_6 [88, 89]. It is also found that turbulence is necessary for SF_6 arcs [90]. Other fundamental aspects of the gas blast arc have also been investigated by the same group, which include arcs with mild nozzle ablation, turbulence [91, 92], electrode erosion, arc-shock interaction [93] and arc instability [94, 95].

1.4.4 Recent development of arc modelling

The governing equations for high pressure thermal arcs have been well formulated in the past thirty years. The source terms specific to circuit breaker applications have also been well identified although their accurate calculation method is still under development. For high voltage circuit breakers arcs two dimensional axis symmetric model is normally used. There has been great success in computer modelling which is enabled by the availability of the power commercial computational fluid dynamics tools [96]. The representative models are the two-zone model [96] and the Liverpool's self-consistent model [97, 5]. For most of the cases the models are applied to the high current phase where due to the large size of the arc column axisymmetry can be assumed. The current zero phase has been modelled by Zhang *et al* for a simple supersonic nozzle with well defined experimental conditions and results [98]. Meanwhile, other research on computer modelling [99, 100] follows a similar approach as in [97] but focusing on different aspects of the switching process.

1.5 Aims, Objectives and Major Achievement of This Research

Previous work in the Liverpool group has laid down a good foundation for further extending the research work into circuit breakers arcs produced with a more complex structure. The work to be described in this thesis can be divided along the following lines:

- To study the characteristics of the mechanical components such as valves, moving piston and moving contact as well as to establish suitable numerical schemes to represent their effects in the model. The main focus here is on the operation of over-pressure valves, especially its operation on a moving piston. These numerical schemes have to be verified using simple cases to make sure they work with the rest of the arc model and produce satisfactory results. The migration from an old version of the CFD package to a newer version is also necessary since technical support for the old versions is withdrawn. Academically it is not important however it is an essential part of the research work. Considerable effort has been spent on this issue in the past four years.

- To construct an arc model for an advanced auto-expansion circuit breaker designed by ABB Switzerland to simulate the high current arc and verify the results using test results. Simulations are also done for other types of auto-expansion circuit breaker to evaluate the overall performance of the arc model and any discrepancies between the measurement and prediction are analysed. Results from the Liverpool model are also compared with the results produced by the ABB two-zone model and there is detailed analysis as regard the question why the two models produce similar results with different assumptions. The analysis gives sound argument to the question and thus increases the confidence in using both models. There is also detailed balance analysis of mass and energy in the arcing domain. Results have confirmed that it is the thermal energy that is brought into the expansion volume that is responsible for the pressurisation process. The mass of PTFE vapour flowing into the expansion volume is negligible. This conclusion will have practical implications to circuit breaker design. Details will be given in chapters 4 and 5.

- To study the global thermal and flow environment prior to thermal interruption, or the current zero period. Previous studies have been more focused on the specific aspect of switching process which is essential for gaining knowledge. However for design engineers it is necessary to see how the global environment changes during the arcing process thus obtaining an overall picture of the breaker operation. Emphasis here is given to the transient nature of pressure field in the arcing space where both thermal interruption and the subsequent dielectric recovery take place. Our results have indicated that large pressure variation does exist shortly before the current zero period. The profile of this pressure variation depends, not only the current waveform, but more importantly, the design parameters. Changing the key design parameters can effectively reduce the level of pressure fluctuation near current zero thus increasing the consistency in the performance of circuit breakers. We have devised a novel structure of the arc chamber where the large pressure oscillation can be effectively smoothed. Further work is necessary to experimentally verify this finding.

1.6 Organisation of Thesis

This thesis is organised as follows:

- This chapter provides an introduction to the thesis. It includes the history of various circuit breakers' development. It also reviews arc modelling history and breakthroughs. Finally it outlines the aims and objectives of this work.
- Chapter 2 introduces the arc models which apply in the simulation, such as the turbulence model, radiation transfer, PTFE ablation. It also introduces the fundamental concepts of fluid dynamics as it applies to arc models, such as the governing equations and the calculations of electric and magnetic field strengths. An electric arc is introduced as a plasma at the beginning of the chapter.
- Chapter 3 focuses on the implementation of arc models in the computational fluid dynamics package, PHOENICS. It describes the geometry of the breakers used in the simulation, followed by the initial and boundary conditions used in the model. The use of convergence control is introduced at the end of the chapter to promote a more stable solution of the underlying differential equations. Choice of time step is also described.
- Chapter 4 gives the results for an ABB circuit breaker for no-load simulations. Results from simulation are verified with measurement. It also explains the numerical scheme for the operation of the moving boundaries such as moving contact, piston and valves.
- Chapter 5 describes the overall Liverpool arc model for high current phase. A complete description of this model is given, including the mass and energy balance. Results for some typical instances are presented.
- Chapter 6 investigates pressure transients present in model circuit breakers, where the thermodynamic and aerodynamic behaviour of the gas flow are of primary interest. Computer simulation of the arcing process in various virtual circuit breakers with different geometries and dimensions were carried out and typical results analysed.
- Finally the work is summarised in chapter 7. Future work is also suggested.

Chapter 2

The Arc Model

We believe that electricity exists,
because the electric company keeps sending
us bills for it, but we cannot figure out how it travels...
– Dave Barry

2.1 The Features of Arc Discharges in High Voltage (HV) SF_6 Circuit Breakers

For voltage ratings above 100kV SF_6 breakers are still exclusively used in power systems. The filling pressure in such breakers is usually not lower than 5 bar. At such a high pressure frequent particle collisions ensure that the arc between the two contacts in the interrupter is characterised by:

1. All constituent species of the SF_6 arc attain a single temperature;
2. The distribution of particles among various energy levels obeys the Boltzmann distribution;
3. The influence of the micro processes associated with photons is negligible in comparison with its counterpart due to particle collisions (*e.g.* photon ionisation is negligible in comparison with impact ionisation).

An arc which has the above characteristics is known in local thermal equilibrium (LTE). For such an arc its properties are characterised by two thermodynamic variables (*e.g.* temperature and pressure). If the arc is in motion, frequent particle collisions ensure the use of mass averaged velocity for all constituent species. Thus, an arc in a high voltage circuit breaker can be treated as a single electrically conducting fluid. Its

behaviour can be described by the familiar conservation equations of mass, momentum and energy for an ordinary fluid but modified to take into account of electrical magnetic fields and radiation transport. The electric field which is necessary for the maintenance of a current also provides the energy source to sustain the arc discharges through Ohmic heating. The Lorentz force due to the interaction of the arcing current with its own magnetic field exerts a force on the arc. Radiation energy transport is often a dominant energy transport process for temperatures above 12,000K [101]. It is therefore necessary for a full description of the arc behaviour to couple the mass, momentum and energy conservation equations with the relevant Maxwell's equations for electromagnetic fields and the radiation transport equation.

HV SF_6 interrupters are characterised by the intense interaction of the arc with its surroundings due to the very high power levels encountered. For example, in an SF_6 breaker with a rating of 500kV and 60kA electrical power input into the arc can reach 50MW at the peak of a short circuit current. A large proportion, no less than 25% for SF_6 arcs, of the electrical power input is taken out by arc radiation. Intense radiation flux hitting the surface of the arc confining vessel (usually a PTFE nozzle) causes the ablation of the wall. The ablated vapour entrains into the arc, thus greatly modifying the characteristics of the arc. It is therefore necessary to consider the effects of wall ablation on the interruption capability of behaviour of the arc [74, 5].

The arc discharge in an HV SF_6 interrupter is highly transient as current varies sinusoidally. The velocity along the axis of the arc can reach a few thousand meters per second. Such a flow situation together with the steep density gradient at the edge of the arc core often produces instability [94]. In comparison with nitrogen or air the superior thermal interruption capability of SF_6 is mainly due to turbulence enhanced momentum and energy transport [102].

The effects of electrode melting and the influence of the electrode region will not be considered in the present investigation. Contact erosion often occurs during the operation of a breaker. The present thesis is exclusively concerned with auto-expansion (also known as self-blast) breakers in which the flow is arranged towards the contacts. Such a flow arrangement prevents electrode vapour from entering the arc. The length of the arc in an SF_6 interrupter is at least a few centimetres. The arc is therefore dominated by its column. The two electrode regions, which are often in a non-equilibrium

Table 2.1: Mass, momentum and energy conservation equations.

Equation	ϕ	Γ	S_ϕ
Continuity	1	0	0
z-momentum	w	$\mu_l + \mu_t$	$-\frac{\partial P}{\partial z} + j_r B_\theta$ + viscous terms
r-momentum	v	$\mu_l + \mu_t$	$-\frac{\partial P}{\partial r}$ - $j_z B_\theta$ + viscous terms
enthalpy	h	$\frac{(k_l+k_t)}{c_p}$	$\frac{dP}{dt} + \sigma E^2 - q$ + viscous dissipation
PTFE mass concentration	c_m	$\rho(D_l + D_t)$	0

state and are space charge dominated, are therefore not considered.

2.2 The Arc Model and Its Governing Equations

The features of the arc in an HV SF_6 breaker are given in the previous section. An arc model is a mathematical description of these important features. As mentioned previously the arc can be treated as an electrically conducting fluid in a turbulent state. Its behaviour can therefore be described by the time averaged Navier-Stokes equations modified to take into account the electromagnetic fields (Ohmic heating and the Lorentz force) and radiation transport. Assuming axisymmetry, we can write the conservation equations in cylindrical coordinates in the following form:

$$\frac{\partial(\rho\,\phi)}{\partial t} + \frac{1}{r}\frac{\partial}{\partial r}\left[r\rho\, v\phi - r\Gamma\frac{\partial \phi}{\partial r}\right] + \frac{\partial}{\partial z}\left[\rho\,\omega\phi - \Gamma\frac{\partial \phi}{\partial z}\right] = S_\phi \tag{2.1}$$

where ρ is the gas density, z and r the axial and radial coordinates, w and v the axial and radial velocity components respectively. ϕ is the dependent variable, Γ the diffusion coefficient, and S_ϕ the source term, which are tabulated in Table 2.1 for mass, momentum, and energy conservation equations.

In Table 2.1, h represents enthalpy, P for pressure, μ_l and μ_t laminar and turbulent viscosity respectively, whereas k_l and k_t are the laminar and turbulent thermal conductivity respectively, c_p is the specific heat at constant pressure, D_l and D_t the laminar and turbulent diffussivity respectively, E the electric field, j_r and j_z the radial and axial components of current density, σ electrical conductivity, and B the magnetic

flux density. θ indicates the azimuthal direction of a cylindrical polar coordinates system. q in the enthalpy equation is the net radiation loss per unit volume and time. The calculation of q requires a model for radiation energy transport which is given in Section 2.4.

The laminar part of the transport properties (viscosity and thermal conductivity) and electrical conductivity are determined by two thermodynamic variables, enthalpy and pressure. The equation of state and the aforesaid transport properties are tabulated for SF_6 by Frost and Liebermann [101]. Gas density as a function of temperature and pressure is also given in [101]. For temperatures below 300K the equation of state is assumed to have the same form as that for an ideal gas with a gas constant of $56\mathrm{N}\cdot\mathrm{M}/(\mathrm{kg}\cdot\mathrm{K})$.

The discussions of the calculation of the electromagnetic field and the turbulent enhanced momentum and energy transport are deferred to Section 2.3 and 2.6 respectively.

For auto-expansion circuit breakers, the effects of ablation of the PTFE caused by intense arc radiation need to be taken into account. An extra conservation equation needs to be introduced to calculate the concentration of PTFE. This will be discussed in Section 2.5.

The solution of the governing equations requires appropriate initial and boundary conditions. These will be discussed in the chapter 3 where the numerical solution of these equations are discussed.

2.3 Electric and Magnetic Field Calculations

The calculation of Ohmic heating in the energy equation and the Lorentz force in the momentum equations requires the knowledge of electrical and magnetic fields in an interrupter. Since the breaker is operated at a very low frequency (50 or 60Hz), the effects of displacement current are negligible in comparison with the conduction current. In addition the induced electric field due to arc motion in its own magnetic field is also much smaller than that externally imposed through the two contacts. Under these conditions the low frequency magnetohydrodynamic approximation holds [103]. Thus, Ohms Law takes its simplest form,

$$j = \sigma E \tag{2.2}$$

The current continuity equation gives

$$\nabla \cdot j = 0 \tag{2.3}$$

The electric field is related to the gradient of electrostatic potential by E = - ∇ ϕ. Equations 2.2 and 2.3 can be combined into one equation which determine the potential:

$$\nabla \cdot (\sigma \nabla \phi) = 0 \tag{2.4}$$

For an axisymmetrical arc, the magnetic field only has an azimuthal component, which can be derived from Ampere's law:

$$\frac{1}{r}\frac{\partial}{\partial r}(rB_\theta) = \mu_0 j_z \tag{2.5}$$

where μ_0 is the permeability of space.

2.4 Approximate Method for the Calculation of Radiation Transfer

In the source term for energy conservation equation, q is the net radiation loss per unit volume per unit time (emission minus absorption), which is related to the radiation flux vector, $\vec{F}$ by

$$q = \nabla \cdot \vec{F} \tag{2.6}$$

The radiation flux, $\vec{F}$ is the integration of monochromatic radiation intensity I_ν over arc's emission spectrum and then over the solid angle.

$$\vec{F} = \int_0^\infty \oint_0^{4\pi} I_\nu(\vec{r}, \vec{n})\vec{n}\, d\Omega\, d\nu \tag{2.7}$$

where $\vec{n}$ is the normal unit vector, Ω is the solid angle, and ν the frequency of radiation. For a high pressure SF_6 arc, the frequency range of arc radiation spans from infrared

to ultra vacuum violet. The monochromatic radiation intensity I_ν at a given frequency can be derived from the radiation transport equation which is given by

$$\vec{n} \cdot \nabla I_\nu(\vec{r}, \vec{n}) = \epsilon_\nu - K'_\nu I_\nu \tag{2.8}$$

where ϵ_ν is the volumetric emission coefficient and K'_ν the absorption coefficient at frequency ν.

The calculation of q therefore requires the solution of radiation transport equation in three-dimension for the whole spectrum of the arc radiation and in the volume occupied by the arc. For SF_6 arcs radiation transport is dominated by a few hundred lines, which are neither optically thin nor thick [90]. Even with the computing power of the present day computers, the computational cost for such a $3-D$ radiation transport calculation is still prohibitively high. In practice, such a detailed radiation transport computation also encounters difficulties in that the spectra data required for such calculation is not complete. In addition, SF_6 arcs in circuit breakers are often contaminated by the ablated vapour of the nozzle wall and contact materials. This makes such an approach impossible as the spectra data for a contaminated arc is largely not available. Thus, an approximate method for calculating q needs to be found, which avoids the detailed calculation of radiation transport.

For cylindrical wall stabilised arcs Lowke demonstrated that the use of net emission coefficient, which is a function of arc radius, temperature and pressure, can predict satisfactorily the temperature distribution [1]. Lowke's method is commonly known as the net emission coefficient method. This method was modified by Zhang *et al* [66] to calculate the radiation transport of a nitrogen arc burning in a supersonic nozzle with much success. Their modification includes a region where a large proportion of the radiation escaping from the edge of the arc core is reabsorbed. For the arc core the radiation loss is computed using net emission coefficient. The method of Zhang *et al* is therefore essentially one dimensional. Other approximate models, such as $P1$ model [104] and the method of partial characteristics [105, 106, 107], have also been employed. Dixon *et al* [103] applied the three radiation transport models (*i.e.* that of Zhang *et al*, the $P1$ model and the partial characteristic model) to a nozzle SF_6 arc. It was concluded that the method of Zhang *et al* produced the best results when

compared with the experimentally measured temperature profiles. Thus, we adopt the method of Zhang *et al*, which has been modified to take account of the special features of an arc affected by wall ablation. Since this method is concerned with radiation transport in the radial direction, we call this method as one dimensional radiation model for later reference. The partial characteristics model and the P1 model, do not necessarily produce results that are closer to experimental results, thus in the present work, one dimensional radiation model has been adopted.

This one-dimensional model is strictly valid for a monotonic radial temperature profile [66]. For arcs in auto-expansion circuit breakers under the influence of ablation the maximum temperature could be off axis (figure 2.1). Thus, modifications to the one dimensional model are necessary. The procedures for the calculation of the net radiation loss for the modified one dimensional model are given below:

1. Search the maximum temperature, T_m . There will be no net radiation loss if T_m is lower than 8000K;

2. Search in the negative r-direction (from the cold gas surrounding the arc towards the arc axis) for the radial position at which the temperature is 5000K, its radial position is designated by R_{5k} ;

3. Search in the negative r-direction for the radial position, R_{83} , at which the temperature is $0.83T_m$; the region defined by $0 \leq r \leq R_{83}$ is commonly known as the arc core.

4. The arc's radiation radius is defined as $0.5(R_{5k} + R_{83})$;

5. The net radiation loss, q_e , in the arc core, is calculated using the net emission coefficient for a given radiation radius at the local temperature and pressure. The total amount of radiation emitted from the arc core (*i.e.* at the core edge), Q_e , is then calculated by integrating q_e over all emitting volumes ($r < R_{83}$) for a unit length;

6. The radiation coefficient (*i.e.* the absorption per unit volume and time) for the region, $R_{83} < r < R_{5K}$, is assumed to have a radial profile

$$\frac{q_a(r)}{q_0} = 1.1 - \left(\frac{R_{5k} + R_{83} - 2r}{R_{5k} - R_{83}}\right)^2 \tag{2.9}$$

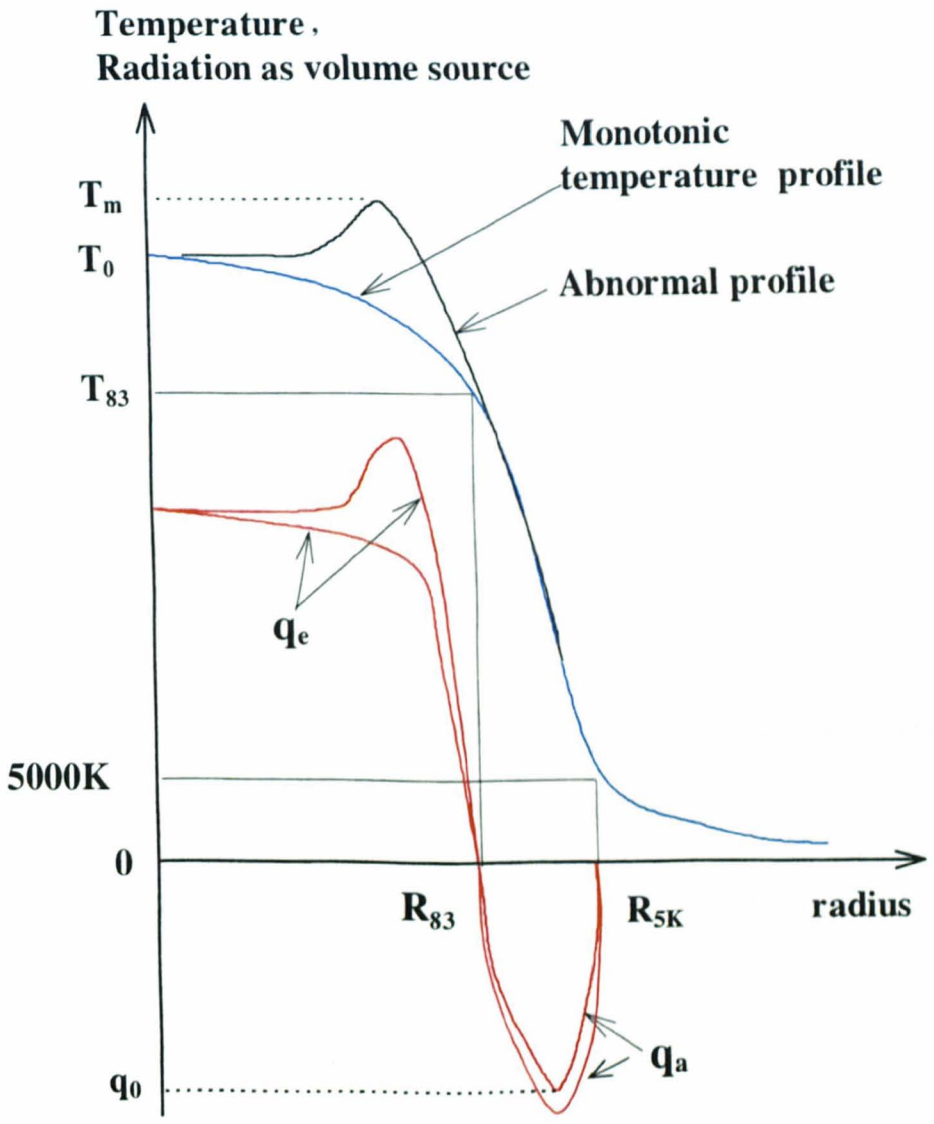

Figure 2.1: Schematic diagram showing the radiation model used in the simulation

where q_0 is the maximum absorption coefficient which is located at $0.5(R_{5k} + R_{83})$. This region is known as the radiation absorption region.

7. Calculate the total radiation absorption, Q_a , in this region by integrating $q_a(r)$ over the absorbing volumes ($R_{5K} \geq r \geq R_{83}$) per unit length.

8. Assume that x% (for auto-expansion arcs, x may change with current) of the radiation emission from $r = 0$ to R_{83} is re-absorbed in the radiation absorption region. Thus, from the known Q_a, q_0 in equation 2.9 can then be determined;

9. After q_0 is known, calculate $q_a(r)$ according to equation 2.9;

10. Set q_e to be positive and q_a to be negative.

The above radiation transport model is modified version of that of Zhang *et al* to take care of non-monotonic radial temperature profile. It is semi-empirical. The net emission coefficient for an arc burning in a mixture of SF_6 and PTFE vapour is not known. For such an arc we use the net emission coefficient for SF_6 arcs (Figure 2.2) as an approximation.

2.5 The Calculation of the Radiation Induced Nozzle Ablation and the Entrainment of Ablated Material

2.5.1 Radiation induced ablation of the inner surface of the nozzle

For HV SF_6 circuit breakers, the interrupter is made of a PTFE nozzle for its mechanical strength as well as for insulation coordination with other commonly used insulation materials in switchgear. PTFE is a polymer and it does not have distinct phase changes. To ablate PTFE the radiation needs to supply the energy required for depolymerisation and then raise the PTFE vapour to a temperature around 3400K [108].

The approximate radiation transport model of section 2.4 indicates that the radiation flux, Q, at the arc edge, defined by the radial position at which the temperature is 5,000K is equal to Q_e - Q_a where Q_e is the radiation flux at the arc core edge and Q_a is the amount of radiation absorbed. If the arc is surrounded by SF_6 (at low current), Q will reach the nozzle inner surface without being reabsorbed in the region between

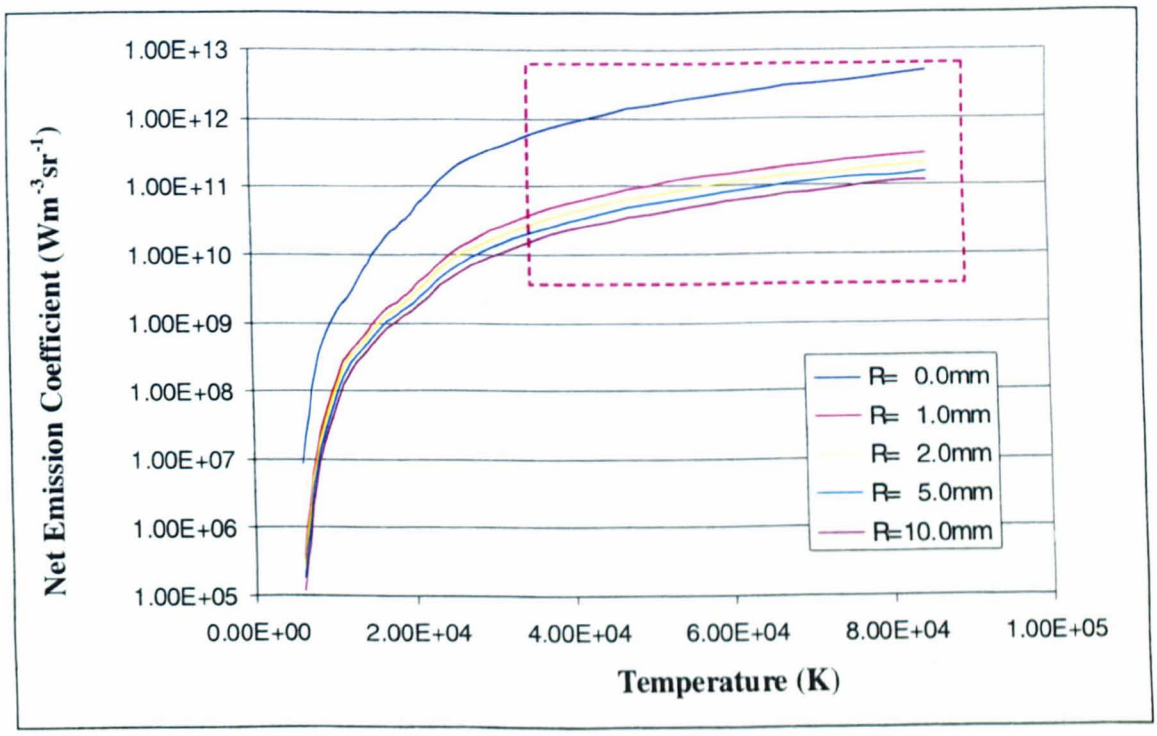

Figure 2.2: Calculated net radiation emission coefficients from cylindrical SF_6 arc plasmas of various radii ($p \approx 1$ bar) [1]. Results above 34, 000K (enclosed in the doted box) are those extrapolated for numerical stability of the computation.

the arc edge and the nozzle wall. However, if ablation of the nozzle inner surface takes place the wall vapour entrains into the nozzle, thus results in a change of temperature profile between the arc edge and the nozzle inner surface. Energy is required to heat the entrained vapour before it enters the arc. Thus, part of the radiation flux at the arc core edge, Q_e, is reabsorbed to heat the ablated vapour. The influence of ablation depends on the instant arcing current and the nozzle size. For currents less than 5kA, ablation does not have much influence on arc radial temperature profile. Radiation re-absorption outside the arc core edge in such a situation should be independent of the rate of nozzle ablation. The radial temperature profile is then controlled by axial convection and radial energy diffusion.

At higher currents, only a fraction of the radiation flux at the arc edge, θ, reaches the nozzle inner surface. θ is called the transparent factor. Part of the remaining radiation flux at the core edge, $Q_e(1-\theta)$ is used to raise the enthalpy of the ablated material from its vapour temperature, h_v, to that of the enthalpy at the arc edge, h_a. The other part of the remaining radiation flux is used to compensate the energy transported in the re-absorption region by convection, which is denoted by $a_N Q_e$. Thus, the energy

balance in the re-absorption region is given by

$$(1-\theta)Q_e = cm(h_a - h_v) + \alpha_N Q_e \tag{2.10}$$

where c is the percentage of ablated vapour entering the arc column, m is the ablation rate of nozzle inner face material per unit axial length, h_a the typical value of enthalpy at the arc edge, and h_v the enthalpy of the ablated vapour leaving the nozzle wall. h_v is also the sum of the energy required to change the phase from solid through the liquid phase to the boiling temperature and then convert it to vapour at the boiling temperature [74]. h_v in equation 2.10 for PTFE is $1.19 \times 10^7 \mathrm{J} \cdot \mathrm{kg}^{-1}$ [109]. The ablation of PTFE is discussed in the next section.

Only part of the radiation flux reaching the nozzle wall, $\beta\theta Q$, is used to ablate the nozzle, the remaining, $(1-\beta)\theta Q$, is passed through the nozzle, which is lost to the surroundings. For evaporation dominated ablation [74] the rate of ablation is given by

$$\beta\theta Q_e = mh_v \tag{2.11}$$

Eliminating Q and m from equations 2.10 and 2.11 gives

$$\theta = \frac{1-\alpha_N}{1+\beta c(\frac{h_a}{h_v}-1)} \tag{2.12}$$

The introduction of the parameters a_N and c in the above equations is due to the fact that at present there is no radiation model that can be used to accurately calculate the radiation flux reaching the nozzle surface for the complex ablation controlled arc in auto-expansion circuit breakers. The determination of these parameters will be deferred to chapter 5.

2.5.2 The calculation of the PTFE vapour concentration

The ablated PTFE vapour enters the nozzle and mixes with SF_6. The arc is therefore no longer burning in pure SF_6 rather in a mixture of SF_6 and PTFE vapour. The thermodynamic and transport properties of such a mixture are different from those of pure SF_6 [5]. These properties are a function of PTFE concentration, which can be calculated from a PTFE conservation equation in terms of its mass concentration, c_m. If we let

the dependent variable, ϕ, in equation 2.1 be c_m, the diffusivity becomes that of PTFE vapour diffusing in SF_6, which is denoted by D. Since the flow is turbulent, diffusion is dominated by turbulence. The calculation of turbulent part of D_t is discussed in Section 2.6.

2.6 Turbulence Model

The stability analysis of arcs in gas flow by Blundell *et al* [94] shows that there are strong mechanisms which make the arc unstable. However, how an unstable arc evolves to its turbulent state is not known. At present the turbulence models for arcs in gas flow are borrowed from those for incompressible fluids. Two such turbulence models, the $K-\epsilon$ model and the Prandtl mixing length model, have been widely used to model the turbulent arc. A recent comparative study of these two turbulent models when applied to arcs in gas flow [90] shows that the conventional values for the 5 parameters of the $K-\epsilon$ model need to be adjusted to fit the experimental results. Such adjustment makes the use of $K-\epsilon$ model no longer attractive compared with the Prandlt mixing length model for which only one parameter needs to be adjusted. It was also found [90] that the mixing length model with the turbulence parameters fixed by one set of experimental results can give reasonably accurate predictions within a wide range of experimental conditions. Therefore the Prandtl mixing length is used to compute the turbulence enhanced viscosity, thermal conductivity and the diffusion coefficient of PTFE vapour in SF_6.

In analogy with shear layer or high-velocity fluid jet, the mixing length is related to the jet radius. In arc context, this is related to the high-temperature region as the velocity in this region attains a very high value due to its low density. Thus, the mixing length for turbulence-enhanced momentum transfer is given by

$$l_m = c\delta \tag{2.13}$$

where δ is the arc thermal radius. c in equation 2.13 is the turbulence parameter to be determined by matching one predicted critical rate of rise of recovery voltage ($RRRV$) with the measured value [98]. It is fixed to a value of 0.1 [5]. The arc thermal radius is defined as the radial distance from the axis to the position of 5,000K in the present

work.

Turbulent viscosity μ_t is defined as

$$\mu_t = \rho {l_m}^2 \left| \frac{\partial w}{\partial r} + \frac{\partial v}{\partial z} \right| \tag{2.14}$$

The turbulent thermal conductivity k_t is related to the turbulent viscosity through the turbulent Prandtl number, which is assumed to be unity

$$Pr_t = \frac{\mu_t}{k_t / c_p}. \tag{2.15}$$

The turbulent diffusion coefficient is related to the turbulent viscosity through turbulent Schmidt number Sc_t by

$$D_t = \frac{\mu_t}{\rho Sc_t}. \tag{2.16}$$

The magnitude of Sc_t is around unity [110] and is set to 1.0 in this paper.

2.7 Summary

The governing equations of a turbulent arc in local thermal equilibrium are given in this chapter. These equations are supplemented by the gas properties for SF_6 or for a mixture of SF_6 and PTFE vapour and by the equations for the calculation of radiation transport, nozzle wall ablation, and turbulent enhanced momentum and energy transport, and PTFE diffusion. Some parameters in the supplementary equations are determined by matching predictions with experimental results. These equations are highly non-linear. They can only be solved numerically with appropriate initial and boundary conditions. This forms the main topic of next chapter.

Chapter 3

Implementation of Arc Models in PHOENICS

Everybody's a mad scientist, and life is their lab.
We're all trying to experiment to find a way to live,
to solve problems, to fend off madness and chaos.
– David Cronenberg

3.1 Introduction

The governing equations together with the supplementary equations given in chapter 2 give a complete description of a turbulent arc in LTE. Attention has been paid to the interaction between the arc and its confining vessel. The effects of radiation induced ablation have been discussed. The emphasis on ablation is aimed at a specific application, *i.e.* the operation of high voltage SF_6 circuit breakers. For the present investigation our objective is to simulate the whole operation an auto-expansion circuit breaker.

The thermodynamic and transport properties of SF_6 or of a mixture of SF_6 and PTFE are highly non-linear functions of temperature at a given pressure. For such coupled, highly non-linear partial differential equations one has to resort to numerical solutions by a computer. Numerical solutions can only be obtained for a specific system under specific operational conditions. In contrast to analytical solutions it is usually difficult to derive general conclusions from computer solutions. The vast amount of data produced by computer needs to be compressed to exhibit the salient features of the dominant processes occurring in the system. The process, numerical solution of the governing equations and the display and visualisation of the computer results, is commonly known as computer simulation.

This chapter is concerned with the implementation of computer simulation of an auto-expansion breaker on a commercially available computational fluid dynamics (CFD) package, PHOENICS [111].

3.2 The PHOENICS CFD Package

The choice of CFD package is an important aspect in simulation. It is often described as a black box where users have no access to the core code where solution procedure is implemented. In order to attain confidence in the CFD package, substantial effort is needed to check the solution of well defined cases against experimental or analytic results. Sometimes users have to use user-defined subroutines to check if mass, momentum and energy are balanced in the solution. In some packages there are logical parameters that can be set to activate certain numerical schemes. One has to be very careful about these settings since inappropriate settings can lead to converged but physically incorrect results. PHOENICS is a general-purpose software package which predicts fluid flow quantitatively. It solves partial differential equations governing the conservation of mass, momentum and energy of mass flow.

For arc simulation, there is also a need to resolve the steep temperature and velocity gradient at the arc edge. Very fine grids are needed in certain regions of the computational domain. The presence of large gradients of physical properties together with high gas speed often leads to difficulties in convergence. On one side, there are areas in the domain where gas has low temperature and high density. In this region a weak relaxation is needed and is sufficient to guarantee rapid convergence. In contrast, gas in the arc region has a very low density. With highly changeable energy source (Ohmic heating and radiation) the energy and momentum equations require strong relaxation for smooth convergence. Special measures may be required to produce reasonably well converged solution within affordable computational time.

Commercially available general-purpose CFD solvers have been widely used in circuit breaker simulations [112, 96, 113, 114, 115, 116]. The use of commercial CFD packages has not proven an easy task. A majority of these packages are based on the finite volume method of Spalding and Pantankar [117]. PHOENICS [111] has perhaps the longest history. PHOENICS has been used in Liverpool for more than 15 years

and its capability and correctness of solution have been studied rigorously. Although it is not very user-friendly, it does have user interfaces required by arc simulations. Its specific way of specifying boundary conditions as explicit source terms makes the software very powerful in dealing with arc modelling. In the present work PHOENICS is used to implement the model.

In the present work, simulation of the arcing process is done in a two dimensional domain. Non-orthogonal grids are needed to accurately represent the shapes of various components. An additional aspect important for choosing the software is the capability of its solution method in handling the non-orthogonality of the grid system to obtain correct results.

The numerical algorithm included the integration of governing equations over the control volume, the discretisation of the terms in the integrated equations representing flow processes such a convection, diffusion and sources; resulting in a solution of the algebraic equations. The flow variables remain conserved after the discretisation of the partial differential equations, which is essential for the correct simulation of any physical processes. The resulting algebraic expression can still be arranged in the following form

Rate of change of ϕ in the control volume with respect of time
= Net flux of ϕ due to convection into the control volume
+ Net flux of ϕ due to diffusion into the control volume
+ Net rate of generation of ϕ inside the control volume due to physical or chemical processes.

Special attention needs to be paid to the generation of the grids, which are usually non-uniform and non-orthogonal with some of the cells occupied by moving parts such as moving contact and piston. The density of grid cells should increase where the gradient of the physical properties of the fluid is large. The calculation of electromagnetic fields often requires a calculation domain bigger than that of the fluid field. These issues will be discussed later. During the modeling of the circuit breaker, the flow geometry varies as a function of time due to moving parts. Considerable effort was devoted to simulate the movement of the moving electrode, piston and also the

operation of the valves.

3.3 Approximation of Circuit Breaker Geometry and Operations

The auto-expansion breaker to be simulated is provided by ABB in Switzerland. A computation model was derived from the detailed drawings of the breaker. A good computation model of the breaker should be as simple as possible yet encompass all important physical processes and retain the main characteristics of the geometry. It is often necessary to make simplifications and approximations to save computational effort without compromising the accuracy of the results. The following approximations and simplifications were made following detailed discussions with ABB.

1. Rounded ends of the metallic field shapers are replaced by square corners (MFL, MFM and MFH in Figure 3.1).

2. There are altogether three valves (two attached on the piston, labeled MPT in Figure 3.1 and one in between the cylinder and the heating chamber). The valve near the bottom of the piston is not simulated because its operation will not critically affect the flow field during the high current phase. The valve has an annular shape.

3. There are eight holes in the hollow contact and auxiliary nozzle in the original ABB circuit breaker design which are not considered in the model. In this work, holes are filled with solid material. Due to the small size of the holes ABB has indicated that these holes can be neglected in the simulation to render the geometry axisymmetric.

4. A flat tip is used for the moving contact. In reality the tip has a semi-spherical shape which creates difficulties in modeling the moving contact. When the breaker contacts separate, the contact gap length is much larger than the axial dimension of this tip. Making it flat in the model does not significantly influence the results since arc rooting is not important in the present work.

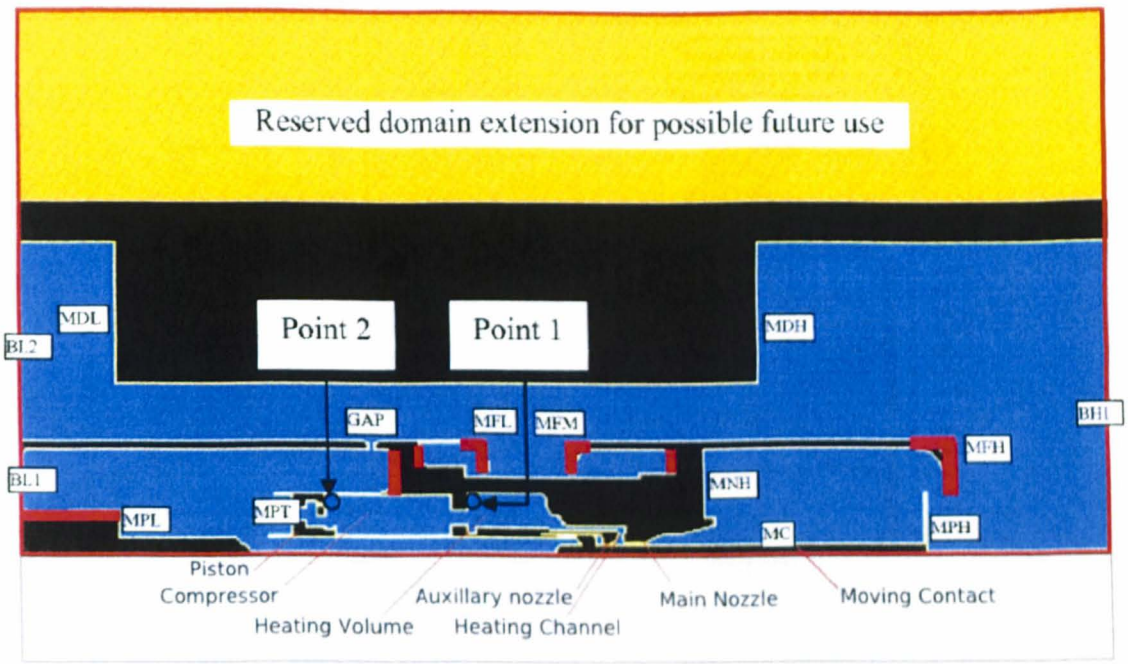

Figure 3.1: Computational domain and geometry approximation for arc simulation in the ABB 170PM40(SW10) auto-expansion circuit breaker.

5. In the simulation, a moving frame of reference was adopted whereby the observer was placed on the nozzle assuming everything else move in relation to it. Therefore the electrode and the piston move while other parts stay stationary. This is the converse of what happens in the actual circuit breaker where the electrode and piston are stationary and the other parts move away from the electrode. Since the relative motion has a speed of less than 10ms^{-1} which is much small the gas flow speed, this type of setting does not make much difference in the final results.

3.3.1 Grid system generation

The body fitted coordinate (BFC) grid system is used in order to model the complex geometry of the auto-expansion circuit breaker. The BFC grid system is particularly suitable for flows with smoothly-varying non-regular boundaries. It provides a good representation in both geometry or surface boundary layers, wall friction and heat transfer. It is useful to accurately simulate flow around curved bodies (eg. in nozzles, circuit breakers etc). The BFC model itself rounds the actual geometry although pre-

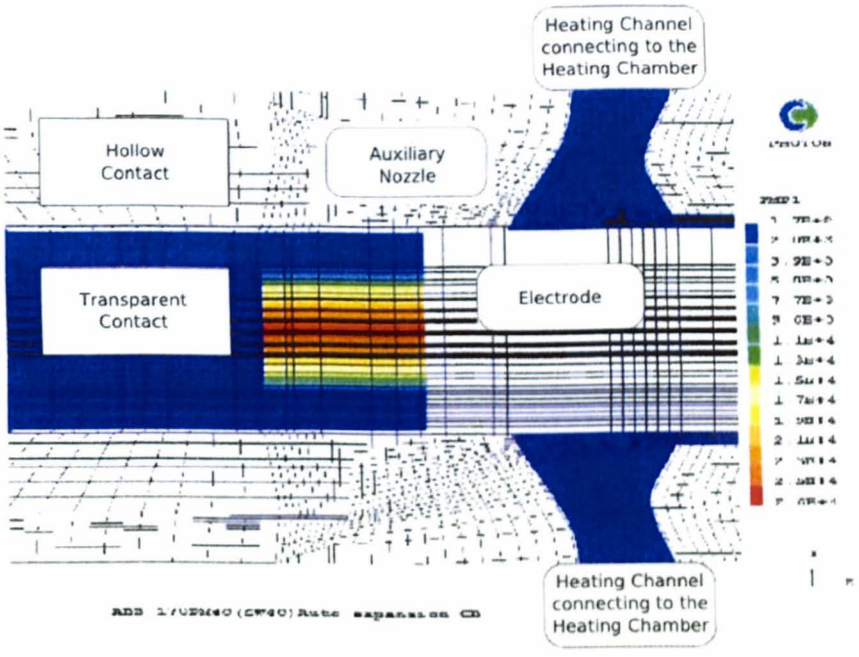

Figure 3.2: Magnified diagram showing grid system and arc initiation.

cautions must be taken so as to make sure the cell angles are not too skewed in order to avoid the difficulty in convergence and also numerical accuracy. It can also be used to reduce the numerical false-diffusion errors, by aligning the grid with the local flow direction where possible. A part of the grid system is given in Figure 3.2. The typical cell size is 1.0mm (axial) by 0.2mm (radial) in the contact gap, and 2.8mm (axial) by 3.0mm (radial) in the heating chamber.

Due to the large CFD domain, a compromise between the total number of cells and computational cost has been made. The grid is densely populated in the arc region in the radial direction. In the axial direction dense grids are used in regions where the flow field undergoes rapid change. There are 105 cells in the radial direction and 245 cells in the axial direction for most simulations. Dense grids are applied in regions where physical processes might undergo drastic change during the simulation. A sudden, dramatic change in cell volume should ideally be avoided.

3.4 Input of Thermodynamic and Transport Properties and Net Emission Coefficient

The solution of the governing equations requires the thermodynamic and transport properties of the arcing gas. As discussed in chapter 2, the inner surface of the PTFE nozzle will be ablated under intense arc radiation. The ablated PTFE vapour entrains into the SF_6 arc, thus changing the composition of the arcing gas. The numerical solution of the governing equations requires the input of equation of state, which relates the density to pressure and temperature, and the transport properties, namely the laminar part of the viscosity, that of the thermal conductivity, the laminar diffusion coefficient of PTFE vapour in SF_6 and electrical conductivity. In addition, the computation of radiation transport needs the data for the net emission coefficient.

The material properties in the presence of PTFE vapour are functions of both enthalpy and PTFE mass concentration. PHOENICS provides user interfaces to the solver in a subroutine called Ground. Sub-level subroutines can be called from Ground to calculate and set the material properties according to user's formula and method. In the present work, material properties are calculated using double interpolation, first in the concentration space, then in the enthalpy space.

3.4.1 The equation of state

For a complex gas such as SF_6 or the mixture of SF_6 and PTFE vapour the gas density at a given pressure is a complex function of temperature and pressure because the gas composition varies greatly with temperature in the temperature range of interest from room temperature to 30,000K. The relationship between gas density and temperature at a given pressure has been tabulated for SF_6 (*e.g.* [101, 5]) and for a mixture of SF_6 and PTFE [5]. Such a relationship is known as the state equation. The tabulated equation of state of Zhang *et al* [5] was written as a user defined subroutine in PHOENICS.

Table 2.1 indicates that enthalpy is a chosen dependent variable (also known as solved-for variable) which is obtained from the numerical solution of the governing equations. As the equation of state and the transport properties are customarily tabulated as a function of temperature. Thus, a relationship between enthalpy and temperature is also required. This relationship is also coded as a subroutine using the data

given in [5].

3.4.2 Transport properties

Of the required transport properties the most important one is the electrical conductivity as the other three, *i.e.* the laminar part of viscosity, thermal conductivity and diffusion coefficient, are of little importance in comparison with their turbulent counterparts. The tabulated values of electrical conductivity as a function of temperature at a given pressure and at a percentage of the PTFE mass concentration in the mixture [5] are inputted into PHOENICS in a subroutine. Subroutines for laminar viscosity, thermal conductivity and diffusion coefficient have also been written which are incorporated into PHOENICS.

3.4.3 Net emission coefficient

The commonly used net emission coefficient for pure SF_6 is that of Libermann and Lowke [1]. The net emission coefficient of SF_6-PTFE vapour mixture is not known. Chervy *et al* [118] calculated the net emission coefficient for SF_6-CF_4 and SF_6-C_2F_6 mixtures with two plasma radii of 0 and 2mm at 0.1MPa by assuming isothermal and homogeneous plasma. Their results indicate that for optically thin plasma (*i.e.* zero radius), a pure CF_4 or pure C_2F_6 plasma radiates more than pure SF_6. If account is taken of the optical thickness, the radiation of carbon is subjected to strong absorption and this can lead to a weaker net radiation for CF_4 and C_2F_6 than for pure SF_6. However, the net radiation of the SF_6-CF_4 or SF_6-C_2F_6 mixture with CF_4/C_2F_6 volume concentration of 50% is always greater than that of pure SF_6. For temperatures above 18,000K the net emission coefficients for the two mixtures, pure SF_5, pure CF_4 and pure C_2F_6 are very close to each other. The net emission coefficient of the mixture of SF_6-PTFE (C_2F_4) is therefore approximated by that of the pure SF_6 in the present work.

3.4.4 Differences in thermodynamic and transport properties

Thermodynamic and transport properties for pure SF_6 and PTFE have been calculated by different researchers (*e.g.* [101, 5, 119, 120]). However, no two sets of data are identical because of the differences in the atomic and molecular data used. When they are

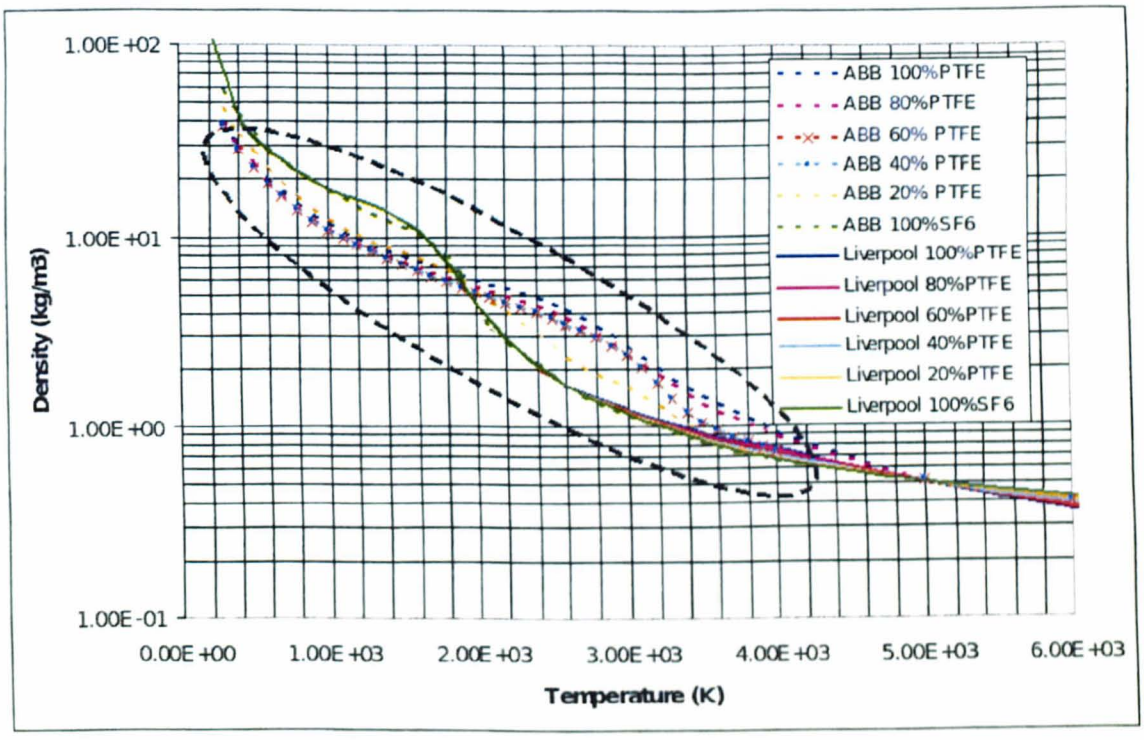

Figure 3.3: Density vs. Temperature at 10 bar

compared it has been found that the data of [5] are very close to those of [119]. Data given in [5] and [120] the gas density (figure 3.3) shows some difference at temperature below 5,000K. This implies that the gas composition of [5] is very different from that of [120]. For electrical conductivity a comparison between the two shows that the electrical conductivity of [5] is consistently higher than that of [120] for temperature above 15,000K (figure 3.4). Since arc temperature is usually below 30,000K, the discrepancy in electrical conductivity is on average less than 10%. Calculations have been performed for the same operational conditions for the data of [5] and those of [120]. However, the results, for example the arc voltage, are very close to each other. On balance more confidence is placed in the data of [5] because its good agreement with the data of [119].

3.5 Initial Conditions, Boundary Conditions and Source Terms

The correct specification of initial conditions, boundary conditions and source terms is important in obtaining meaningful solutions for computer simulation. Initial and boundary conditions indicate how a system under simulation (confined in the compu-

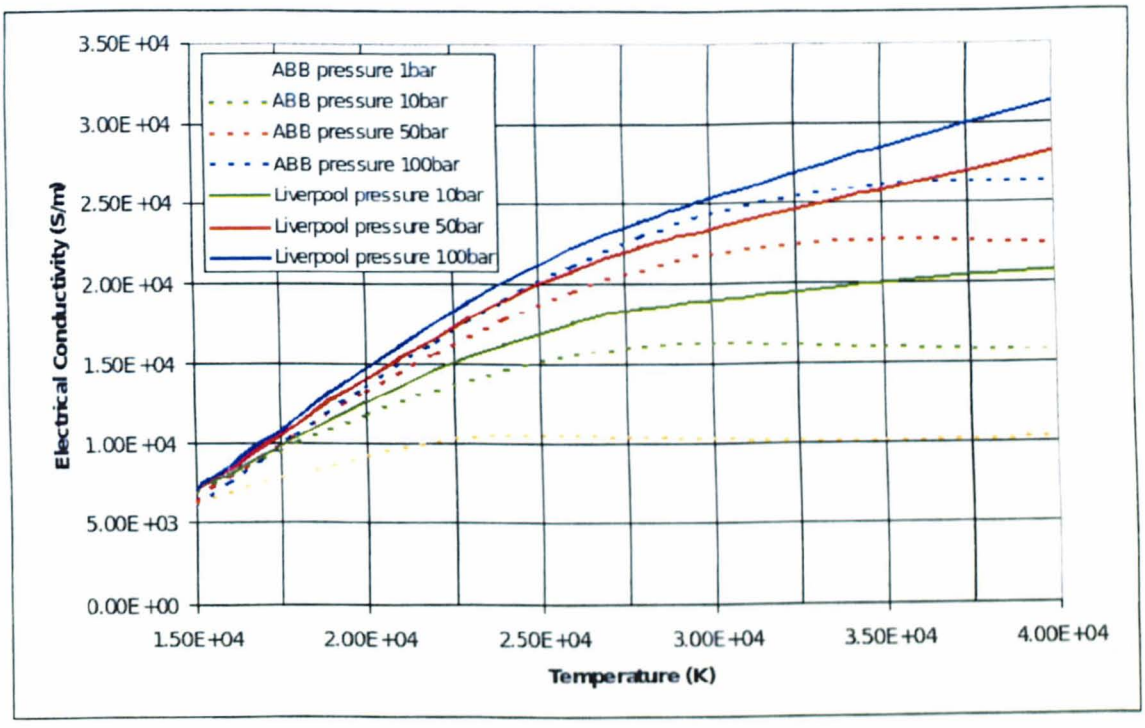

Figure 3.4: Electrical conductivity vs. Temperature for pure PTFE vapour

tational domain) interact with the environment, either mechanically (moving contact and piston), aerodynamically (gas flow), electrically (electrical potential and current), thermally (energy exchange on surface), or in other ways such as ablation (PTFE ablation in this work).

Initial conditions are necessary for the solution by PHOENICS' partial differential equation solver. They define the state of the system at the beginning of the process. In a steady-state calculation, the initial conditions are just a first guess at the answer. The finial solution however is independent of the starting values. Nevertheless, a good initial conditions can accelerate convergence and reduce the computation time. In a transient calculation such as described in this work, the initial conditions are the 'boundary' conditions corresponding to the 'time dimension'. This is because time is parabolic in nature and conditions are required only at the beginning of the time dimension.

The number of boundary conditions needed to specify depend on the nature of the partial differential equations and the types of boundary. Boundary conditions should be specified according to the physics involved and need to be consistent with the initial conditions. In order to guarantee a unique solution of the partial differential equation,

boundary conditions should not be over or under specified.

The necessity for specifying boundary conditions can be clearly seen from the following integro-partial differential equation:

$$\iiint \left[S_\phi - \frac{\partial(\rho\phi)}{\partial t} \right] dV = \iint [\rho\vec{v}\phi - \Gamma\nabla\phi] \cdot d\vec{A}. \tag{3.1}$$

where A is the surface area of a cell.

The convective and diffusive fluxes are specified at the domain surfaces while the true source terms have a volumetric nature, as shown on the left hand side of equation 3.1. This means in PHOENICS we need to use two types of source terms, one is surface source and the other is volumetric source. PHOENICS takes as default a zero flux on for the terms on the right hand side of equation 3.1 on all boundaries of the calculation domain.

The finite volume discretisation of the general partial differential equation yields, for each cell (or control volume), p, in the computational domain, the following algebraic equation:

$$a_p\phi_p = \Sigma(a_i\phi_i) + S_\phi + TC(V - \phi_p) \tag{3.2}$$

where a_p and a_i are coefficients representing convection or diffusion link between neighbour cells, S_ϕ the built-in source terms (terms in the Navier-Stokes equations that cannot be place on the left hand side of equation 2.1) appearing in Table 2.1 and the term $TC(V - \phi_p)$ represents any additional source terms (such as radiation and Ohmic heating in the enthalpy equation or Lorentz force in the momentum equation) or boundary sources. T is the type (area or volume), C a coefficient, V a value and finally ϕ_p the local value of the variable to be solved for.

There are two ways commonly used to specify the source terms. The first one is a 'fix flux' type. The user is required to directly provide a single value for the term $TC(V - \phi_p)$. In this case PHOENICS sets C to a tiny value (10^{-10}) and CV to a user given value, thus eliminating the effect of ϕ_p.

The other type is called 'fixed value' that can be used to fix the solved for variable to a value given by a user. In this case, PHOENICS sets C to a large value (10^{10}) and V to the user given value. Dividing all other terms in equation 3.2 except $TC(V - \phi_p)$ by

the large value of c, they become negligible in comparison with $T(V - \phi_p)$. Equation 3.2 for the local solution is governed by the resultant equation

$$T(V - \phi_p) = 0 \tag{3.3}$$

which gives a solution $\phi_p = V$ where V is given by the user. Linearisation of the mathematical expression of source terms is often used to accelerate convergence.

3.5.1 Inlets and outlets

For arcs in an axisymmetric flow field, the derivative of all dependent variables with respect to the radial coordinate, r, is set at zero on the axis where $r = 0$. At the inlet, stagnation pressure and temperature are normally specified for gas flow. This means the inward mass, momentum and energy fluxes are calculated by assuming isentropic expansion of gas from the stagnation pressure to the local pressure at the inlet. The local pressure is part of the solution to be obtained by the solver. So it is constantly adjusted in the solution process.

In the present work, there is no gas injected into the computational domain through a conventional inlet. Thus no inlet conditions are needed. However in the present work we need to consider the entrainment of PTFE vapour into the arcing space. The mass, momentum and energy associated with nozzle ablation are added into the solution process using surface sources.

The mass flux is calculated by using the method given in section 2.5 (equation 2.11). The mass flow rate per unit area as surface source is independent of the local gas state. The determination of whether a part of the solid surface is ablating or not depends on two conditions. Firstly, the surface must be ablatable and in the present work it means the surface must be a PTFE surface. Secondly, there must be radiation available for ablation. It is assumed that radiation travels only in the radial direction. If a surface cell can radially 'see' the arc column then PTFE vapour is generated by the radiation flux on the surface. Therefore in the present work the total area of ablating surface increases with time until the moving contact stops moving. The momentum associated with the ablated vapour is assumed to be perpendicular to the ablating surface. Given a mass flux, its entry velocity is inversely proportional to the local

density.

Results have shown that the momentum flux interface condition does not noticeably affect the computational results since the flow is dominantly generated by pressure gradient. The energy flux of the PTFE vapour can be obtained by the vapour temperature and its specific heat. The enthalpy of the vapour is a constant as given in chapter 2. Principally, all the energy used to ablate PTFE vapour should be brought back into the gas flow by the vapour. All the interface sources are implemented as 'fixed flux' surface sources, which is a specific type defined in PHOENICS meaning the flux is directly given by the user to the solver.

For solid walls other than ablating surface, there is no mass, momentum and energy exchange between the wall and the gas. This implies a zero flux in terms of mass, momentum and energy exchange. The effect of this setting has been discussed in [90] and it was shown that for switching processes the energy exchange through the wall including the electrode surface plays an unimportant role in the solution.

In circuit breaker applications, the exit of the arcing chamber is either connected to a low pressure vessel or a large volume (exhaustion volume) and gas leaves the chamber at a high Peclet number. Under such conditions, the convective energy and momentum fluxes dominate the diffusive fluxes. Thus, downstream boundary conditions other than the pressure at the exit are not necessary. In the two different types of geometries that have been used in this work, only the smaller computational domain (used in chapter 6) requires the specification of the outlet conditions where a fixed pressure has been specified. The large domain (used in chapter 5) represents the real space of the interrupter and there is no outlet. Experience has shown that sometimes an inappropriate choice of the outlet could render part of the outlet as an inlet where flow reverse occurs. In these circumstances, the fixed pressure condition at the outlet is no longer sufficient. Additional information such as velocity and temperature of the gas just outside the boundary is required.

For a fixed pressure outlet, the pressure is to be fixed irrespective of the mass flow. The mass flow 'floats' to accommodate the difference between the internal and external pressures at the exit. Using the linear source $TC(V - \phi_p)$, it is recommended by *CHAM*, the CFD package provider, to set C_m to 103 and V_m to the exit pressure:

$$TC_m(V_m - P_p) \tag{3.4}$$

where T is the type (area or volume), C_m a value called coefficient, V_m a value to calculate the source term and P_p the local pressure resulting from the solution procedure.

3.5.2 Initial condition and initiation of arcs

The filling pressure of SF_6 is 6 bar in the present work. There is no gas movement at the beginning of the simulation. For the cases reported in chapters 4 and 5, in the first stage of the circuit breaker operation which last for about 17ms, the moving contact remains electrically connected to the hollow contact and there is no arc. This is commonly referred to as the 'cold flow' stage. Shortly after the two contacts separate at about 17.6ms, an arc is established in the contact gap.

To maintain an electric current path for small current in the axissymetric case, a transparent contact is needed. A transparent contact is a region in the computational domain over which the electrical conductivity of the gas, irrespective of its temperature, is set to a high value ($10^5(\Omega \cdot \mathrm{m})^{-1}$). In the auto-expansion circuit breaker under investigation, this transparent contact is placed in the hollow contact that fills the hole of the latter. Its position is shown in figure 3.2. Ohmic heating is not present in the transparent contact region. The presence of the transparent contact has no blockage to the gas flow.

In practice, the breakdown of the contact gap following contact separation is a rapid and complicated non-equilibrium process. This process is almost not possible to simulate. Moreover, in the worst scenario, the instantaneous current during contact separation could be extremely high. It could be 30kA or higher. A common practice in circuit breaker arc simulation is to start the arc with a hot, conducting column that has a size similar to that of a steady state arc in nozzle flow. The initiation of an arc column at high current creates numerical difficulties because of the sudden input of Ohmic heating. In the present work, a low electric current of 2.69kA is used to start the simulation and the current is then ramped up in a short period of 0.2ms to the actual current. This gives time for the arc column to expand according to the increasing current and the formation of a proper arc column in a short period from the

arc initiation. The arc is initiated when the contact gap is about 15mm by imposing a hot column at the time when the arc should be started (figure 3.2). The initial hot column has a diameter of 10mm.

Once the transient process is initiated, the Ohmic heating and radiation transfer inside the arc column lead to the rapid build-up of a strong heat source. The arc column size is then adjusted according to the governing equations. For auto-expansion circuit breaker arcs, the auxiliary and main nozzles are normally blocked by the moving contact when the arc is initiated. The initiation of the arc with a hot column only affects the arcing process in a short period, typically $1 - 2$ms. Once the arc burns in the auxiliary nozzle, ablation starts to control the arcing environment. Thus the initiation of the arc column does not significantly affect the high current phase and the subsequent current zero period.

3.6 Convergence Control and Time step

3.6.1 Convergence control

In PHOENICS, the solution algorithm proceeds slab by slab, where a slab is a layer of cells perpendicular to the axial position (z direction). At each of these slabs, and for each solved-for-variable ϕ_p, and for each cell P, the following algebraic equation is iteratively solved

$$a_p\phi_p = \sum_{F\in\{S,N,H,L\}} a_F\phi_F + a_T\phi_T + b \tag{3.5}$$

where the coefficients a with different subscripts P, F, and T represents links between neighbour cells, linearised sources, and solution of previous time step. Because of the highly nonlinear nature of the transport properties and radiation transfer, relaxation is needed to ensure convergence of the solution procedure.

Relaxation promotes convergence by changing the rate of convergence (by affecting the smoothness of the iteration process). It slows down the changes made to the values of the variables during the solution procedure. When linear relaxation is applied to the iteration process of a variable ϕ, the new value of the variable at each cell is taken as

$$\phi_{new} = \phi_{old} + \alpha(\phi^* - \phi_{old}) \tag{3.6}$$

where ϕ_{old} is the current in-store value, resulting from the previous iteration; ϕ^* is the value which results from the current iteration; α is the relaxation factor $(0 < \alpha \leq 1)$. ϕ_{new} is the relaxed value which is to be used for the next round of iteration. Linear relaxation is normally used for pressure, electrical potential and vector potential. Solutions for all these variables are based on the whole field solver. The choice of the relaxation factor requires some experience or trial simulation. For pressure in auto-expansion arcs, a linear relaxation of 0.4 to 0.6 is a good choice. A value of 0.8 is used for the electric potential solution.

In numerical solution of the governing equations, the iteration process within a time step resembles a 'transient process' where the intermediate values continuously changes from the values of the last time step to the converged value of the current time step. PHOENICS provides a relaxation method called 'false-time-step'. This method adds the following extra retarding source term to the balance equation (3.5):

$$\frac{\rho V_p}{\Delta t_f}(\phi_p - \phi_{p,old}) \tag{3.7}$$

where ϕ_p is the cell-value in cell P, $\phi_{p,old}$ is the cell-value resulting from the previous iteration; V_p is the cell volume; and Δt_f is user-set false-time-step. The above expression indicates that if the solution is well converged then the term is negligibly small. A small value of Δt_f produces a large term thus slows down the change of the concerned variable. Given the value of Δt_f, the relaxation term is then proportional to the difference between the old value and the new value of the variable concerned. This means that if the change during the iteration is too abrupt, then a large retarding 'force' will be automatically added to the process to slow down the change, thus promoting convergence. It is similar to add a frictional force to a moving object: the faster the object moves, the bigger the friction is.

Choice of the false time step depends on an understanding of the nature of the process and also on experience. Sometimes a trial-and-error approach may needs to be used. For auto-expansion circuit breaker arcs, it is found that using a single false time step leads to unrealistically long computing time. This is because in the relatively

cold region, there is no radiation or Ohmic heating and the gas density is usually high. Thus a weak relaxation is needed for rapid convergence. However in the arc region, there is strong Ohmic heating and radiation and the gas density is very low. Different regions of the domain therefore require different values of false-time-step. In the present work, a two-zone relaxation method is used. The false time step in the cold region, which is defined as the region whose temperature is lower than 10^4K and the magnitude of energy source is lower than $10^{10}\mathrm{J}/(\mathrm{m}^3 \cdot \mathrm{s})$, the false time step is set to 10^{-5}s to 10^{-6}s for both energy and momentum equations. Otherwise, the false time step is set to 10^{-7}s to 10^{-8}s.

3.6.2 Choice of time step

The choice of time step is an important aspect for the simulation. Ideally, use of fewer time steps is preferred because it is computationally cheap. However, if the time step is much larger than the characteristic time of the physical process, the solution will be less accurate and the solution process may easily diverge. The size of the time step should be determined based on the characteristic time of the physical process. For circuit breaker arcs, there are several time scales to be considered. Firstly the duration of the current waveform needs to be considered. The time step should be small when the current changes rapidly. Secondly, the time scale for variation of enthalpy under the influence of radiation transfer and Ohmic heating is much smaller. This can be estimated by dividing the expected typical enthalpy change with the magnitude of the volume energy source. Thirdly, we also need to consider the time scale for flow field change. It is difficult to estimate due of the complex flow field encountered but needs to be checked based on typical flow speed. Sharp velocity field change can take place when the moving contact is just leaving the main nozzle. The distribution of the time step over the whole arcing process should be determined by considering the combined effect of the above mentioned factors. In this study, a time step size in the range of 2 to 20μs is used for the high current phase.

3.7 Summary

This chapter is concerned with the implementation of the arc model in the PHOENICS package. A number of issues of practical importance are discussed and the method for implementation is explained in detail. The concept of false time step and the specification of boundary conditions as source terms are two important aspects in obtaining a well converged solution which is physically sensible. A method of two-zone relaxation is developed for auto-expansion arcs based physical considerations and also experience. The numerical implementation of piston movement and valve operation is deferred to next chapter when we discuss the simulation of the no-load case.

Chapter 4

No-Load Simulation for ABB Auto-expansion Circuit Breaker

Success is going from failure to failure
without a loss of enthusiasm.
– Winston Churchill

4.1 Introduction

There are two situations in auto-expansion circuit breaker operations where gas flow is in a 'cold' environment. Firstly, modelling of the arcing process often involves an initial 'cold flow' stage before the main contacts separate and a subsequent arcing stage. Secondly, for low current switching below several kA, nozzle ablation is negligible and the flow and thermodynamic environment at current zero is significantly different from the flow without the arc. Thus the cold flow simulation is a good representation of the flow pattern for low current switching. The objective of this chapter is to simulate the cold flow in the ABB auto-expansion circuit breaker, analyse the flow patterns and also verify the numerical methods for contact and piston movement and also the operation of the valves.

A diagram of the circuit breaker geometry used in the simulation is shown in figure 4.1. Red indicates the solid wall (either metal or PTFE material) whereas blue indicates the gas-filled region. In the current model the solid parts are only differentiated by their electrical conductivities. The electrical conductivity of the insulating material is set to a small value of $10^{-3}(\Omega \cdot \mathrm{m})^{-1}$ while that in the conductor is set to a large value of $10^{5}(\Omega \cdot \mathrm{m})^{-1}$.

Gas flow in the no-load case is generated as a result of the relative movement of

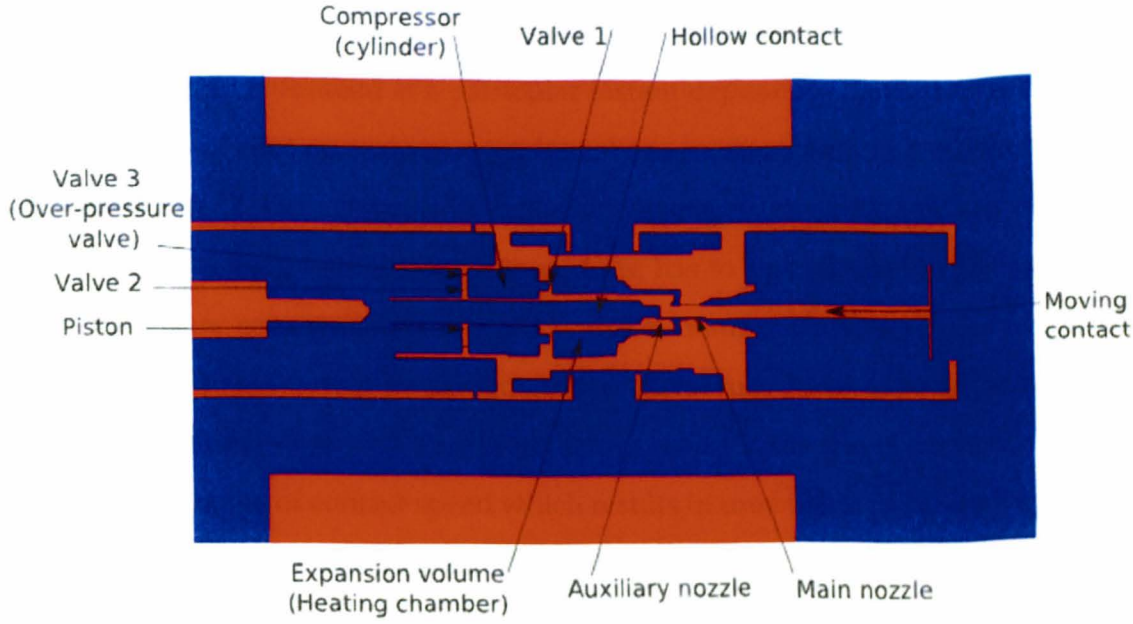

Figure 4.1: Geometry used in the simulation of the ABB circuit breaker (170PM40).

the piston in the compressor (cylinder). Over-pressure valves are used to control the maximum pressure in the compressor. The accuracy and efficiency of the computational model depends on how the computational domain is discretised (grid system) and how the effects of piston movement and valve operation are implemented in the numerical scheme. Figure 4.2 illustrates a scheme used in the present work to guarantee mass, momentum and energy balance when the contact or piston moves. The solid object is moving towards the right hand side in the diagram. Details are given in next section.

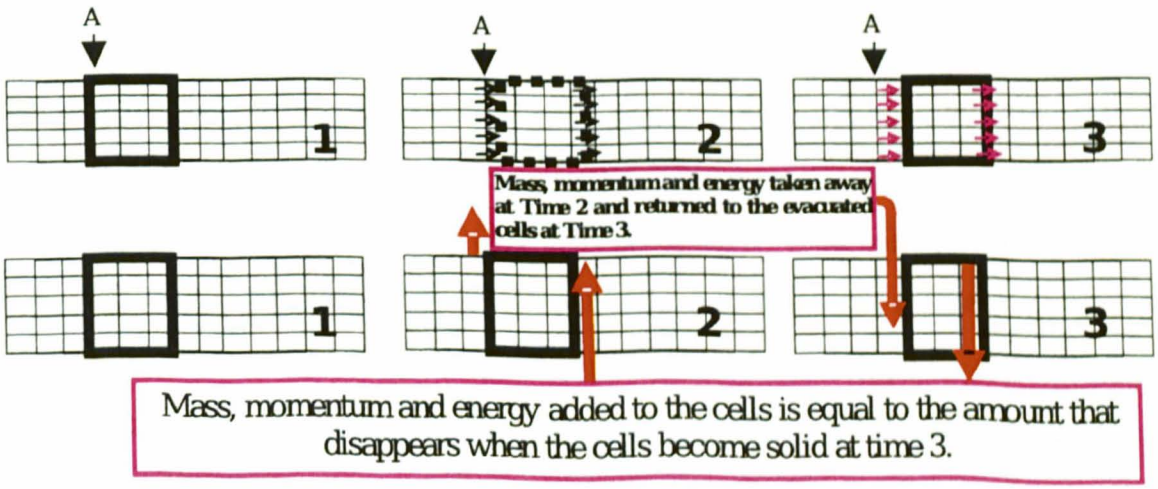

Figure 4.2: Schematic diagrams showing numerical scheme for moving a solid part.

Although piston movement takes place in a discrete manner, namely, a blocked cell is completely evacuated at a particular instant depending on the travel of the piston; its effects of continuously moving have been implemented in a manner which is close to reality. This is conveniently realised by using continuous (in time) volumetric source terms in the governing equations. Care has to be exercised in the implementation to ensure correct results when the piston changes its direction of movement. Experience has shown that measured contact travel may have to be smoothed when used in the simulation since a small fluctuation/noise in the travel curve can induce a rather large change of contact speed which results in unrealistic pressure waves in the domain. The accuracy of the prediction also depends on the coarseness of the grids. The numerical model for moving piston is described in the section 4.2.1.

4.2 Simulation Conditions with Moving Boundaries

4.2.1 Numerical schemes for the operation of moving contact and piston

In a real operation, during the opening of the circuit breaker, the hollow contact which is surrounded by PTFE main and auxiliary nozzles, is mechanically connected to a cylinder which slides over a fixed piston. In this work, the geometry of the circuit breaker requires a body-fitted coordinate grid system and this has made it difficult to simulate the movement of the complicated parts which includes the hollow contact, cylinder, heating chamber and nozzles. In the simulation, the fixed electrode, which is much simpler in shape, 'moves' whilst the whole hollow contact-nozzle system is assumed to be at rest. This practice is well accepted in circuit breaker arc simulation. The same approach is applied to the fixed piston in the cylinder, where the piston 'moves' with respect to its surroundings in this simulation.

As indicated in figure 4.2, a cell originally occupied by solid will be evacuated only when the solid object completely moves out of the cell. The mass, momentum, energy and PTFE concentration (when vapour is present in the arcing process) for the just evacuated cells are copied from the upstream cells, which are the cells on their left hand side. This amount of copied mass, momentum, energy and PTFE concentration are equal to the amount of loss of the corresponding quantities from the cells originally in front of the solid surface, which is represented in figure 4.2 by the red arrow

pointing away from the cells. The loss of a physical quantity is realised in the model by using a negative volumetric source proportional to the contact speed. In this manner, the numerical scheme maintains mass, momentum, energy and PTFE concentration balance. On the right hand side of the solid surface, the cells originally occupied by gas will be changed to solid when the cells are completely occupied by solid due to movement of the solid object. Since in reality the moving surface constantly pushes the gas towards the right handed direction, surface sources are specified for mass, momentum, energy and PTFE concentration.

Conservation of mass, momentum and energy and/or PTFE concentration is represented by source terms in two layers of cells which are immediately adjacent to the moving surfaces. Mass loss from a upstream gas cell (cell pointed by A in figure 4.2) is given by $\Delta A \cdot \rho \cdot w_p$, where A is the cross sectional area, ρ the gas density, and w_p speed of the piston. The surface sources for mass, momentum and energy for the cells upstream of the piston are converted into a volume mass source, $\frac{\rho \cdot w_p}{\Delta z}$, where Δz is the axial width of the cell. In PHOENICS, when a negative volume source of mass (sink) is defined, the momentum and energy associated with the outgoing mass are automatically removed.

Numerically, when a cell is completely evacuated/unblocked within a time interval, Δt, we have the relationship that $\Delta z = w_p \cdot \Delta t$ for the newly evacuated cell. The mass copied from the upstream cell is therefore $\Delta V \cdot \rho = \Delta A \cdot w_p \cdot \Delta t \cdot \rho$. The total mass lost from an upstream cell during this period is $\Delta A \cdot w_p \cdot \Delta t \cdot \rho$. So clearly the mass is balanced. Using a similar argument we can prove that all other quantities are also balanced in the scheme. The movement of the right handed moving surface in figure 4.2 is implemented in a similar way. Figure 4.3 and figure 4.4 show the pressure and velocity distribution shortly after the piston starts to move.

A validation test was performed where SF_6 gas is isentropically compressed in a cylinder as shown in Figure 4.5. The theoretical result is obtained by assuming isentropic compression of SF_6. The pressure drop after 36ms is associated with the reversed motion of the piston. Typical cell size in the direction of piston movement is 4mm and the time step used is 0.1ms. The accuracy of prediction deteriorates when the gas is compressed into a smaller volume because of the finite cell size used. An overall accuracy of 4% is attained with a typical cell size of 4mm in the direction of

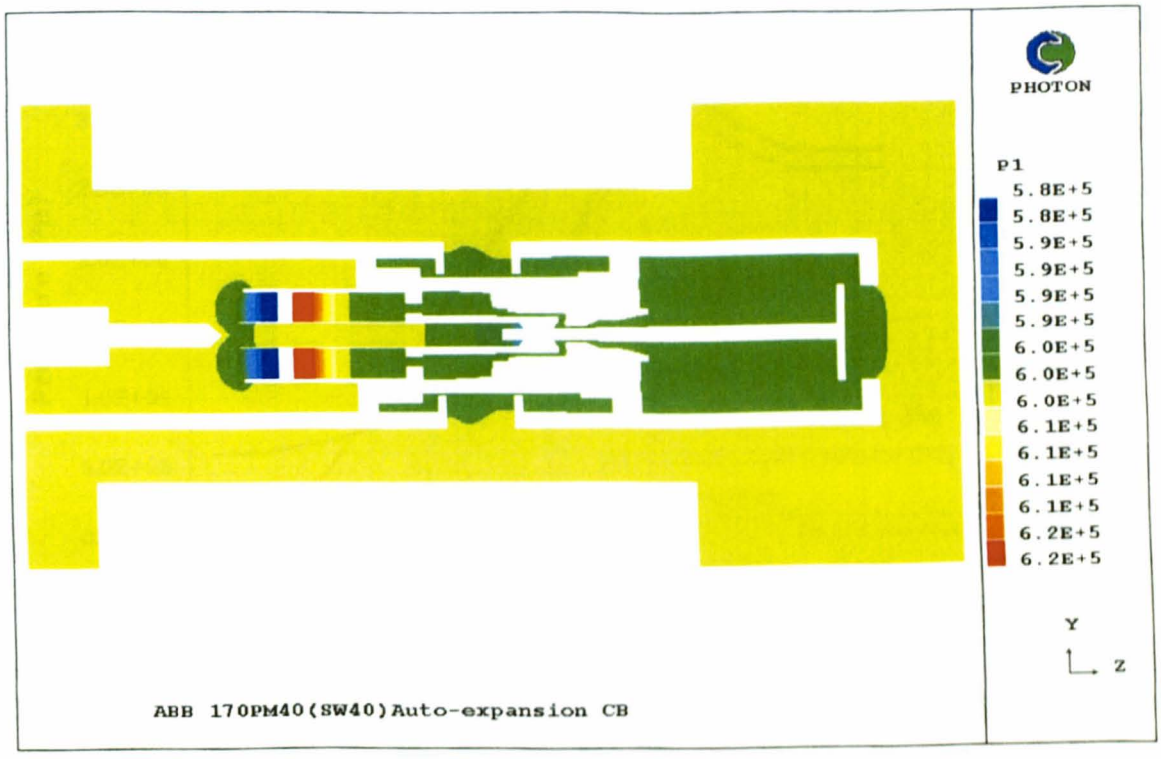

Figure 4.3: Diagram showing pressure distribution shortly after piston movement (0.2ms) with a speed of 2.5ms^{-1}. Filling pressure is 6 bar.

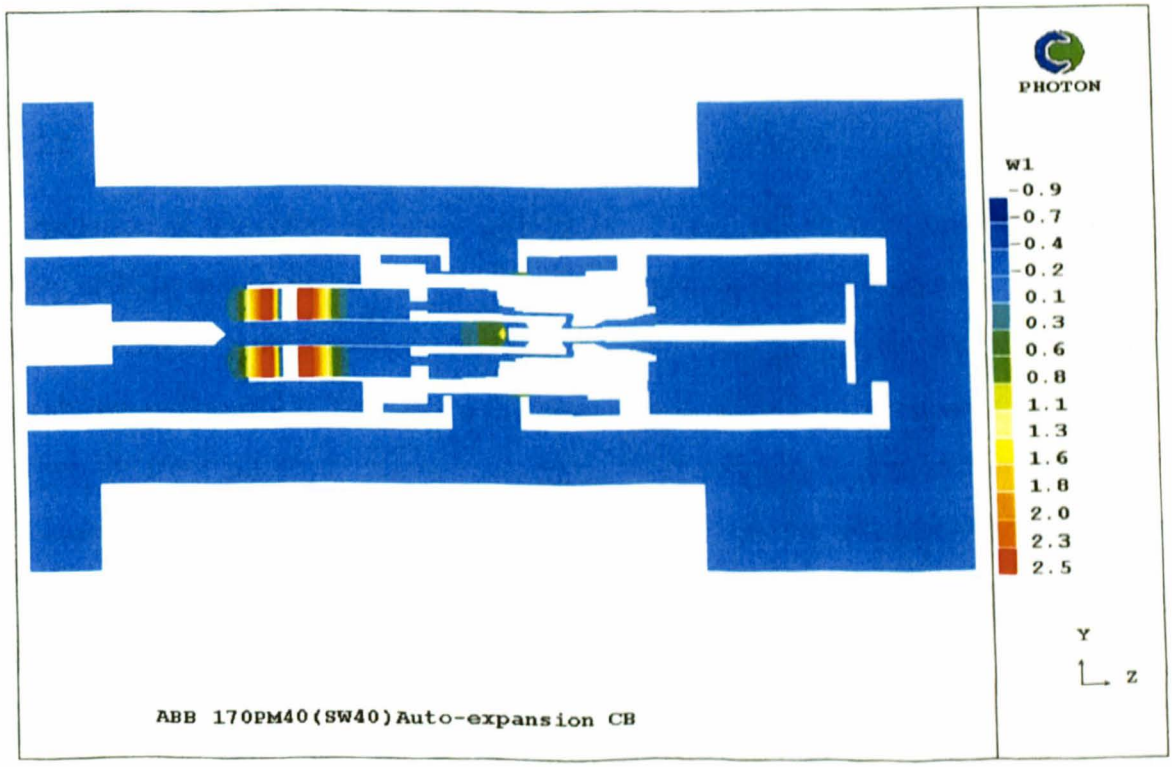

Figure 4.4: Diagram showing velocity distribution shortly after piston movement (0.2ms) with a speed of 2.5ms^{-1}.

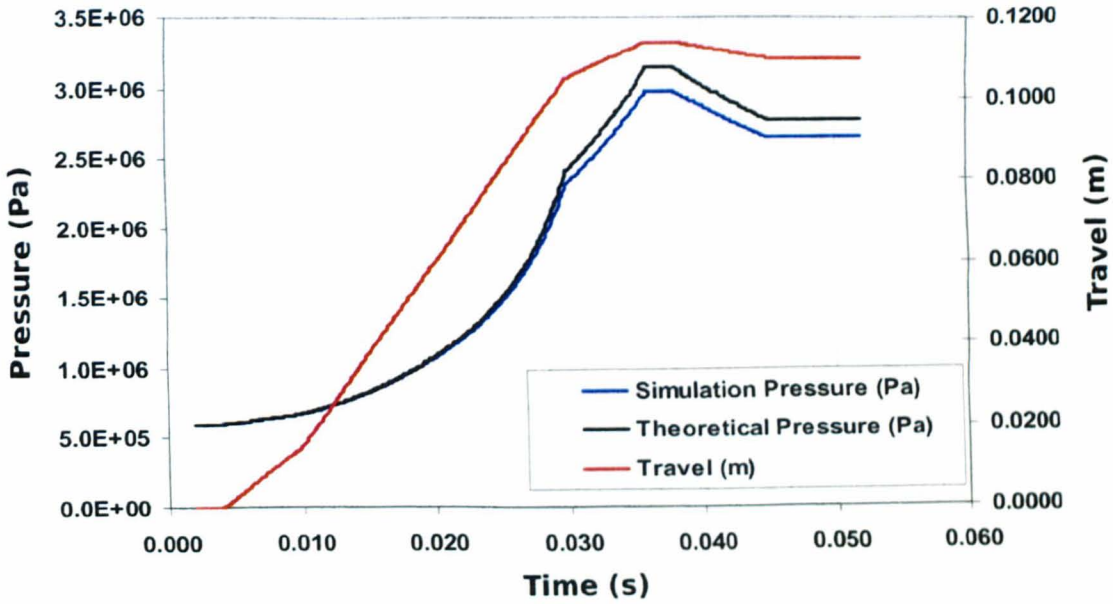

Figure 4.5: Pressure variation in a cylinder with all valves closed (no gas outlet from the cylinder).

movement. Further refining the cell size leads to better prediction but the associated computing cost has increased. The implementation of contact (*e.g.* solid electrode) movement can be understood in a similar way.

4.2.2 Method and implementation of valve operation

Simulation of the valve operation, especially a valve moving with a piston, is not an easy task. In reality, the operation of over-pressure or under-pressure valves involves the movement of solid surface away or towards an annular opening located in a wall, as shown in Figure 4.6. The opening of the valve is a continuous process, which means when the force resulting from the pressure difference on both sides of the valve plate is larger than the pre-force (see figure 4.7), the gap between the plate and the annular hole gradually increase leading to gas exhaust from the compressor. This is shown in Figure 4.7.

There are altogether three valves in this circuit breaker. Valve 3 which is called over-pressure valve has a critical effect towards pressure in the heating chamber. To accurately model the valve opening process, the inertia of the valve components, the pre-force and the detailed pressure distribution surrounding the plate need to be con-

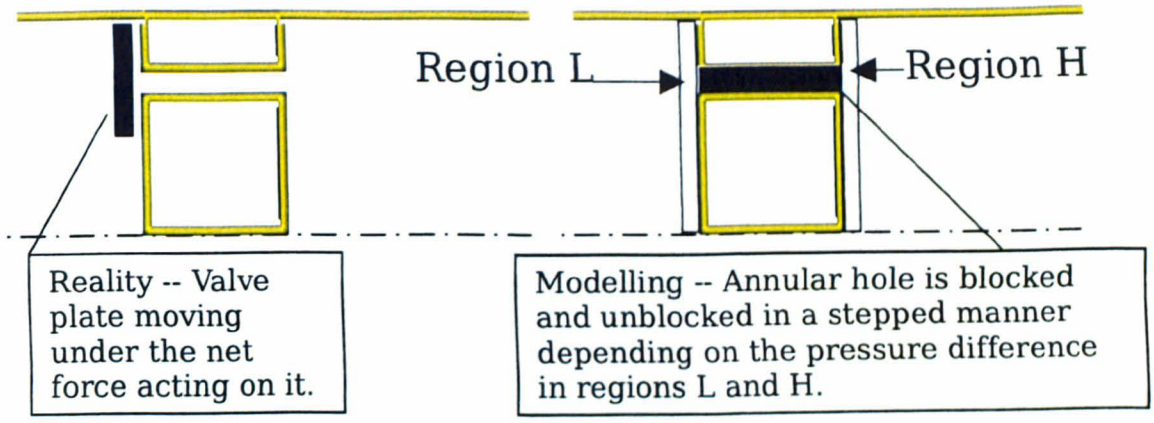

Figure 4.6: Diagram showing a real valve and the numerical simulation of its operation.

Table 4.1: Relationship between acting force and percentage of opened cross section of the valve hole.

Force (N)	Valve Condition
$0 \sim 50$	valve fully closed
$50 \sim 160$	opening one-fifth of full width (considering possible leakage area)
$160 \sim 200$	opening two-fifth of full width.
$200 \sim 240$	opening four-fifth of full width.
more than 240	fully opened.

sidered. This requires the use of extremely fine grids and time step to catch the transient pressure field around the plate. In the present model, we use the method of filling and evacuating of the annular holes based on the pressure difference in regions L and H and the area of the valve plate (figure 4.6). To simulate the changing gap between the wall and the valve plate, the hole in the present simulation can be blocked at different percentage of its maximum cross area. This percentage is correlated to the ratio of the net force to the pre-force with a simple linear relationship as described in Table 4.1:

Mass, momentum and energy need to be conserved in the opening process. When filling a part of the hole, mass is drawn from regions L and H (figure 4.6). This automatically transports momentum and energy into the hole. When unblocking part of the hole, mass, momentum and energy is dumped into regions L and H causing a small increase of pressure in the two regions.

The consequence of this technique is that the flow field immediately at the back

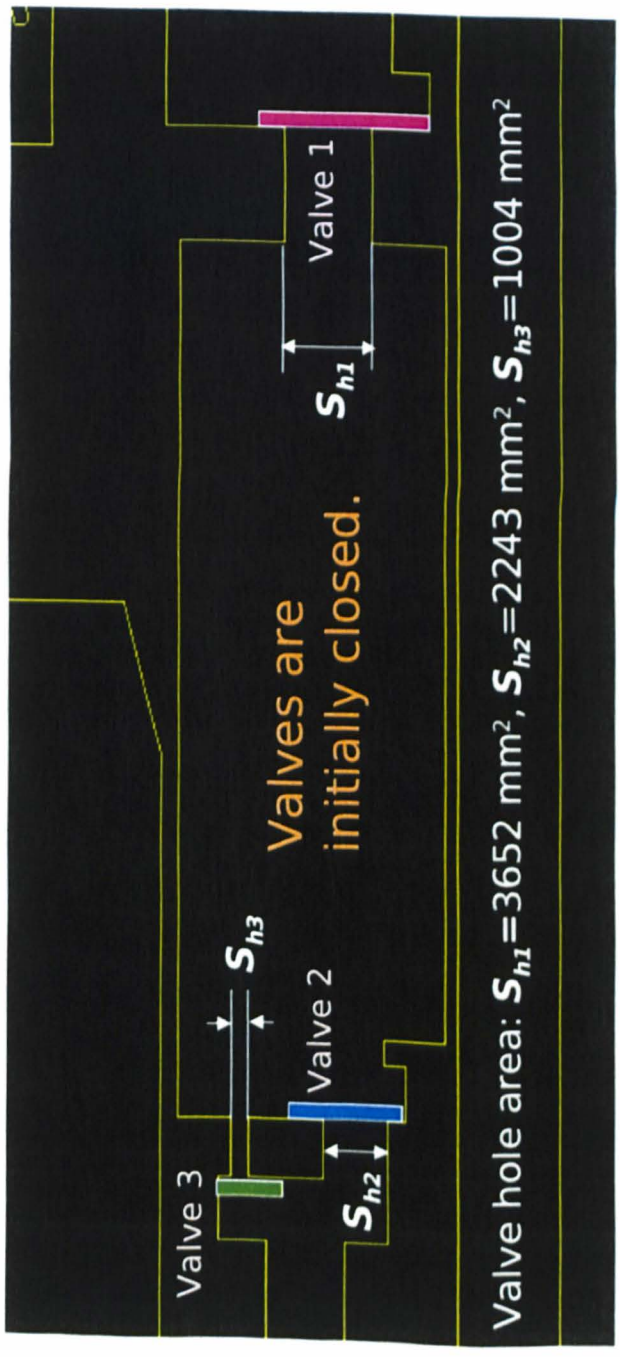

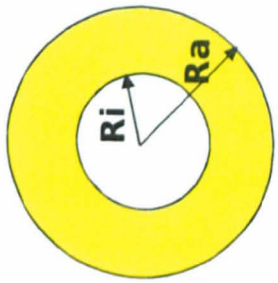

Valve Parameter	Valve 1	Valve 2	Valve 3
Ri (mm)	21.75	25.75	45.75
Ra (mm)	47.75	42.49	56.75
Thickness (mm)	2	2	2
Mass (kg)	0.02	0.02	0.02
Spring constant (N/m)	0	0	46500
Pre-force (N)	0	0	120

Figure 4.7: Diagram showing the location of the valves and their dimensions and mechanical parameters.

of the valve plate no longer reflects the real situation since there is no valve plate in the present simulation. However this region does not critically affects the circuit performance therefore the difference will not be discussed further. The flow and pressure field inside the compressor (cylinder) will however not be substantially affected (in the region containing region H). Thus this model is adequate for the present simulation.

Valve 1, which is the valve between the compressor and the expansion volume has also been simulated. The method used for this valve is similar to that for Valve 3. The pre-force for this valve is small and in the simulation is set to zero.

The other valve, which is attached to the bottom of the piston, seldom operates according to ABB and is thus not simulated in the work.

4.3 Typical Results and Comparison with Measurement

Results are shown in figure 4.8 for both heating chamber and compressor together with measurement. The prediction agrees with measurement within 5% of the latter. Since the method of contact movement is verified in figure 4.5, the small difference is possibly caused by approximations in the geometry and also by the simplification introduced for modelling the valve operation. It is noted that the pressure minimum inside the cylinder after its peak can be predicted but the time when the minimum occurs critically depends on the peak pressure.

Figure 4.9 gives the pressure and velocity field at 5.6ms. The pressure inside the volume is about 6.1 bar. The over-pressure valve is closed at this stage. It can be seen that gas is drawn from the area around the cylinder into the space that piston evacuates. Pressure inside the cylinder is higher than that in the heating chamber.

At 13.6ms, the solid contact has moved into the narrow section of the hollow contact (figure 4.10). Since the auxiliary nozzle is still blocked by the solid contact, the pressure in the heating chamber and cylinder continues to rise to about 6.8 bar. Compared with the situation at 5.6ms (figure 4.9), the pressure is much more uniform inside the chambers. Further compression of the cylinder by piston movement pushes the pressure to over 7.5 bar (figure 4.11) and because of the pressure difference between both sides of the valve, the overpressure valve is now opened. The pressure in the valve hole decreases rapidly from 7.7 bar to 5.9 bar. At this time the moving con-

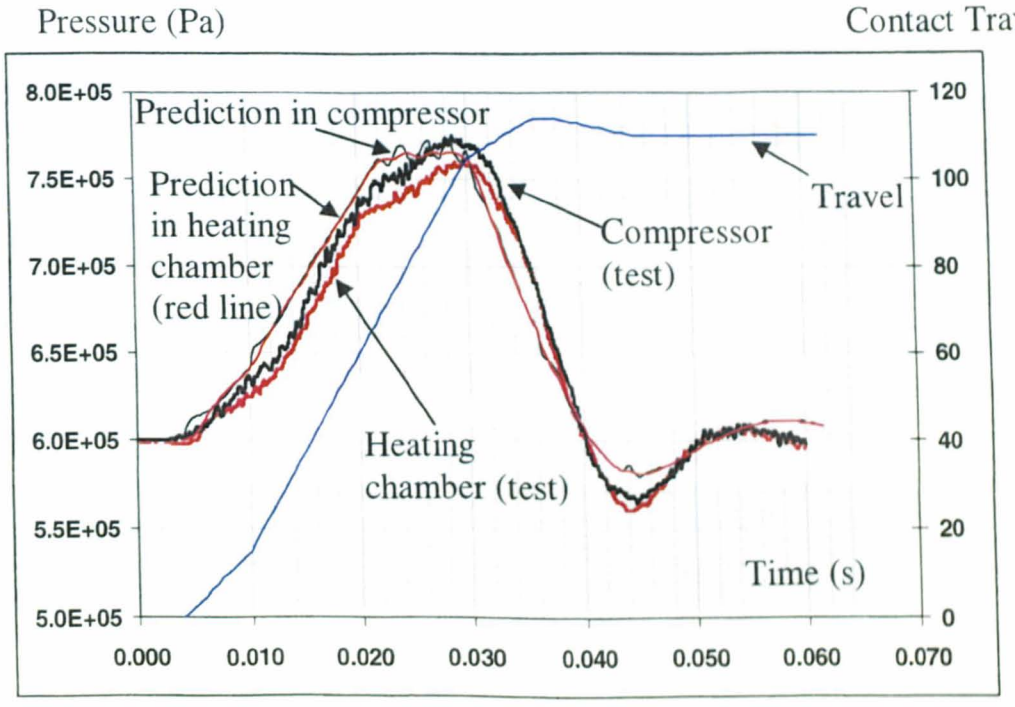

Figure 4.8: Comparison of predicted and measured pressure variation in the compressor and heating chamber of the $170PM40$ breaker for a no-load case.

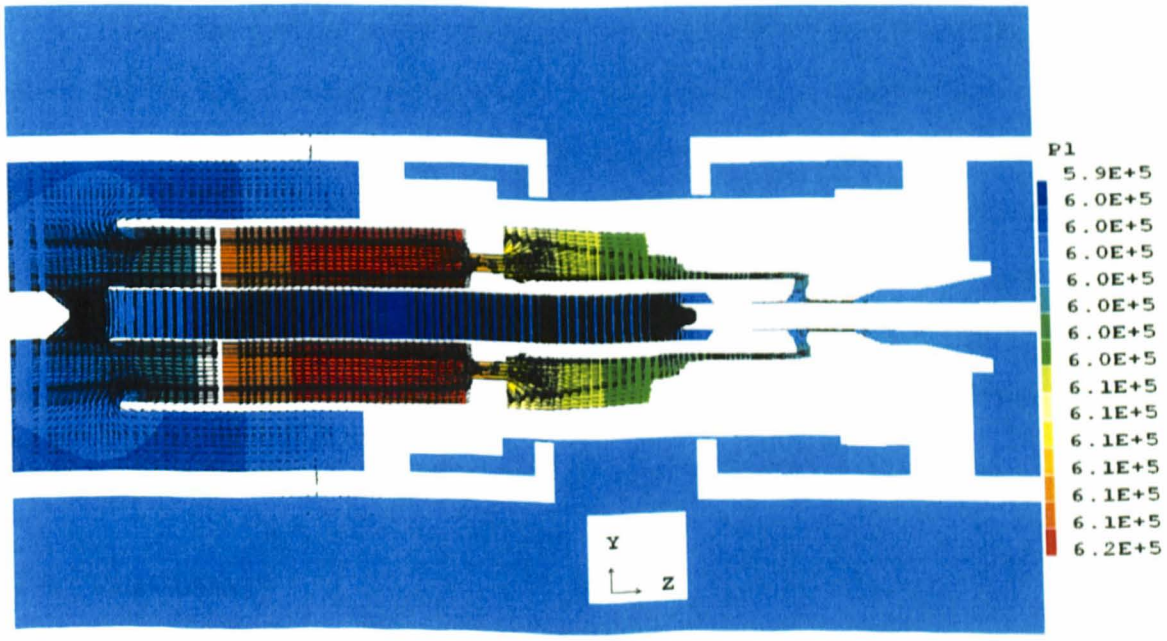

Figure 4.9: Pressure and velocity field at 5.6ms. Filling pressure of SF_6 is 6 bar. The velocity vectors are only an indication of the direction of gas flow.

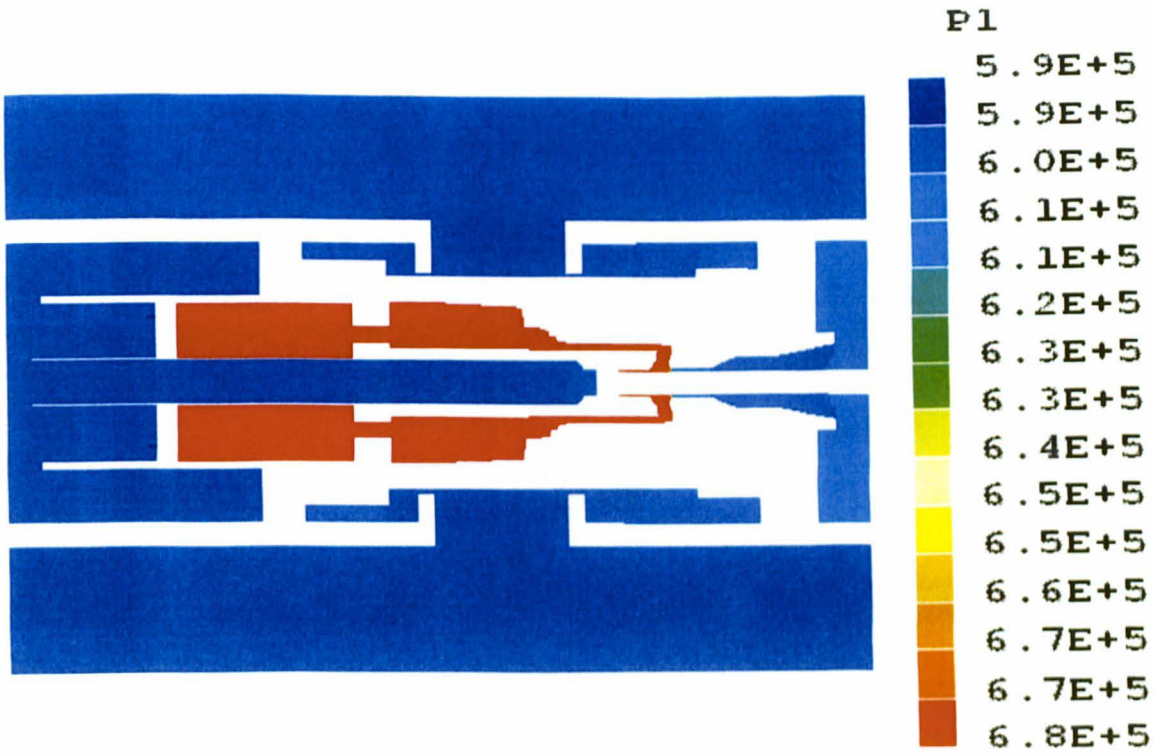

Figure 4.10: Diagram showing the pressure in the heating chamber and cylinder at 13.6ms

tact has cleared the auxiliary nozzle and velocity field is established inside the hollow contact (figure 4.12).

At 33.6ms, the moving contact has cleared the main PTFE nozzle and the pressure inside the heating chamber decreases to 7 bar. It can be seen from figure 4.13 that velocity in the main nozzle reaches $75ms^{-1}$ and $85ms^{-1}$ in the hollow contact. A stagnation point is developed in the space between the auxiliary and main nozzles with a pressure similar to that in the cylinder. In view of the agreement between the predicted pressure and measurement by ABB, it can be concluded that the present model can be used to simulate the cold flow situation in high voltage circuit breakers with good accuracy.

4.4 Summary

This chapter first discusses the implementation of the moving parts especially the operation of the valves. Comparison with analytical results has shown that the numerical scheme is sufficiently accurate for such applications. The predicted pressure rise

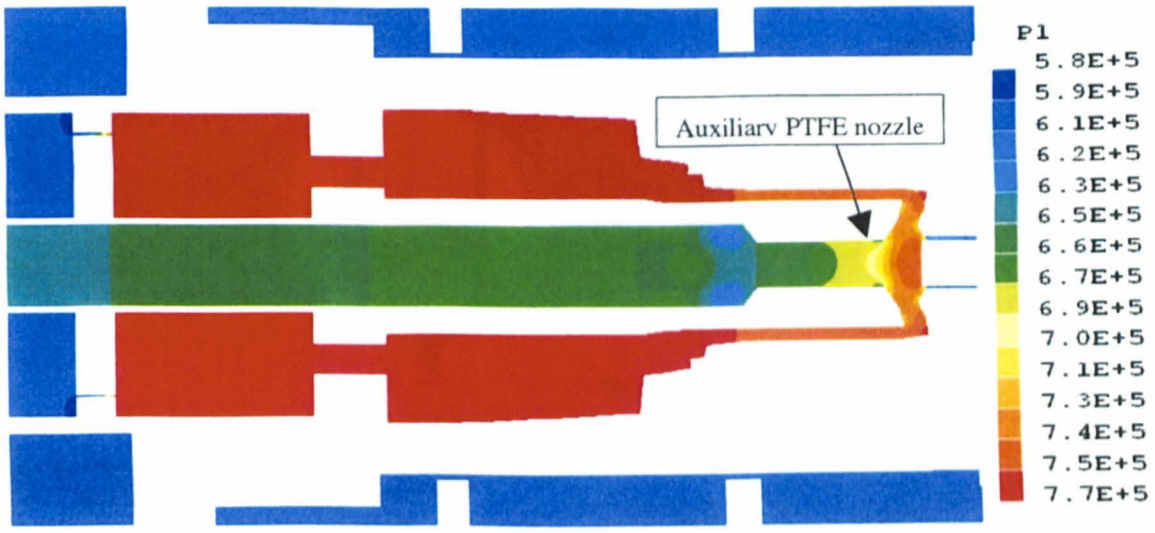

Figure 4.11: Diagram showing the pressure variation in the arcing region and its surrounding at 23.6ms.

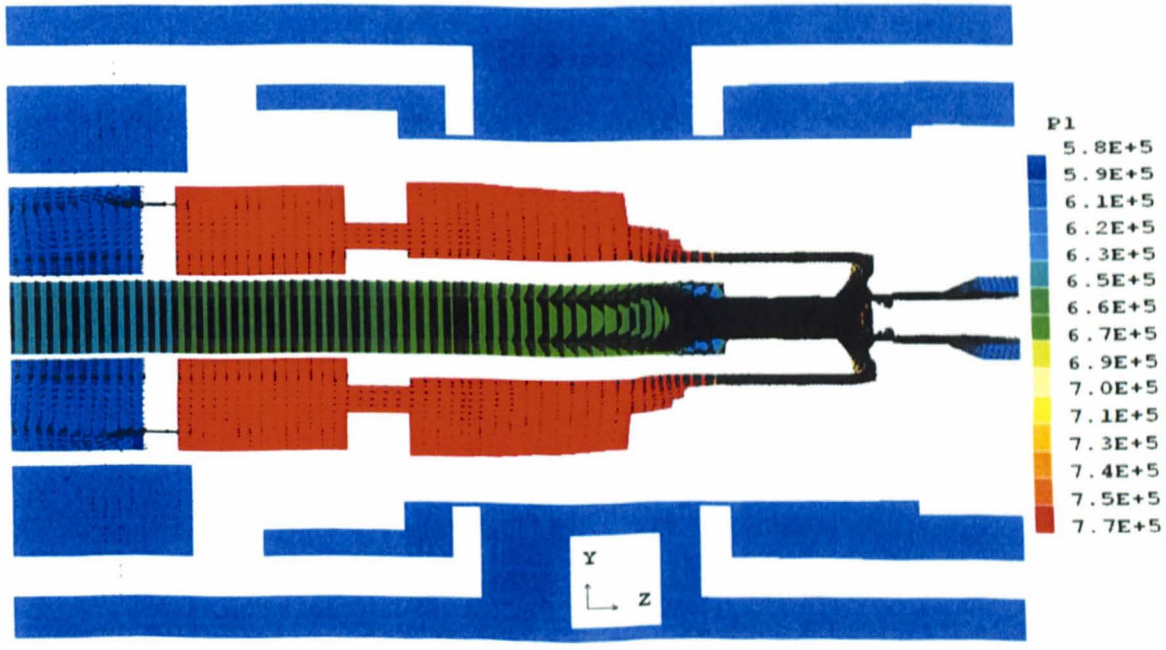

Figure 4.12: Diagram showing the velocity vector at 23.6ms. The velocity vectors are only an indication of the direction of gas flow.

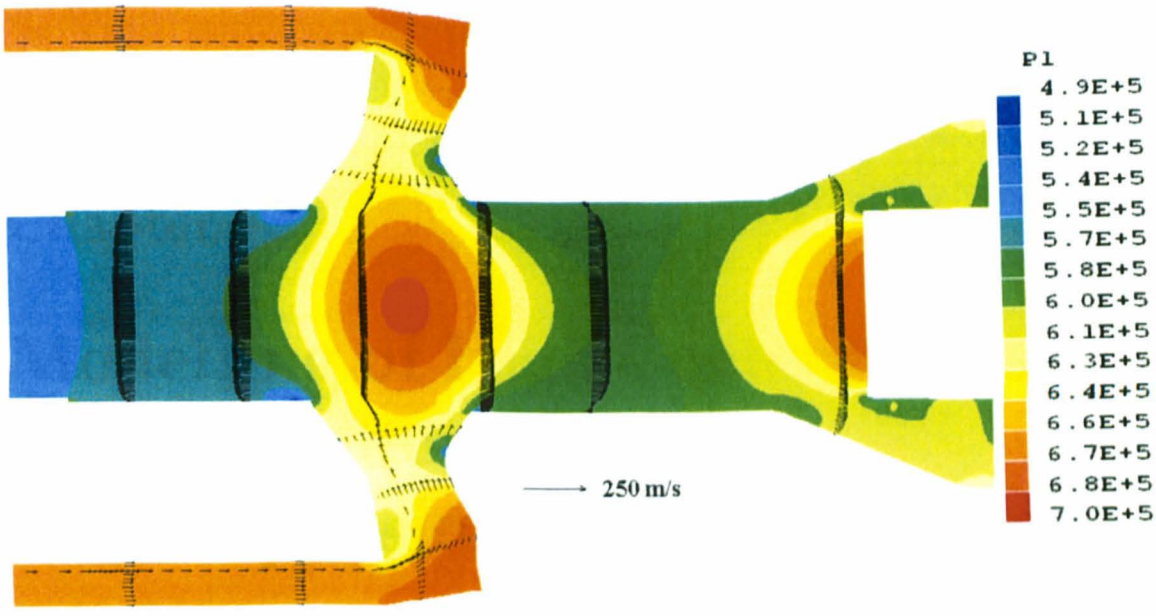

Figure 4.13: Pressure and velocity at 33.6ms. Gas speed in the main PTFE nozzle is 76ms^{-1} and that in the hollow contact is 85ms^{-1} on the axis.

in the heating chamber for the no-load case agrees reasonably well with test results despite the approximations that have been made on the geometry and the valve operation. Detailed pressure and flow field at several important instants have also been presented. In the next chapter, arc simulation starts from the instant when the contacts separate. The arc will be started in the flow field that is obtained from the cold flow case but with a contact travel which is measured for the high current case.

Chapter 5

Modelling of High Current Phase (Pressurisation Phase) in Auto-expansion Circuit Breakers

Research is creating new knowledge.
– Neil Armstrong

5.1 Introduction

There has been considerable success in simulating the high current arcing phase of a number of models and real circuit breakers [121, 96, 3, 97, 122, 123, 124, 125, 126, 4, 5, 6]. The performance of a model is normally judged by the agreement between prediction and measurement for arc voltage and pressure at important locations, and total amount of nozzle ablation. The gas mixture temperature in the heating chamber and heating channel (or flow passage, an annular, long, thin channel connecting the arcing space and the heating chamber) is an extremely important parameter but unfortunately due to the measurement difficulties there have been no experimental results. Following the work in chapter 4, this chapter is concerned with the establishment of an arc model that can be used for different auto-expansion circuit breakers and different short circuit conditions.

In this chapter and the following chapter, the terms 'heating chamber' and 'expansion volume' are interchangeable. They both refer to the space where pressurised gas is stored.

Auto-expansion circuit breakers rely on pressurisation of the heating chamber by nozzle ablation to create the environment for thermal and subsequent dielectric in-

terruption. The accuracy of the model depends strongly on how the physical mechanisms are represented. When the arcing current waveform is known, the predicted arc voltage directly determines the total electrical power that is dissipated in the contact gap. This is the primary parameter for comparison. Pressure variation in the expansion volume is largely dependent on the amount of (PTFE) vapour generated by nozzle ablation, on the pumping efficiency of the breaker arrangement (percentage of vapour entering the expansion volume), and on the temperature of the incoming vapour at the entrance of the expansion volume. The latter two factors are closely related to the electric power dissipation which dominates not only the shape/size of the arc column but also the radiation reaching the nozzle wall causing PTFE ablation. The pressure variation in the expansion volume can also be affected by the propagation of pressure waves, however the extent of this influence is generally small in comparison with the overall pressure variation during the high current phase.

There are limiting factors in the performance of the arc model for the high current arcing phase. Calculation of radiation transfer in the arc and its surrounding region is the most dominant one since it is a mechanism rapidly re-distributing energy and supplying ablating radiation to the nozzle. Arc rooting is another one that can affect the calculation of Lorentz force near the arc root. As a result it is not possible to correctly calculate the Lorentz force in the hollow contact where uncertainties exist in the location of the arc root and also the size of the root. Using a transparent contact, we place the arc root on the tip of the transparent contact. The uncertainty caused by the arc rooting problem is however expected to be small since at high current the arc size is comparable to the inner size of the hollow contact and more importantly, for most of the time in the high current phase the flow in the hollow contact is controlled by the axial pressure gradient resulting from nozzle ablation.

In this chapter the performance of two existing models, namely Liverpool's arc model and ABB 'two-zone' model, has been studied for the ABB short line fault (SLF) case. This case has an arcing duration of approximately 13ms and a peak current of 53kA. Details of the current waveform are given when results are presented later on. The predicted arc voltage and the pressure variation in the expansion volume are compared with the measurements and arc behaviour at typical instants in the arcing history studied. The treatment of some physical processes in the two models is exam-

ined. Suggestions are then made in order to improve our Liverpool model. Following this comparison, some of the model parameters are optimized and the model is then used to predict the pressure rise in the heating chamber and also the arc voltage for another two arcing cases with a different circuit breaker. An important objective of this chapter is to ascertain the validation of the arc model for the high current phase thus gaining confidence in the following chapter when we discuss the important pressure fluctuation phenomena.

5.2 Overall Description of the Liverpool Arc Model

Liverpool's arc model solves the mass, momentum and energy conservation equations as well as the electric current continuity equation in the full differential form and in a self-consistent manner. Details have been given in chapter 2.

Liverpool's arc model differs from ABB's two-zone model [96] mainly in the following two aspects: Firstly, the temperature in the arc is allowed to adjust itself according to the energy input/removal mechanisms (convection, radiation, Ohmic heating and turbulent cooling) through the coupled governing equations. While in ABB's model the arc temperature is pre-described according to a simple formula. Secondly, the energy sources (Ohmic heating and radiation, including radiation absorption) are calculated according to the temperature and pressure fields from the solution of the computation and there is no restriction applied to their locations). It is in this sense that Liverpool's model is expected to produce more realistic results in the arc region.

5.3 Considerations on Selection of Key Model Parameter

As explained in chapter 2, the radiation re-absorption at the arc edge is an important model parameter that directly determines the amount of nozzle ablation. Because of the lack of an accurate method to calculate the radiation transfer inside and around the arc column, an approximate model has to be used. In order for our arc model to be applicable to different circuit geometries, this parameter needs to be determined first.

In the *ABB* two-zone model, a value of $17\text{mg} \cdot \text{kJ}^{-1}$, which corresponds to $59\text{MJ} \cdot \text{kg}^{-1}$, is used to determine the amount of PTFE ablation. This value of $59\text{MJ} \cdot \text{kg}^{-1}$ directly

relates the PTFE ablation to the total electric energy input in the two-zone model while in the Liverpool's model the ablation of PTFE relates to the radiation flux reaching the nozzle wall [90]. As shown later in the energy balance for Liverpool's model (we further assume 10% of the radiation reaching the nozzle wall is permanently lost), only about 25% of the total electric power input is used to ablate the PTFE. This gives a value of $48\text{MJ} \cdot \text{kg}^{-1}$ for the calculation of PTFE ablation in terms of per total electric energy input. This smaller value gives a slightly larger amount of PTFE ablation of 4.3g from the Liverpool model while the ABB model predicts a PTFE ablation of 3.2g.

ABB's two-zone model also uses a vapour temperature of 5,000K while Liverpool's model uses a vapour temperature which is slightly higher than 3,000K, however, both models produce similar pressure rise in the heating chamber under identical test conditions. Thus an explanation is necessary. It should be noted that the radiation re-absorption zone in Liverpool's model is determined by the radial temperature profile which extends from the arc core edge into the colder vapour layer. Radiation re-absorption helps heat up the vapour when it flows from the ablating surface towards the heating channel. The vapor can be heated to a temperature of 6,000K to 10,000K. In this sense it can be argued that the use of a higher vapor temperature in ABB's model implicitly accounts for the role of radiation re-absorption. This has an important implication that the overall mass and energy balance in the two models matches each other although they take different approaches in considering the physical processes.

Optimisation has to be carried out impirically for two radiation model parameters: a multiplication factor to the net emission coefficient of Liebermann and Lowke [1], and the radiation re-absorption percentage (PCT) . PCT was first obtained by matching experimental results in a converging-diverging nozzle, giving a value of 80% [66]. In normal nozzle arcs, where the arc is blown in axially dominant flow, the radial temperature profile at the arc edge is largely determined by convective and turbulent cooling. The simplified radiation model gives acceptable results for this situation. However, in auto-expansion circuit breakers, there are a number of situations that can occur which make the flow/temperature field much more complex. Calibration of the absorption percentage is therefore necessary.

The parameters were calibrated using the ABB SLF90 and the 980947 cases and the

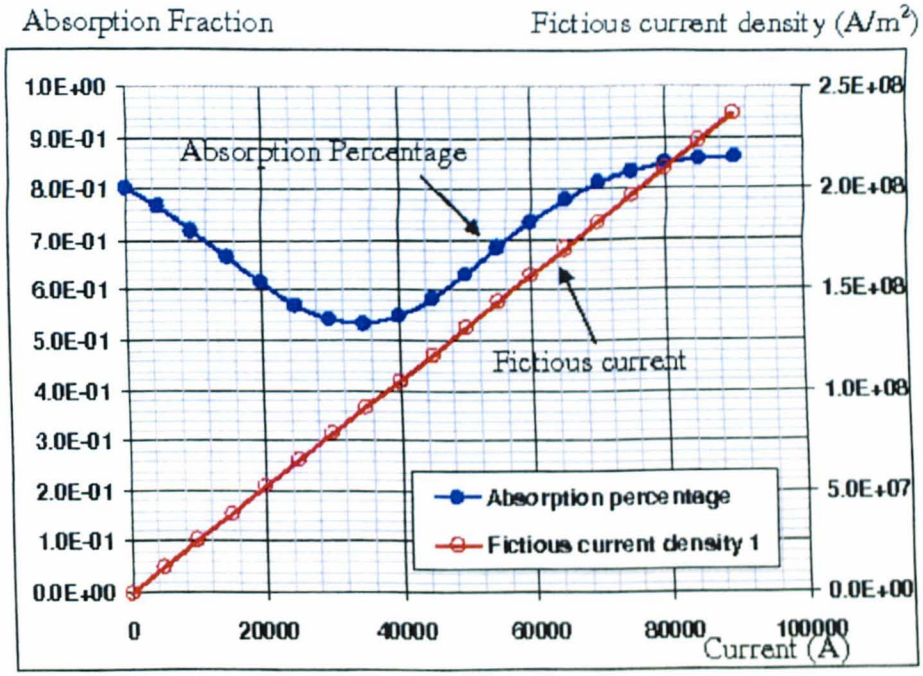

Figure 5.1: Radiation re-absorption percentage as a function of current for a nozzle radius of 11mm. Scheme was proposed by matching modelling results to measurement for the ABB $170PM40$ (one test case) and another auto-expansion circuit breaker $AGGR66$.

calibrated model was then used to predict the 980938 case. The radiation re-absorption percentage as a function of current for a nozzle of 22mm in diameter is given in figure 5.1. A value of 1.5 is used to mulplify the net emission coefficient of Liebermann and Lowke [1]. It is to be noted that since there is no test results available for comparison with a peak current lower than 30kA, the re-absorption curve may bear some uncertainty in the low current end. The test cases are shown in Table 5.1 with a peak current level (final loop) from 35kA to 77kA. Comparison is made on pressure rise in the heating chamber and arc voltage (see next section) for all three cases.

Although the curve in figure 5.1 is obtained by calibration against arc voltage and pressure measurement, it nevertheless has physics imbedded in. Recalling equation 5.1 in chapter 2:

$$\theta = \frac{1 - \alpha_N}{1 + \beta c(\frac{h_g}{h_v} - 1)} \tag{5.1}$$

where θ is the transparent factor which is related to the absorption percentage by PCT $= 1 - \theta$. For low current with strong axial flow, nozzle ablation is negligible thus

Table 5.1: Test cases used for calibrating the radiation model.

Circuit breaker and Test ID	Arcing Duration (ms)	Average contact speed (m/s)	Peak current in last loop (kA)	Maximum pressure rise in the heating chamber in final loop (bar)
ARRG66 : 980938	13.8	6.82	35	16.5
170*PM40* : *SLF90*	15	variable	53	40
ARRG66 : 980947	18.8	7.14	77	30

$c = 0$. However, turbulence energy transfer in the radial direction in SF_6 is strong and according to the model proposed in [66], $\alpha_N = 0.8$. This implies that about 80% of the radiation from the arc core is absorbed at the arc edge where strong turbulence or convection exists. The situation discussed here corresponds to the left part of the curve in figure 5.1 between 0 and 5kA.

When the arcing current is moderate, the diameter of the arc is marginally smaller than the nozzle diameter and there is a substantial part of the vapour coming off from the PTFE enters the arc column and the remaining part of the vapour flows out of the nozzle through the surrounding cold layer. The change of the arcing environment from SF_6 to PTFE-SF_6 mixture and also the relatively cold vapour entering the high temperature arc column leads to a change in the radial temperature profile and the absorption characteristics at the arc edge. The percentage of radiation that is absorbed at the arc edge reduces. This regime corresponds to the middle part of the curve in figure 5.1 up to 30kA.

However, when the arcing current is extremely high, say over 50kA in a 10mm radius nozzle, the arc column size is comparable to that of the nozzle and most of the vapour has to enter the arc column radially and be heated up by radiation re-absorption to a conducting temperature. With strong ablation, it is expected that the radiation re-absorption percentage at the arc edge attains a high value. This corresponds to the right hand part of the curve in figure 5.1 for current higher than 30kA.

We can thus argue that the re-absorption percentage depends on the current (which

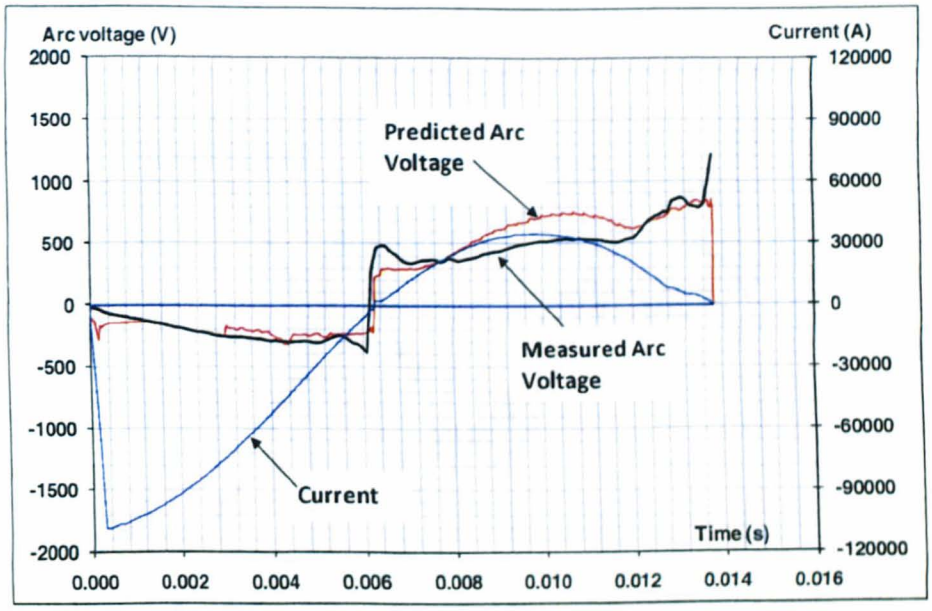

Figure 5.2: Comparison of predicted and measured arc voltage for $ARRG66$ test case 980938. Arc voltage is to be multiplied by a factor of -1.0.

largely determines the arc size and level of ablation), the flow situation and the nozzle diameter since the radial temperature profile is significantly affected by the different arcing situations.

5.4 Overall Behavior of the Arc Model at High Current Phase

Comparison is made on pressure rise in the heating chamber and arc voltage in figures 5.2, 5.3, 5.4, 5.5, 5.6 and 5.7 for all the three cases. It can be seen that the predicted arc voltage agrees very well with measurement in the first loop; the prediction is higher than measurement by a maximum of 15% for $170PM40$ and 25% for $ARRG66$. The predicted pressure rise at current zero in the heating chamber agrees with measurement within 10%.

There are however noticeable discrepancies between the measurement and prediction. For the $ARRG66$ 980938 case, the predicted arc voltage is higher than the measurement in the second half of the current loop (figure 5.2). This over-prediction also happens in the 980947 case as shown in figure 5.6. A high arc voltage generally means a thinner arc column. When this simulation was carried out, there are no data of electrical conductivity for pressures higher than 10 bar. We have used an

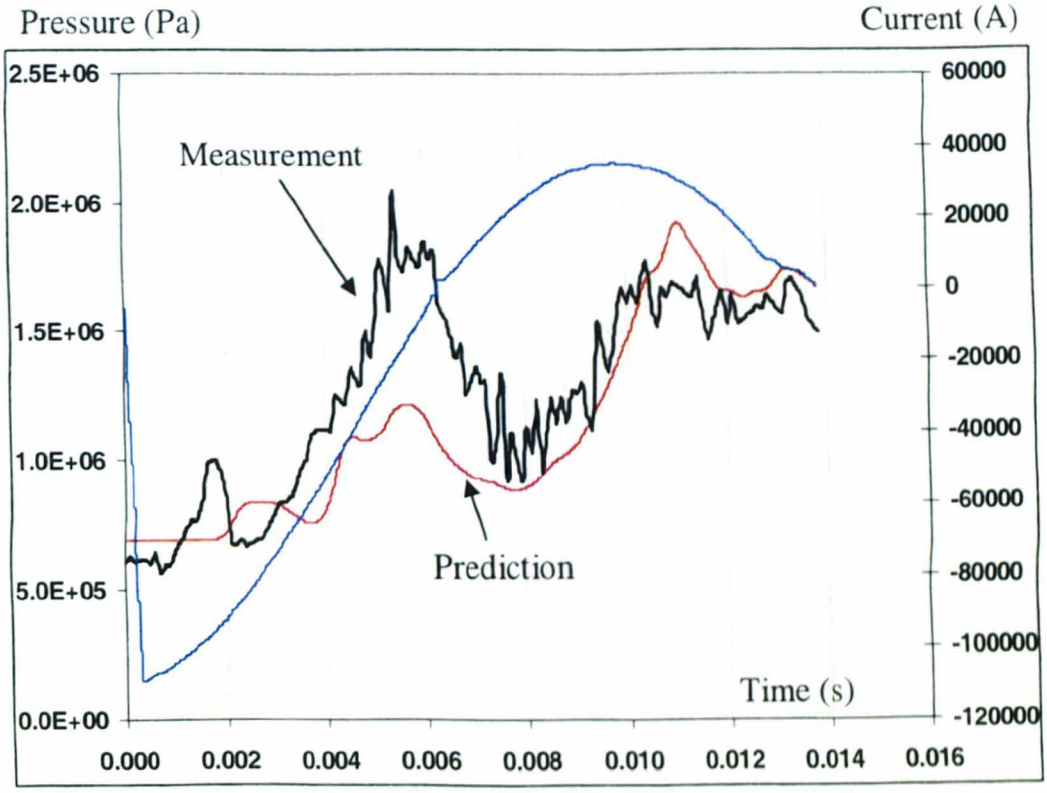

Figure 5.3: Comparison of predicted and measured pressure rise in the heating chamber for case 980938.

approximate formula to take account of the influence of pressure on electrical conductivity of PTFE arc plasma. The other possible reason could be the calculation of radiation re-absorption that also affects the size of the arc. This is especially true when the arc current changes rapidly in the period before and after the current peak. The arc size should adjust itself according to the strength of the ablation and radiation re-absorption at the arc edge. Uncertainties in the exact size of the re-absorption region and the absorption strength could in principle lead to a delayed adjustment of the arc size and therefore introduce deviation in the predicted arc voltage under certain flow conditions.

It is also interesting to note that the predicted arc voltage for the ABB case is closer to the measurement. Looking into the arcing conditions it is noticed that the peak current for the ABB case is 53kA in the main arcing period which is at the middle of the other two cases. It should be pointed out that the absorption percentage presented in figure 5.1 is very approximate and only roughly considered the physics involved in the change of arc temperature in the radial direction when the arc current changes.

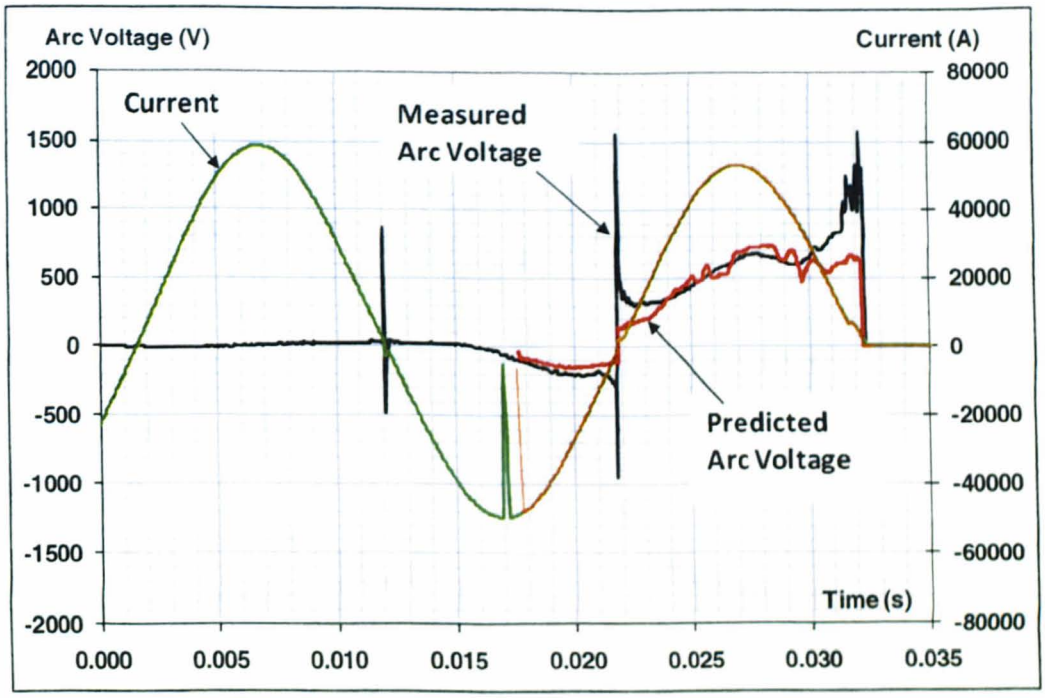

Figure 5.4: Comparison of predicted and measured arc voltage for case *SLF*90.

A more accurate model will require the re-absorption at the arc edge be calculated dynamically according to the pressure, temperature profile and also the PTFE concentration, which at present is not possible due to the lack of fundamental data.

There is also a narrow surge of predicted arc voltage in the 980947 case as indicated in figure 5.6 at 10ms. Detailed analysis reveals that this surge is linked to the rapid shrinkage of the arc size in the simulation as a result of rapid change flow field and Ohmic heating. The temperature field together with velocity vector at three instants, 9.3ms, 9.7ms and 11.3ms are plotted in figures 5.8 to 5.10. It can be seen that the voltage surge is a result of rapid arc column shrinkage. It takes about 2ms for this shrinkage to recover. Although the overall pressure rise in the heating chamber is not significantly affected due to its short duration, the course for its onset will need further investigation in future.

For comparative purposes, the pressure and arc voltage prediction by ABB arc model are shown in figure 5.11 and 5.12.

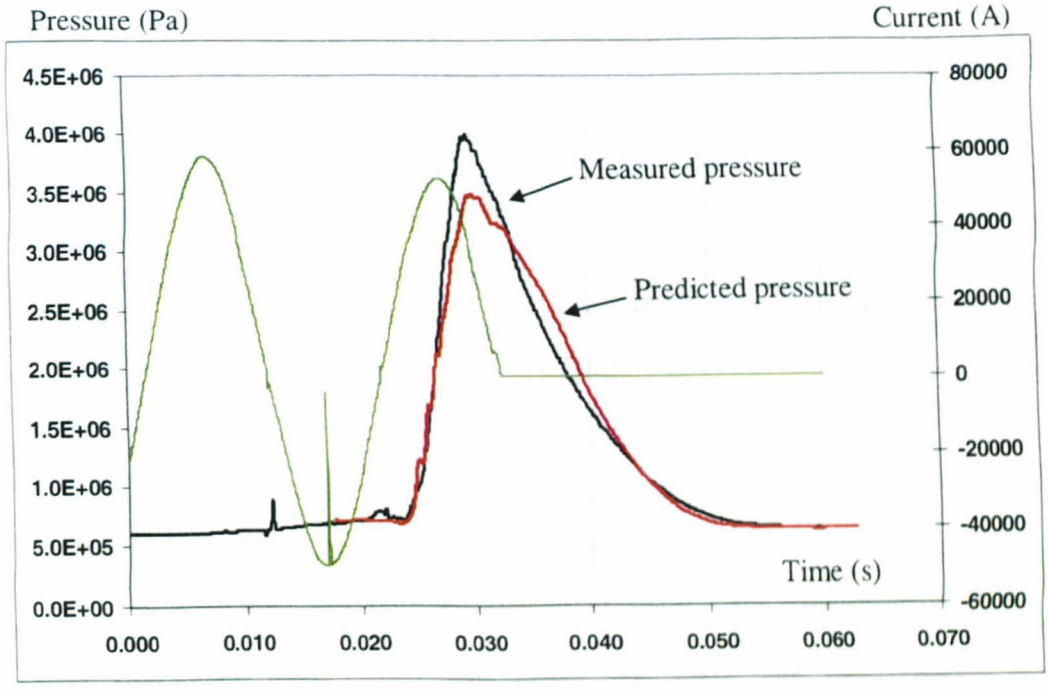

Figure 5.5: Comparison of predicted and measured pressure variation in the heating chamber for case *SLF*90.

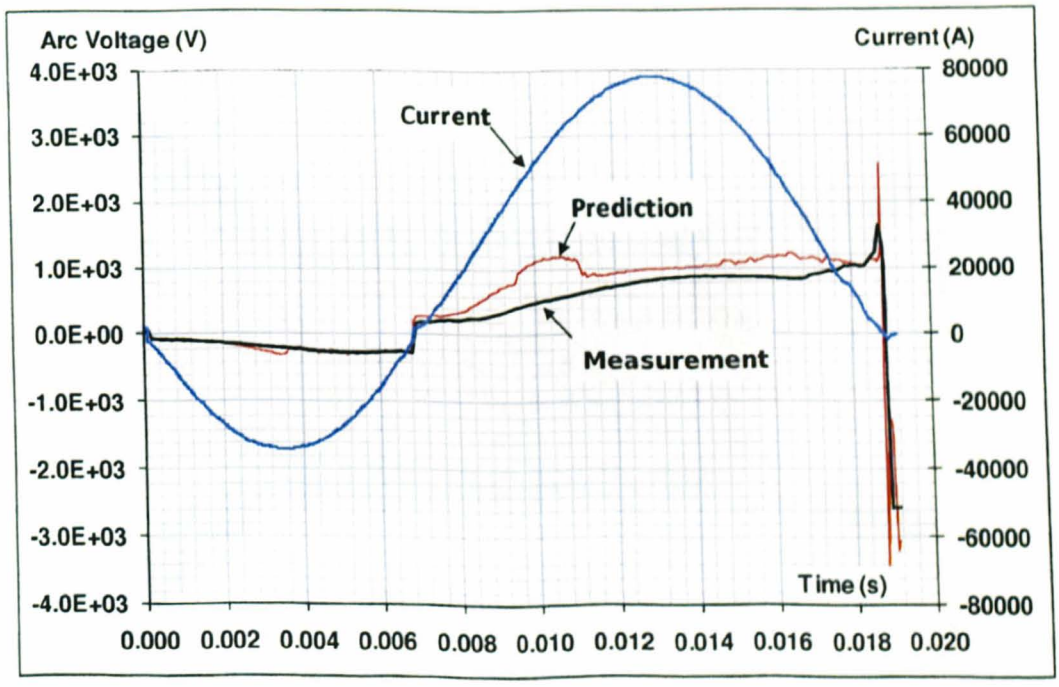

Figure 5.6: Comparison of predicted and measured arc voltage for ARRG66 test case 980947.

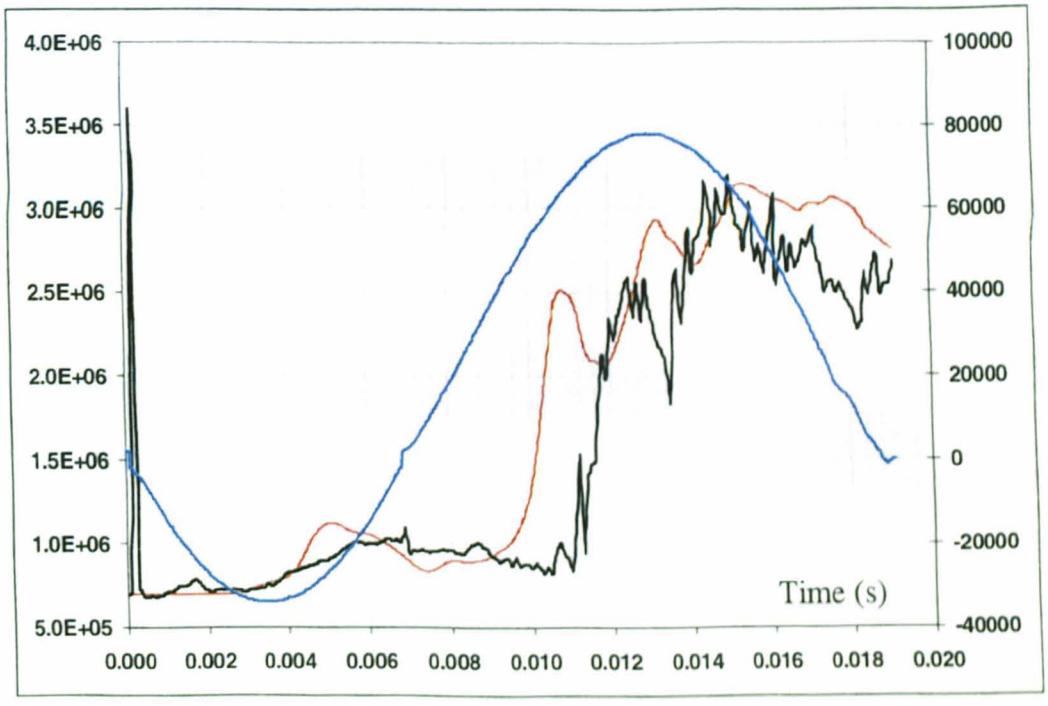

Figure 5.7: Comparison of predicted and measured pressure variation in the heating chamber for test case 980947.

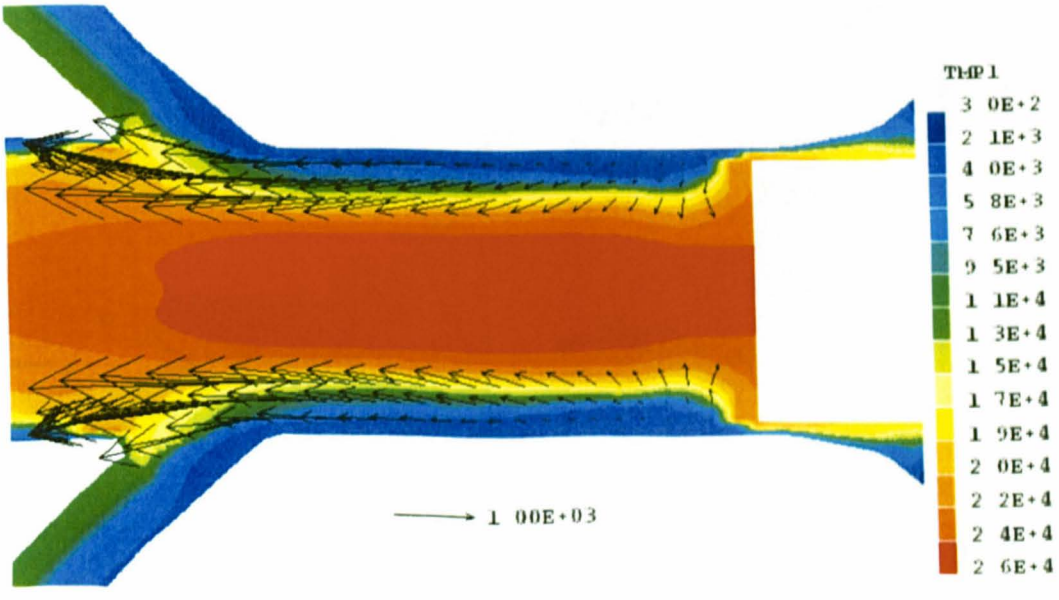

Figure 5.8: Temperature and velocity field at 9.3ms with a current of 40.6kA for case 980947.

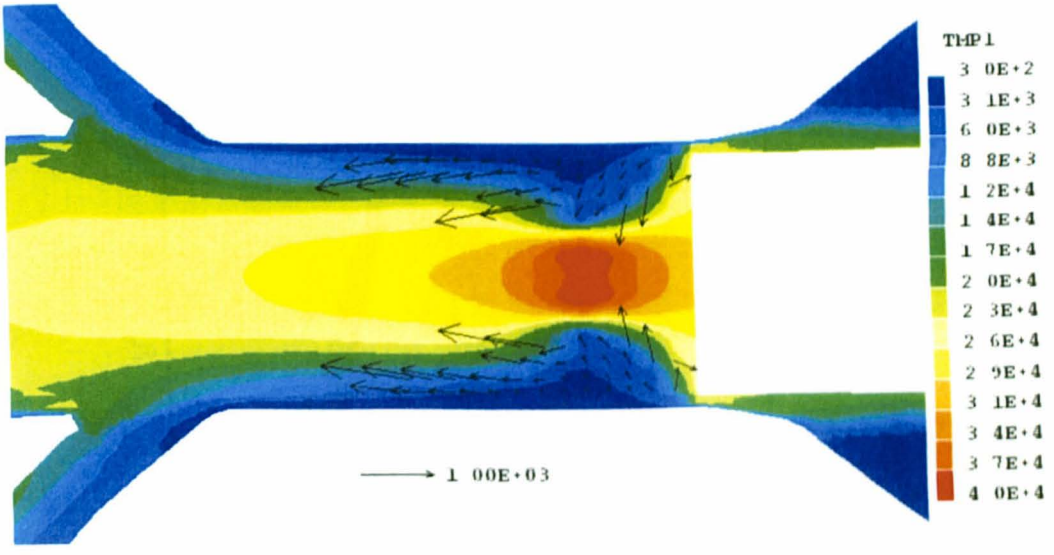

Figure 5.9: Temperature and velocity field at 9.7ms with a current of 47.2kA for case 980947.

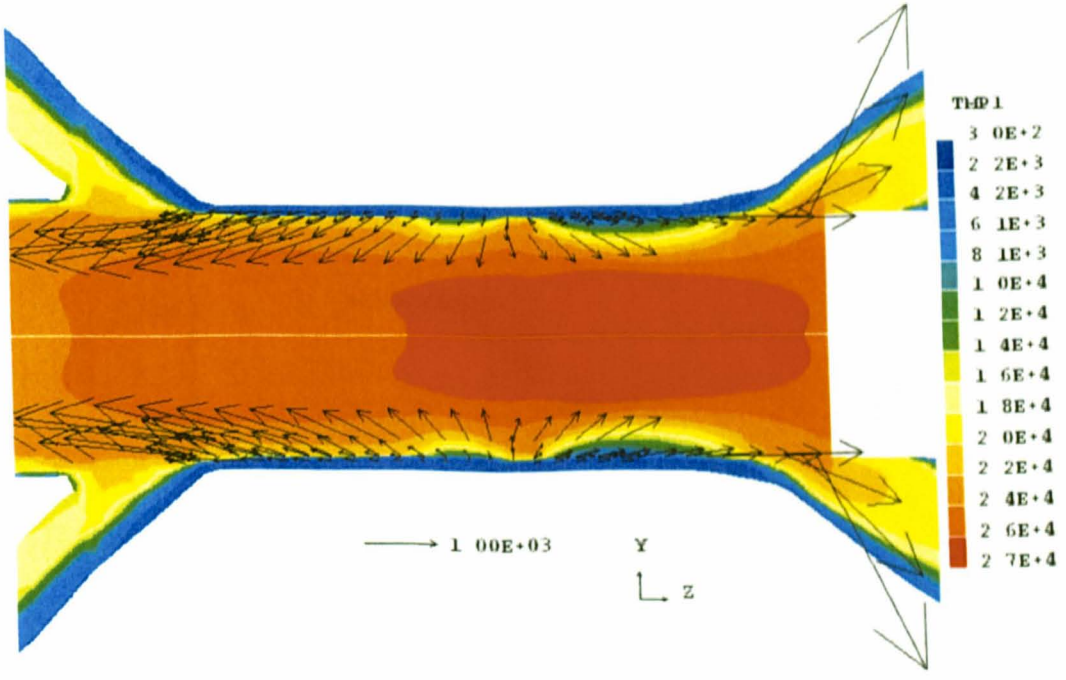

Figure 5.10: Temperature and velocity field at 11.3ms with a current of 58.9kA for case 980947.

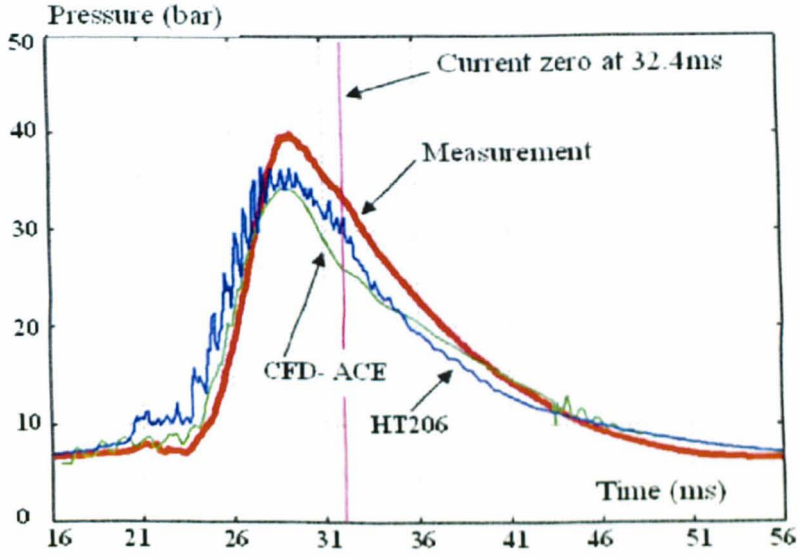

Figure 5.11: Pressure prediction by ABB arc model for case shown in figures 5.4 and 5.5.

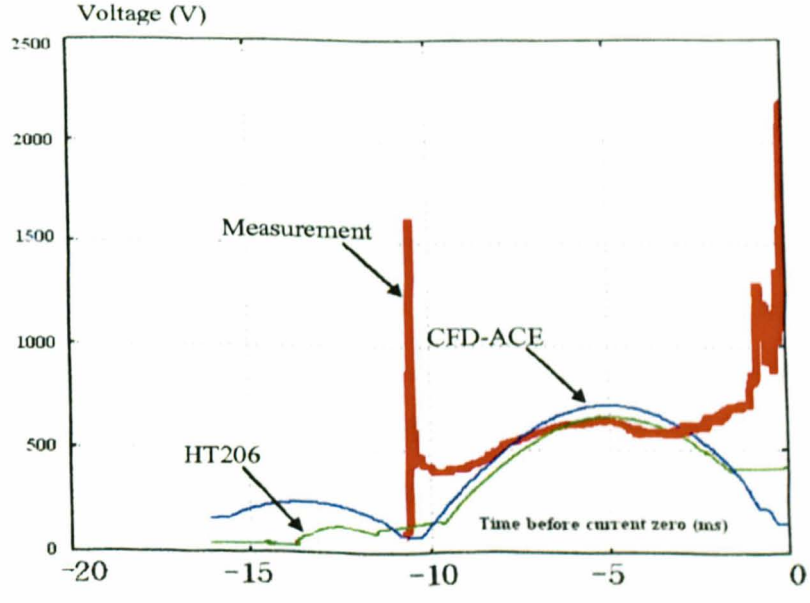

Figure 5.12: Arc voltage prediction by ABB arc model for case shown in figures 5.4 and 5.5.

5.5 Typical Results and Discussions

For the ABB short circuit fault case the predicted arc voltage agrees well with measurement for current higher than 25kA. The maximum difference is less than 100V, which corresponds to a difference of 15% from the measurement. However the prediction is much lower than measurement when the current approaches its final zero. There are three possible reasons for this discrepancy. Firstly, when the current is low, the arc column may deviate from the symmetrical axis and be deformed. This could change the effective arc length. Secondly, the turbulent parameter used in the high current phase may not be applicable to the current zero period which requires calibration using at least one measured rate of rise of the recovery voltage $RRRV$ value or measured arc resistance around the current zero period. Thirdly, since convection and turbulent cooling are the dominant mechanisms to remove energy from the arc column in axial flow, approximation to the geometry of the breaker, especially the replacement of the round solid contact tip with a flat tip in the simulation may affect the local flow field in the main nozzle and result in a broader arc column hence a lower arc voltage. These issues need to be considered in future work when the current zero period is studied. It needs to be mentioned that the pressure built-up in the heating chamber is insensitive to this discrepancy since the current is low and little PTFE vapour is ablated from the nozzle surface.

The predicted pressure peak in the heating chamber is 35 bar which is 87.5% of the measured peak pressure (figure 5.5). The solid contact clears the auxiliary nozzle at 21.37ms with a current of 7kA before the first current zero. The small gap between the solid contact and the auxiliary nozzle allows only a very small amount of gas to flow into the heating chamber during the arcing period before the first current zero. This is why the pressure rise in the heating chamber before the first current zero is negligible (figure 5.5). From 23ms the current increases rapidly and starts to cause strong ablation of the nozzle surface (location of ablation surface indicated in figure 5.13). As a result, PTFE vapour starts to be pumped into the heating channel (velocity vector in figure 5.14). The pressure wave takes about 1.0ms to reach the sensor point, as can be seen from the measurement and prediction (figure 5.5). The shortest flow distance from the ablating surface to the sensor point is 160mm. The speed of sound

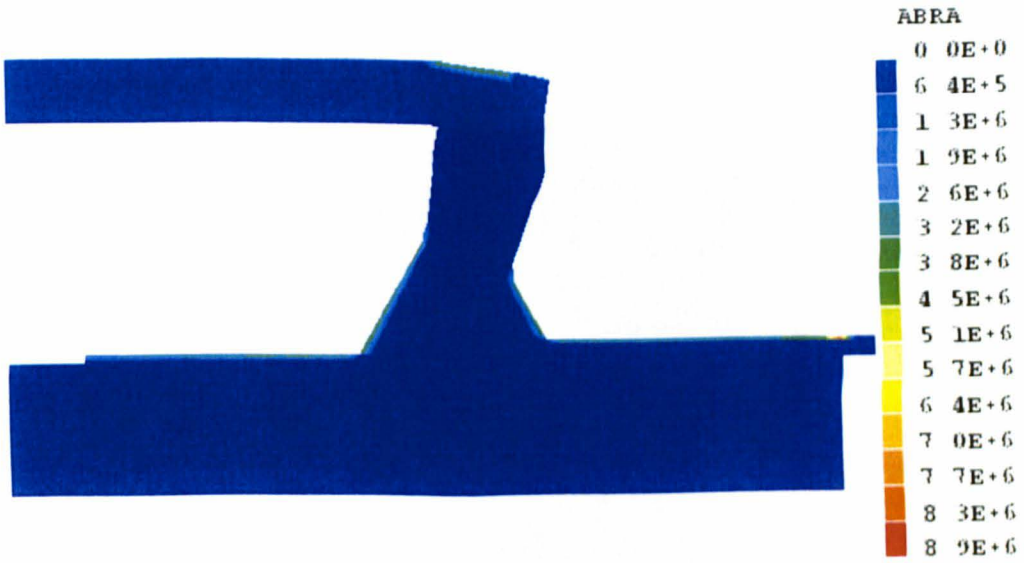

Figure 5.13: Locations of ablation patches (green/red patches) used in the simulation for the *ABB* circuit breaker.

in SF_6 at 7 bar and 300K is 135ms^{-1}. It thus takes 1.2ms for the pressure wave to propagate over such a distance. Theoretical estimation agrees reasonably well with both measurement and simulation.

The pressure reaches its peak in the heating chamber at 29.55ms, which is 2.5ms after the current peak. During the pressure rise period, traces of the pressure wave can be clearly seen in the prediction while they do not appear in the measurement. Measurement error is not available.

When the current starts to decrease rapidly towards the final current zero, the arc column starts to contract and cold gas from the auxiliary nozzle gradually builds up the necessary environment for thermal interruption. A series of arc temperature distribution is given in figures 5.15 to 5.18. More details on the establishment of the necessary flow and thermodynamic environment are discussed in chapter 6.

5.6 Mass and Energy Balance in Arcing Space and in Heating Chamber

A mass and energy balance calculation was carried out to gain a deeper understanding of the arcing process. The calculation was done for the second loop, which is responsible for the pressure build-up in the heating chamber. The domain for the balance

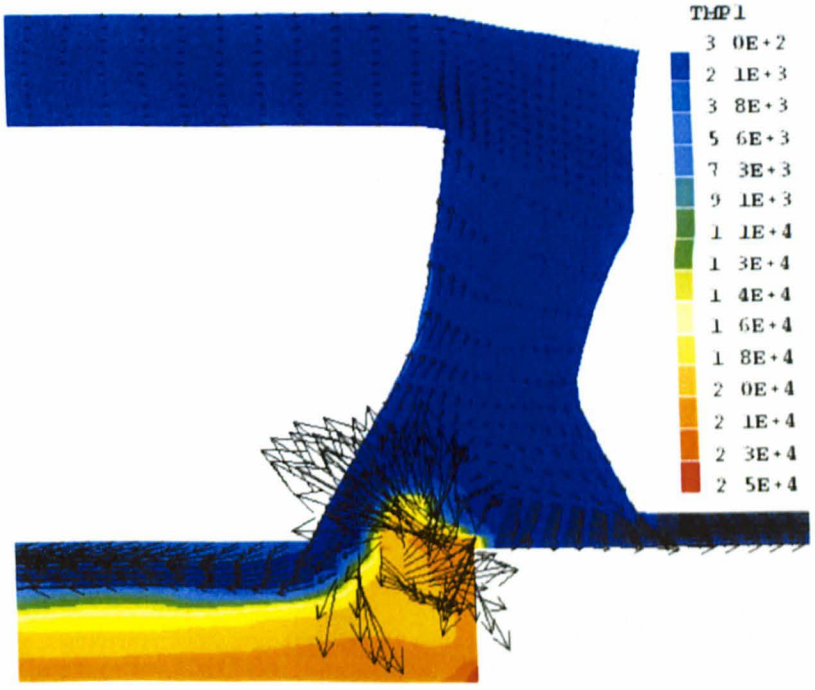

Figure 5.14: PTFE vapour starts to flow towards the heating channel when the current increases to 15.78kA at 23ms. This diagram is for ABB test case.

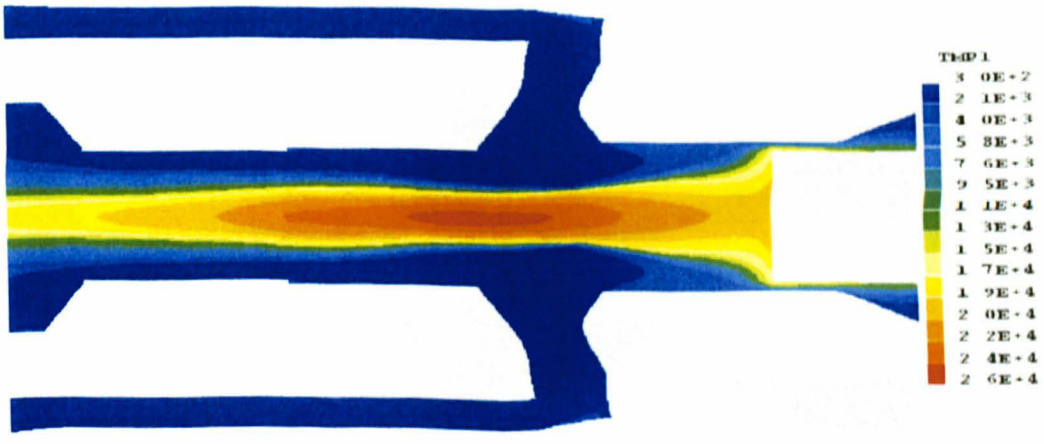

Figure 5.15: Temperature field at 31.4ms with a current of 10kA before final current zero.

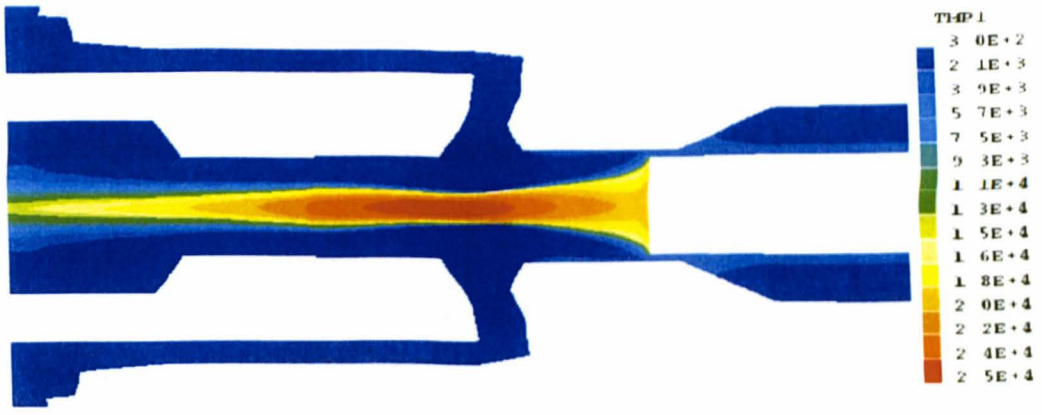

Figure 5.16: Temperature field at 31.8ms with a current of 6.8kA before final current zero.

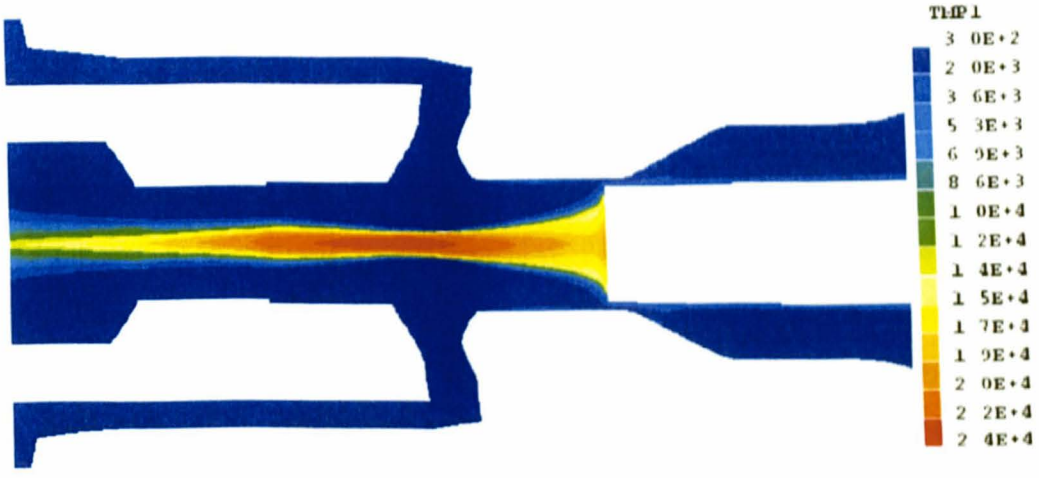

Figure 5.17: Temperature field at 32.19ms with a current of 2.79kA before final current zero.

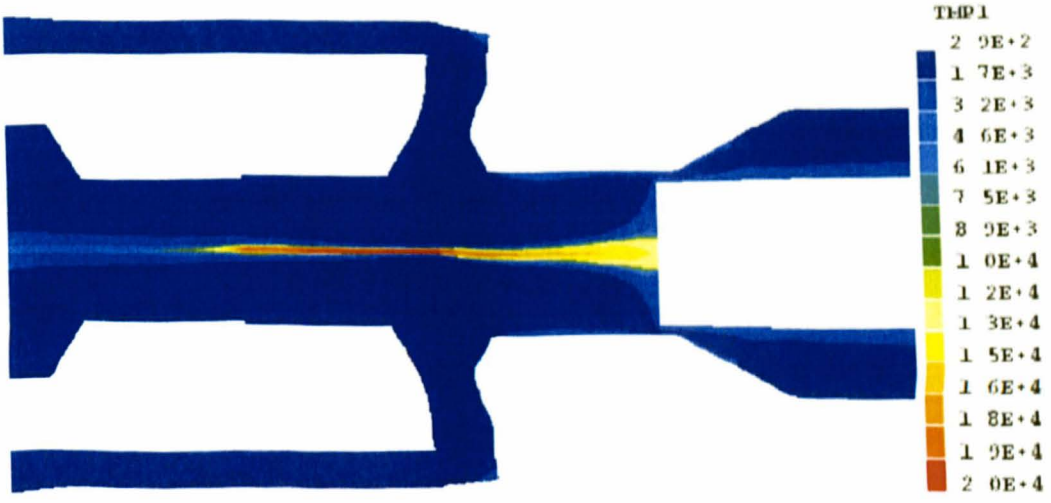

Figure 5.18: Temperature field at 32.39ms with a current of 308A before final current zero.

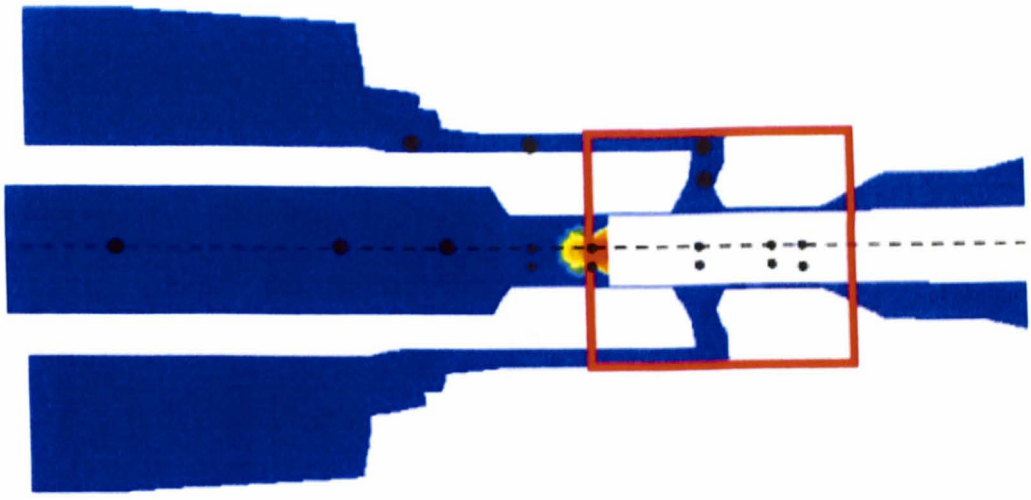

Figure 5.19: Domain of arcing region for energy and mass balance calculation.

calculation is shown in figure 5.19. Results are shown in figure 5.20.

Several observations can be made by closely examine the results in figure 5.20. First of all, radiation emission from the arc core takes away about 75% of the Ohmic heating. This implies that in the arc core, radiation is the dominant energy transport mechanism so that the arc temperature on the arc axis is mainly determined by radiation. At peak current, about 60% of the radiation from the arc core is re-absorbed at the arc edge. Thus the radiation reaching the nozzle wall accounts 25 to 30% of the Ohmic heating.

Among all the convective fluxes at the exit of the balance domain, convection out from the hollow contact is the strongest. This is understandable since the main nozzle is partly blocked by the moving contact. During the pressurization stage, energy flux into the expansion volume is comparable with the energy flux away from the hollow contact (up to 28ms). However, when the pressure inside the expansion volume approaches its peak (30ms in figure 5.5), energy flux into the expansion volume quickly decreases while the convective flux into the hollow contact maintains its strength. This implies that for this case geometry of the hollow contact hole is an important design aspect since it significantly affects the energy exhaustion in the high current phase.

Flow reversal in the heating channel occurs at 30ms, as indicated by the thin pink curve going from negative into positive (energy flux comes from heating chamber now) in the negative half of figure 5.20.

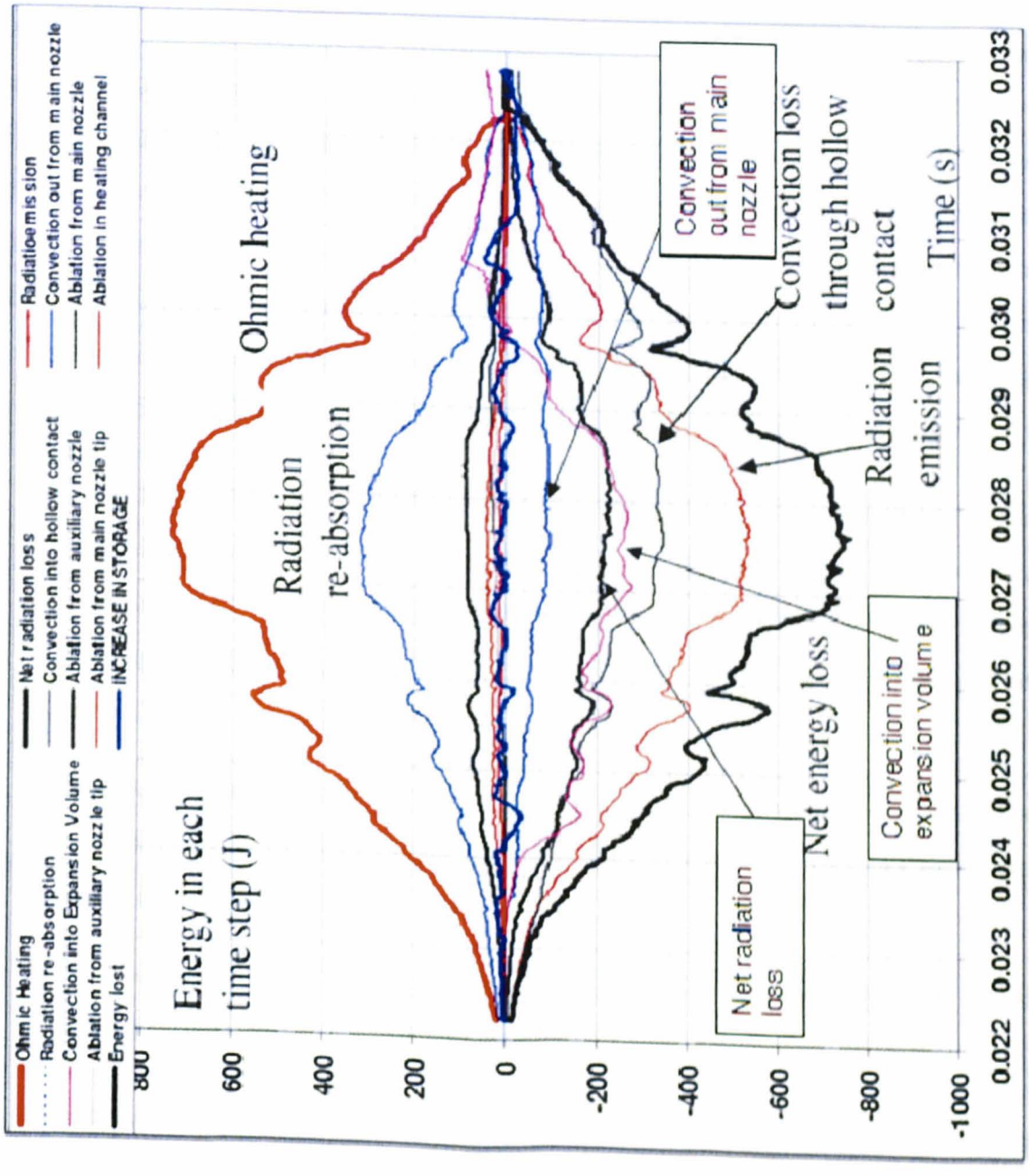

Figure 5.20: Energy balance in the arcing and ablation domain. Values shown are the energy produced or convected within the time step at that time (power multiplied by time step length). The time step is 20μs.

The mass balance has a similar feature to that of the energy balance (figure 5.21). Beginning at 23ms the arc column rapidly expands and mass is pushed away from the domain. This is clearly shown by the fact that the curve labelled as 'total mass into heating chamber' closely follows the curve labelled as 'change in mass storage', which means that the mass convected into the heating chamber (expansion volume) is due to a reduction in the mass stored in the balance calculation domain shown in figure 5.19. It is interesting to note that the rate of change of mass storage rapidly slows down at 24ms, indicating the arc size has settled down at this time. Other convection fluxes also start to change slowly. At 30ms, colder gas from the heating chamber starts to enter the arcing region and the mass fluxes sharply increase. An important aspect in the mass balance is to assess how the mass fluxes change shortly before the final current zero. From the results we have observed the following important features:

- Flow reversal starts at 29.8ms, which is indicated by the curve labeled 'Total mass into heating chamber' changing its sign at this time. The mass storage increases rapidly from 30.5ms to 31.4ms but then experienced a decrease before increases again. This phenomenon is associated with the pressure fluctuations which will be discussed in chapter 6.

- Although there is fluctuation in the mass flux from the expansion volume, the mass flux out of the main nozzle and into the hollow contact increases monotonically from 30ms.

- The fluctuation in mass flux from the expansion volume is expected to be linked to pressure fluctuation in the arcing space.

The total electrical energy input into the breaker is 0.196MJ (the measurement gives a value of 0.217MJ and the ABB model predicts a total energy input of 0.194MJ). 90% of the radiation reaching the nozzle is assumed to ablate the PTFE surface. The ablating energy is 0.0464MJ, which is only 25% of the electrical energy input. The total PTFE vapour produced is 4.3g.

The mass and energy balance for the heating chamber is shown in figures 5.22 and 5.23. During the arcing period, the mass in the heating chamber only increases by 8% but the energy content increases by a factor of 6 in the period from 22ms to 30ms.

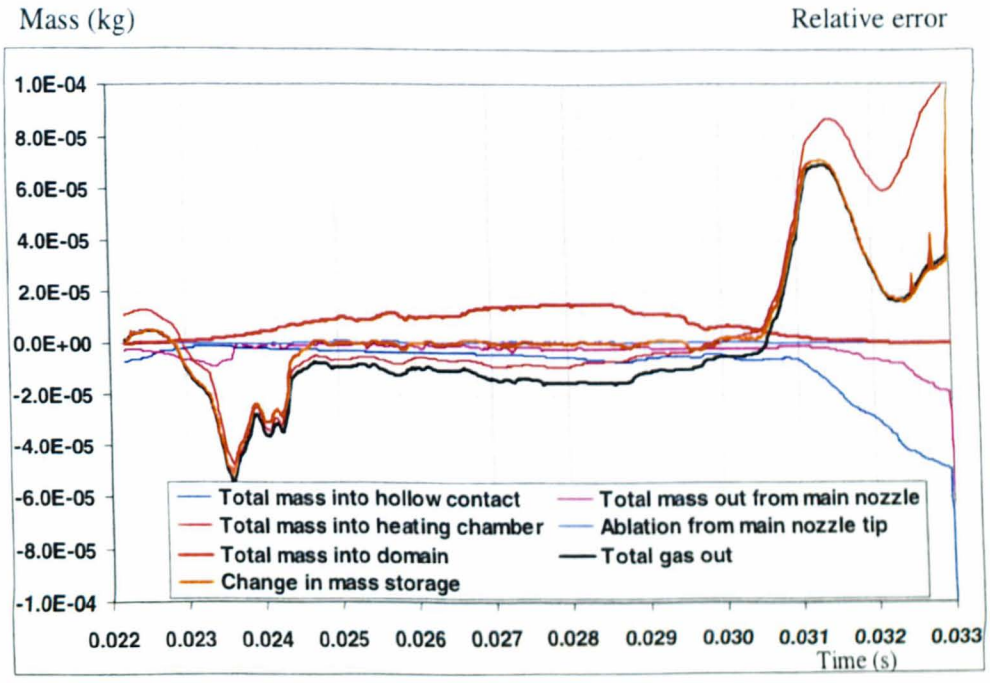

Figure 5.21: Mass balance in the arcing and ablation domain. Values shown are the mass produced or convected within the time step at that time (power multiplied by time step length). The time step is 20μs.

This clearly shows that it is the incoming energy that heats up the SF_6 in the heating chamber to increase the pressure. Optimised design should therefore consider how to best control the thermal flux entering the heating chamber. The total energy that is transported into the heating chamber is about 50kJ, which is larger than the amount of energy used to ablate the PTFE during the pressurisation period. Therefore the use of an optimised thermal (energy) path to the heating chamber may be a critical factor for auto-expansion circuit breaker design. Figure 5.21 also shows that after current zero (32.4ms) mass continues flowing out from the heating chamber under the pressure difference. When the hot gas left in the heating chamber cools down, a low pressure region will be formed and the heating chamber will require refill by either a valve or through the small gap between the contact and the nozzle.

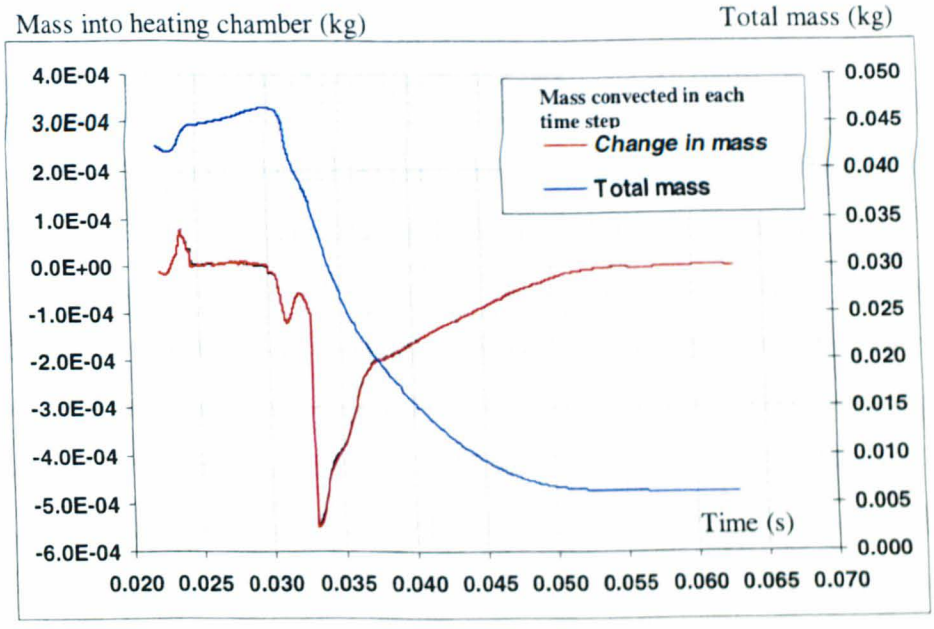

Figure 5.22: Mass balance for the heating chamber of the *ABB* circuit breaker. The mass convected into the heating chamber is for the whole duration of the time step which is 20μs. The value given in this diagram is the mass convected per time step which is integrated over each time step. The sharp change at 33ms is related to the sudden change in time step length.

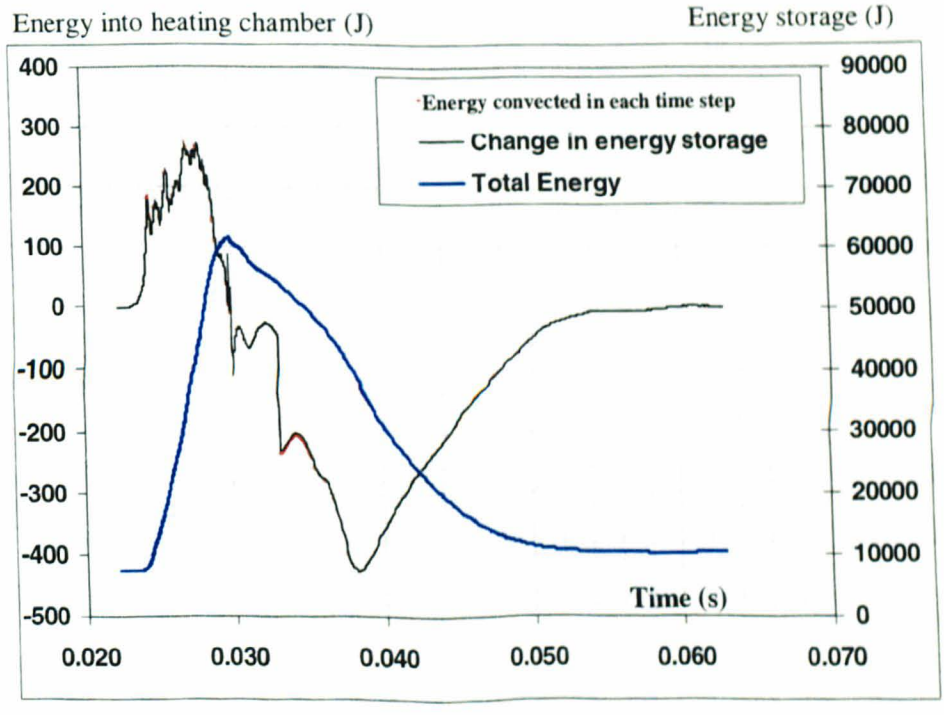

Figure 5.23: Energy balance for the heating chamber of an *ABB* circuit breaker. The energy convected into the heating chamber is for the whole duration of the time step which is 20μs.

5.7 Role of Magnetic Pinch in the Development of High Pressure Zone in the Arcing Nozzles

Without considering the Lorentz force, the predicted pressure rise in the heating chamber is 4 bar lower than that considering the Lorentz force. It should however be noted that the inclusion of Lorentz force may not always result in a higher pressure in the heating chamber. For the ABB breaker ablation in the auxiliary nozzle is very strong and a stagnation region is formed locally at certain stage of the high current phase. In this case the Lorentz force helps pump hot gas into the heating chamber. If in the case where no stagnation point is developed in the auxiliary nozzle, then the higher pressure produced by the magnetic pinch at the arc center results in more gas be exhausted in to the hollow contact and produce a lower pressure in the heating chamber.

There is a big difference between pressure on the axis and that at the arc edge. Around the peak current, the axis pressure can reach a value of 100 bar while that at the arc edge is 37 bar. This gives a difference of 63 bar. Using the radial profile of the axial current density from our simulation, the following one dimensional equation

$$\frac{\partial}{\partial r}\left(P + \frac{B^2}{2\mu_0}\right) = -\frac{B^2}{\mu_0 r} \tag{5.2}$$

produces a pressure difference of 53 bar, where μ_0 is the permeability of space. From our simulation we have a difference of 63 bar which is close to the estimation. This clearly shows that Lorentz force should therefore be included in arc modelling.

5.8 Summary

The results from the Liverpool arc model agree reasonably well with measurement for ABB's circuit breakers and also with those from ABB's two-zone model, if we take into account the approximations that we have made in the model especially the use of the 1D radiation model which is semi-empirical. We also explained why Liverpool's model gives similar results as that from ABB's model. Liverpool's arc model is able to predict the important features of the switching arc in auto-expansion circuit breakers. We also simulated another two cases with different geometries and the agreement is also reasonably good. This gives us confidence in using the model for the work in the

next chapter.

The accuracy of Liverpool arc model is largely limited by the use of the one-dimensional semi-empirical model for radiation transfer that determines the energy for PTFE ablation and also the temperature and size of the arc. Although the model has been calibrated in the current range from 35kA to 78kA (peak) for two circuit breakers, further improvement of the prediction accuracy will require a more accurate model which determines the radiation re-absorption as an intrinsic feature. The use of the five band $P1$ model or the partial characteristics method for circuit breaker arc radiation calculation would be a way forward if the fundamental radiation data can be made available. With these two models, substantial increase in computation load is anticipated. Therefore the use of parallel processing in the modelling process seems to be unavoidable for future improvement.

Chapter 6

Pressure Fluctuation in the Arcing Chamber before Current Zero and Its Implications

Pressure is a word that is misused in our vocabulary.
When you start thinking of pressure, it's because
you've started to think of failure.
– Tommy Lasorda

6.1 Introduction

As discussed in chapter 5, nozzle ablation is the main mechanism for pressurization of gas in the heating chamber in the high current phase. Strong ablation takes place around the current peak when the arc column emits a substantial portion of the electrical power input as radiation which subsequently causes nozzle ablation. When the current decreases rapidly following its last peak, the arc column shrinks and nozzle ablation becomes less fierce. With gas exhausting from the ablating nozzles through nozzle exits the pressure in the contact gap naturally decreases. The most significant change in flow field is the reverse of direction of the flow in the heating channel that connects the contact gap and the heating chamber. This is the starting point in the interruption process to build up the necessary flow and thermodynamic (pressure and temperature) environment for thermal and subsequently dielectric recovery of the contact gap. It is important, for both designers and researchers, to gain a holistic view of what is taking place in the arcing chamber during this critical period and what it implies for the quality and consistency of the performance of the breaker. Because of the complicated design of the interruption chamber and together with the non-uniform

temperature distribution in the heating chamber, the variation of pressure and temperature in the contact gap does not follow a simple pattern. The objective of this chapter is to, based on the verified arc model in chapter 5, perform a systematic study on the detailed evolution of the interruption environment following the last current peak and how the design parameters influence this evolution. A new design is also developed based on the understanding gained from the study and its effectiveness has been numerically tested for suppressing unwanted pressure fluctuations.

6.2 The Reference Case and Characteristics of the Flow Reversal Period

6.2.1 Computational domain and boundary conditions for a reference case

A simple model circuit breaker was used in this chapter to focus our attention on the transient flow and thermodynamic environment shortly before the final current zero and to single out the inherent relations between the design parameters and the evolution of the environment, transient pressure phenomenon. A reference case was chosen for the purpose of comparing the influence of different design parameters on the evolution of the interruption environment. The dimensions and geometry are similar to those of the ABB auto-expansion circuit breaker $170PM40$. The computational domain chosen for this breaker is shown in figure 6.1 together with the location of points where pressure was recorded during the simulation. The length of the channel, which is measured from the joining point of the heating chamber and channel (point immediately left to Point A in figure 6.1) to Point C, is 83mm. The heating chamber has a length (horizontal dimension) of 86.5mm and a width (radial dimension) of 36.25mm. The main nozzle has a diameter of 22mm. The diameter of the auxiliary nozzle is 19mm and that of the solid contact (moving contact in simulation) is also 19mm.

Two exhaustion volumes (the blue region in figure 6.1) are provided for gas released from the arcing space. Fixed pressure (6.0 bar) and temperature (300K) boundary conditions are imposed on the left and right hand side walls to represent a constant pressure environment. The choice of these settings were based on experience that imposing fixed pressure boundary conditions at the joining point of a long nozzle and

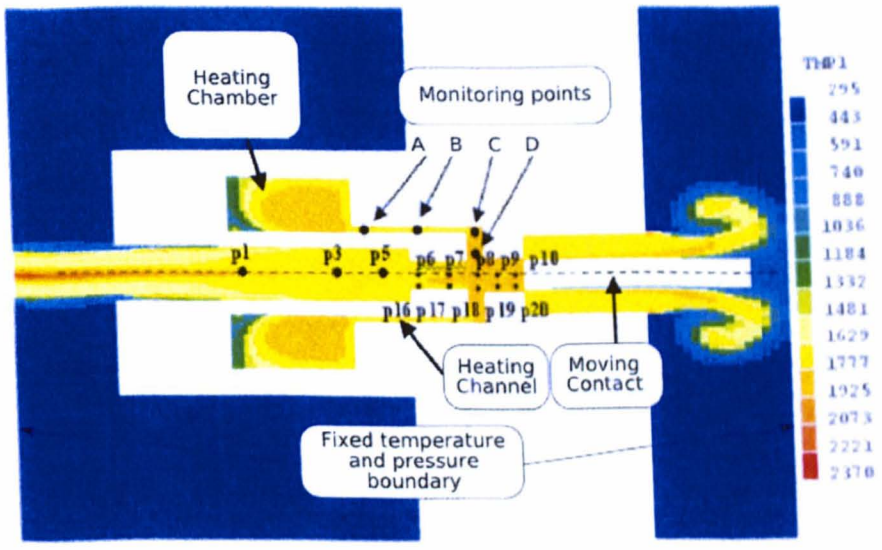

Figure 6.1: Schematic diagram of the model circuit breaker used for the study of the evolution of flow and thermodynamic environment in auto-expansion circuit breakers.

large background environment could lead to inaccurate results due to reverse flow and uncertainty in choosing the exact pressure value. Other boundary conditions are the same as those used in chapter 5.

The filling pressure of SF_6 is 6.0 bar (absolute) at room temperature. The current waveform is same as that used in chapter 5 for the ABB breaker and will be shown when necessary. The number of grids is 183 (axial) by 91 (radial), sufficiently refined to resolve the gradient of the flow and thermodynamic quantities in regions of interest. In all cases the solid contact has a maximum travel of 115mm, moves according to a travel curve with a speed from 6 to 9ms^{-1}.

A simulation with the real circuit geometry but with a smaller computational domain was also carried out. The geometry of the domain is shown in figure 6.1. These two simulations give similar results for the pressure fluctuation investigation with small difference existing as a result of difference in geometry. A small part of the result form the second simulation will also be used in this chapter to demonstrate the nature of the pressure fluctuation.

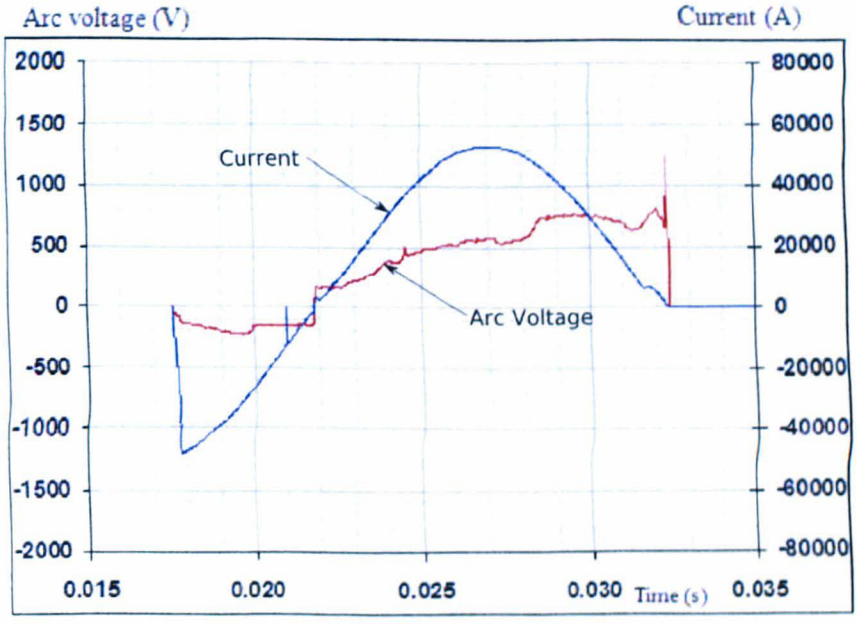

Figure 6.2: Current waveform and predicted arc voltage for the reference case of the model circuit breaker.

6.2.2 Arc behaviour shortly before flow reversal

The arc is initiated at 17.6ms with a contact gap length (between the transparent contact tip and the solid moving contact tip) of 8mm that is filled with a thin hot conducting column. The initial position of the moving contact tip is at Point $p7$ in figure 6.1. The current is ramped up from 2kA to about 48kA in 0.2ms to establish the arc. The current waveform and predicted arc voltage of the reference case are shown in figure 6.2. There are no measurements of arc voltage for comparison but it can be noted that the magnitude of the prediction is very close to the measurement for the real circuit breaker (figure 5.2). In the period up to 29ms where the current has already passed its final peak, hot PTFE vapour is generated and thermal energy is pumped into the heating chamber where pressurization takes place.

As can be seen from figure 6.3 pressure variation inside the chamber is rather smooth. The small ripples superimposed on the smooth trend are caused by pressure wave propagations associated with the contact movement and changing current, as already discussed in chapter 5. The arc in the first loop hardly affects the pressurisation process because the auxiliary nozzle is blocked by the solid contact and little vapour and thermal energy are convected into the heating chamber. The level of pres-

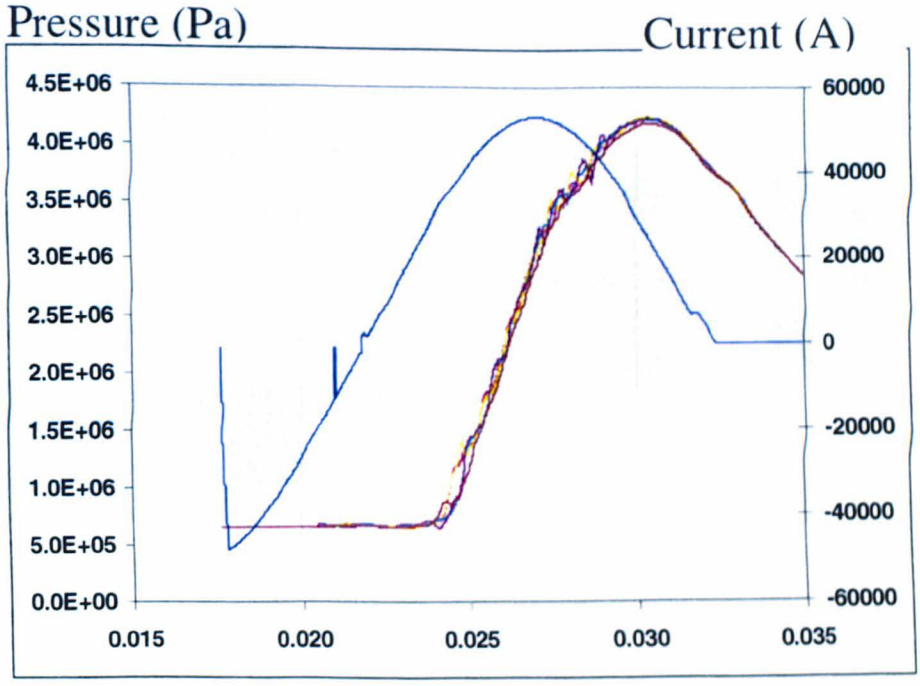

Figure 6.3: Pressurisation inside the heating chamber for the reference case. Curves reflect the record at different monitoring points in the chamber

surisation depends on the location of the arc and the arcing current. Maximum and fastest pressurisation of the heating chamber takes place when the arc burns in both the main and auxiliary nozzles around the peak current. Temperature, flow and pressure field in the contact space at the final current zero bear no memory of the local arc parameters during the high current phase. They are instead determined by the flow reversal process and the properties of gas mixture in the heating chamber, as discussed below.

Because of the propagation of pressure waves and the inertia effect of the arcing gas, heating chamber reached its maximum pressure at around 2 to 3ms after the current peak. Figures 6.4, 6.5, 6.6, and 6.7 show the temperature, pressure and velocity fields at the instant of 27.4ms corresponding to the current peak. Several points need to be explained. Firstly, the arc column at the peak current almost completely fills the arcing nozzles thus exhaustion of PTFE vapour is through the arc column. The thickness of the cold PTFE layer is much smaller than the size of the arc column (figure 6.4). Secondly, the axis pressure in the arc column is much higher than that at the arc edge, which is caused by the magnetic pinch effect (figure 6.5). The effectiveness of the pressurization process is not determined by the maximum pressure inside the arc

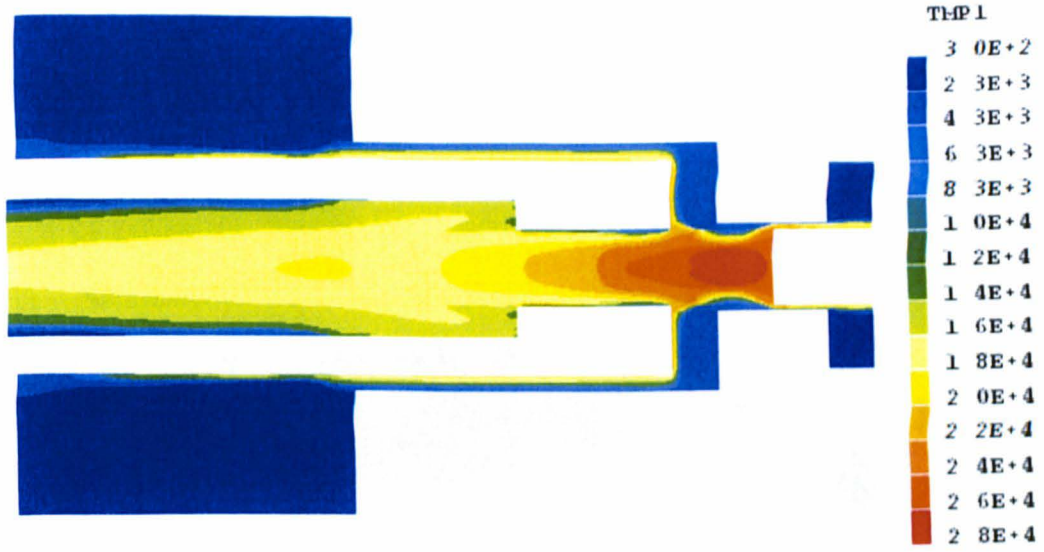

Figure 6.4: Temperature field at 27.4ms corresponding to the peak current of 52.6kA.

column, instead it is determined by the pressure near the arc edge where PTFE vapour is driven towards the heating channel under the action of the pressure gradient (figure 6.6). similar to the pattern described in chapter 5, PTFE vapor follows a narrow path to flow into the heating chamber. The region designated as S in diagram c is rather stagnant since there is an ablating patch specified on surface T. Although the heating channel is only a few millimetre thick, temperature across the radial direction is far from uniform. The mass of PTFE vapour is negligible in comparison with the total mass confined in the heating chamber *(figure 6.7)*.

6.2.3 Flow reversal and formation of interruption environment

Flow reversal means the reverse of flow in the heating channel due to a lower pressure in the arcing nozzle than that in the heating chamber when the current passes its final peak and decreases rapidly towards its final zero. At high current levels, vapour from the main nozzle surface is produced and further heated up by the arc (radiation re-absorption) during its course flowing to the heating channel. This temperature could reach $10,000$K or even higher. Flow reversal occurs normally at $2-3$ms after the current peak. In this reference case it takes place at 30.2ms. Careful examination of the results shows that in the 1ms period before the instant of 30.2ms gas in the heating channel is rather stagnant. It does not flow in either direction. Starting from 30.2ms, cold gas starts to flow into the heating channel (figure 6.8). Since this is a transition

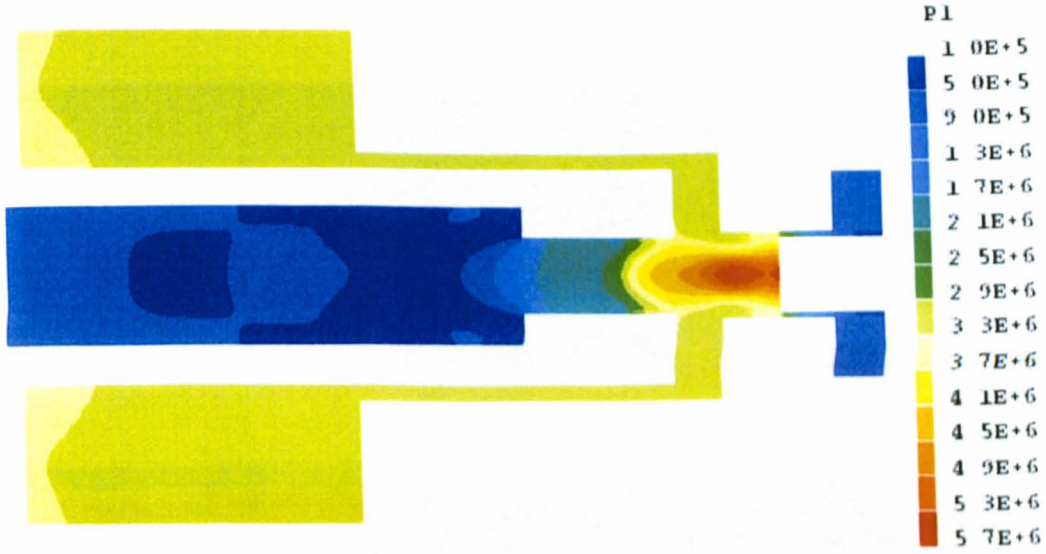

Figure 6.5: Pressure field at 27.4ms corresponding to the peak current of 52.6kA.

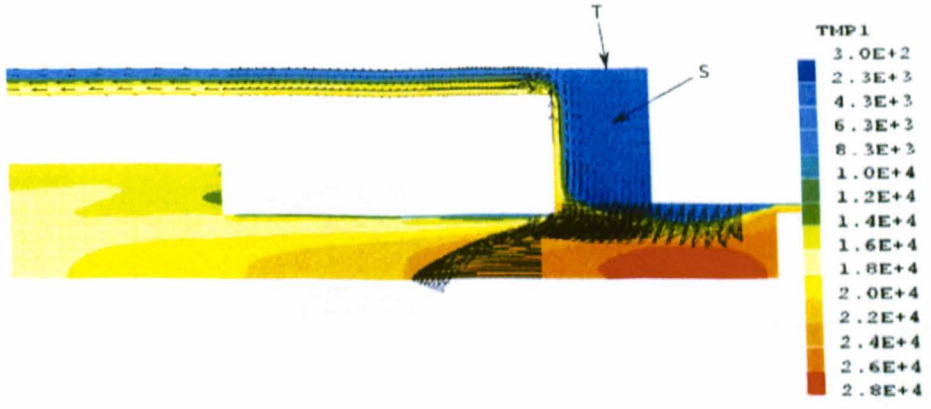

Figure 6.6: Velocity vector showing PTFE vapor pumped into the heating channel, at 27.4ms, current 52.6kA.

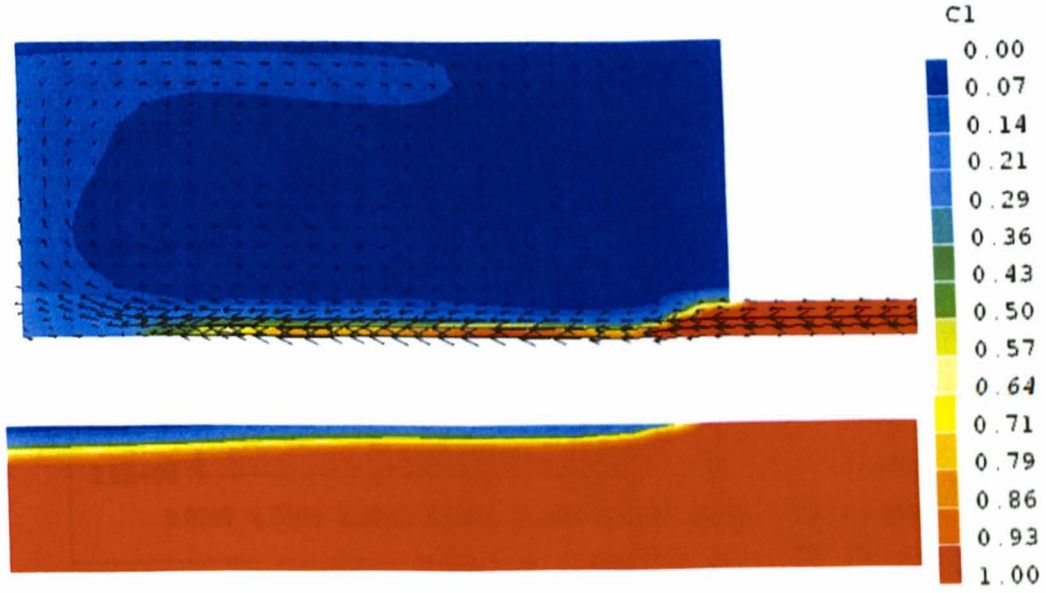

Figure 6.7: PTFE concentration and gas flow velocity vector, 27.4ms, 52.6kA.

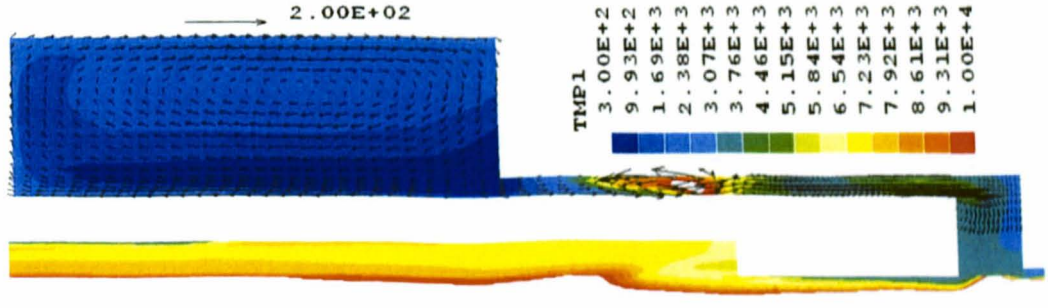

Figure 6.8: Flow field in the heating chamber and heating channel at 30.2ms corresponding to 30.8kA after current peak.

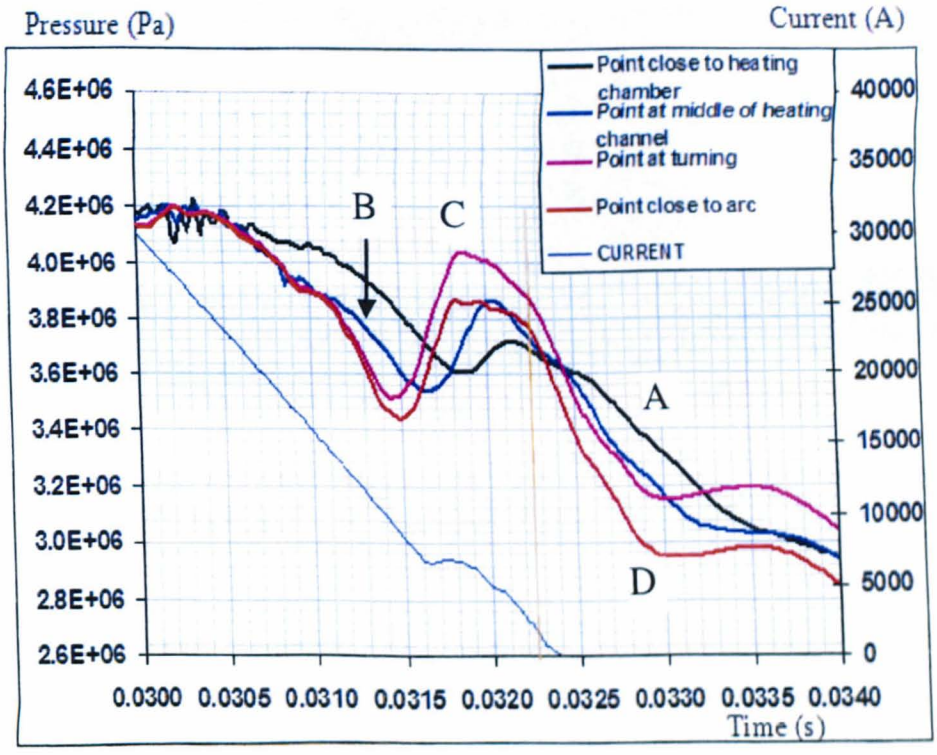

Figure 6.9: Pressure variations in the heating channels after the current peak for the reference case.

stage, a small cloud of gas still remains in the heating channel and flow circulation is observed inside this low density area. Different from the pressurization stage, flow in region *S* (position shown in figure 6.6) is much more uniform towards the arc column.

Since the colder gas in the heating chamber cannot respond rapidly enough to compensate the pressure drop in the arcing nozzle due to arc column shrinkage, the pressure in the arcing space is expected to continuously decrease. This is shown in figure 6.9 detailing the pressure variations at several points whose locations are given in figure 6.1. Between 30.2ms and 31.5ms the pressure near the arcing nozzle (Point *D*) has the largest pressure drop while the point close to the heating chamber (Point *A*) has the least pressure drop. The choice of Point *D* as an indicator of the pressure in the contact gap is based on the consideration that pressure on the nozzle axis is significantly affected by the magnetic pinch effect and does not truly reflect the pressure and temperature environment around the thin arc column at current zero.

Pressure recovery in the arcing space starts to take place when the colder gas from the heating chamber arrives at Point *D*. This is shown by the flow field in figure 6.10 together with the temperature of gas at 31.6ms. Comparing with figure 6.8 it can be

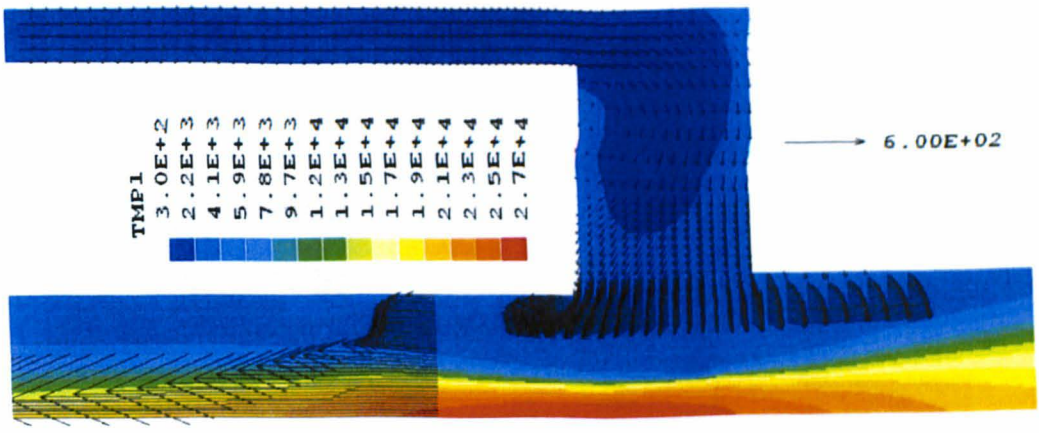

Figure 6.10: Diagram showing temperature velocity field in the heating channel at 31.6ms when the pressure in the arcing space starts to recovery.

clearly seen that the arc column is much thinner in figure 6.10. In view of the fact that it takes time for the pressure field thus the velocity field in the exhausting channel (here the hollow contact) to adjust itself, the high mass flow rate of colder gas from the heating channel cannot be immediately exhausted at a sufficiently high rate. The consequence is that the colder gas is blocked in the arcing space which then develops a temporary high pressure at 31.8ms in the arcing space (curve *D* in figure 6.9). This type of 'blockage' is propagated back to the heating chamber and creates a pressure peak at each of the *A*, *B*, *C*, *D* points with different amplitudes. The maximum pressure recovery peak is at the turning point (Point C) in the heating channel where the gas is forced to turn into a perpendicular direction. This means that the closer the point is to the heating chamber (for example Point *A*) the later the pressure recovery peak appears.

The pressure transient profiles from the Liverpool model show characteristically similar patterns to those obtained by ABB using a simple model for low current arc [127] (figures 6.11 and 6.12). Although the current zero is different in the two diagrams the pressure variation follows a similar pattern. The difference in details is due to the different arc models used and the difference in geometry, contact travel and arcing current.

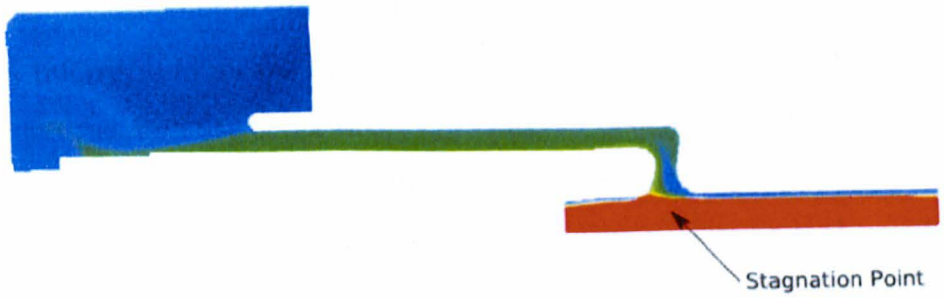

Figure 6.11: Geometry of the arcing chamber and the stagnation point.

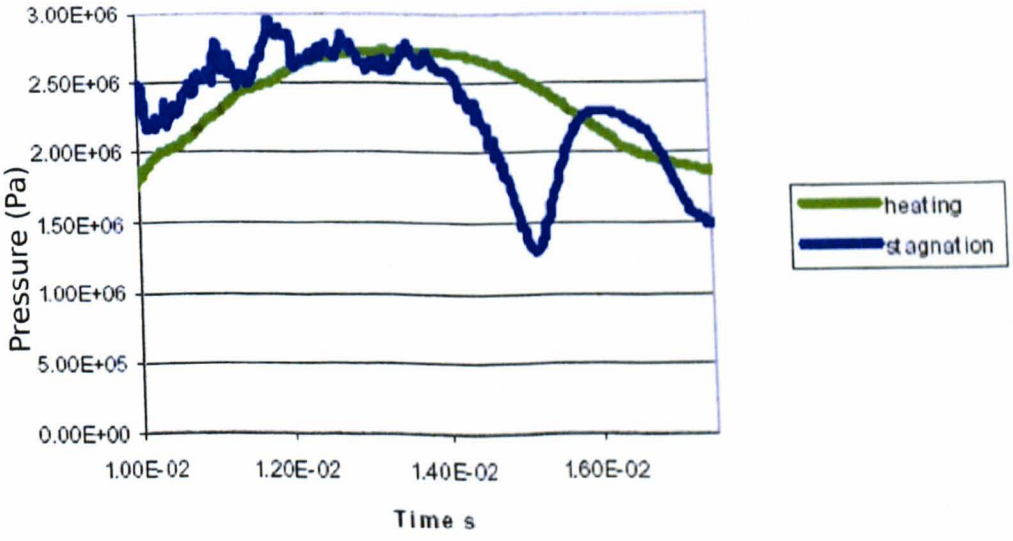

Figure 6.12: Pressure profile at the stagnation point at 15ms. The arcing duration is 14ms with a rms current of 70kA.

6.2.4 Implications of pressure variation in the arcing chamber

The interruption capability of a breaker depends on the pressure and temperature fields (dielectric recovery) and how efficiently thermal energy can be removed from the residual plasma column (thermal interruption) during the current zero period. A successful interruption means the temperature of the plasma column continuously decays with time. Because of the small size of the column at current zero, the temperature, pressure and velocity fields in the arcing nozzle surrounding it basically determine the performance of the breaker. After the recovered pressure peak around 32ms which is 0.4ms before the final current zero, the pressure decays monotonically and more colder gas flows into the arcing space, preparing the immediate environment for thermal interruption. Figures 6.13 and 6.14 show the temperature, pressure and velocity fields surrounding the thinning arc column at 378μs before the final current zero for the reference case. It can be seen that the velocity and temperature fields are rapidly approaching a uniform distribution in the radial direction outside of the arc column. Figures 6.15 and 6.16 show the results using a different geometry with very similar dimensions and identical current and contact travel conditions at 10μs before the final current zero. It is apparent that the closer to the final current zero, the more uniform the velocity distribution is in the radial direction. The pressure field in both cases attains a maximum at the middle of the interspace between the auxiliary and main nozzles. The decay of pressure towards the nozzle exits depends on the exact position of the moving contact.

In contrast to that shown in figures 6.4 and 6.6 where there is large temperature gradient in the heating channel, flow at the same location is more uniform (figures 6.10 and 6.13) when gas in the heating chamber is flowing into the arcing nozzle to form a high speed flow interrupting environment. This is directly related to the temperature distribution in the heating channel where in figure 6.13 the gas is colder and the temperature gradient is negligible. The mixing process in the heating chamber (such as that show in in figure 6.8) directly determine how 'hot' the environment is in the arcing nozzle and how the velocity and pressure field vary in the period shortly before current zero. With a uniform flow in the heating channel, the characteristic time for filling the arcing nozzle by colder gas from the heating chamber will be deter-

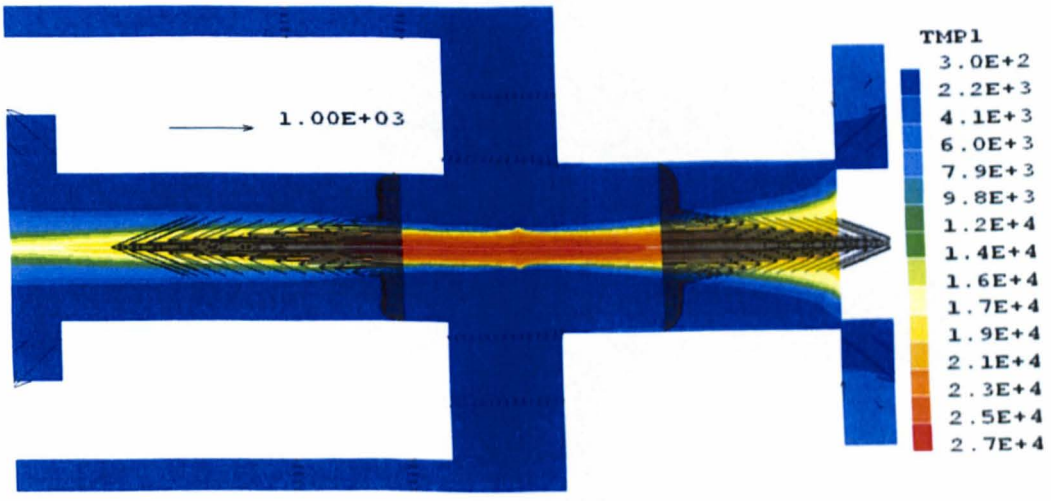

Figure 6.13: Temperature with velocity vector at 378μs before the final current zero for the reference case.

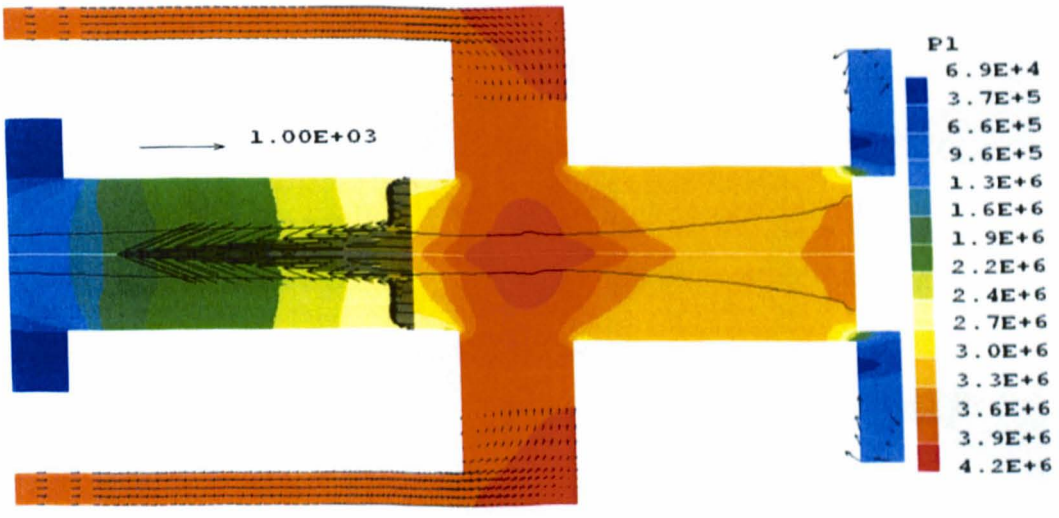

Figure 6.14: Pressure and velocity fields at 378μs before the final current zero for the reference case. The 10,000K isotherm lines are shown.

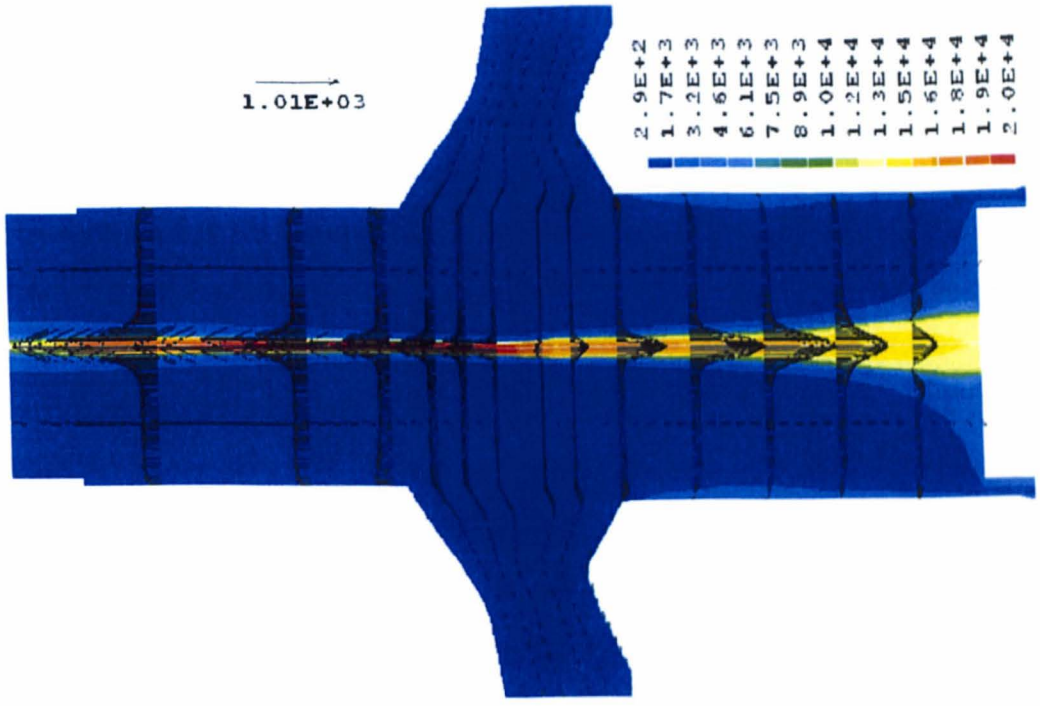

Figure 6.15: Temperature and velocity field shortly before final current zero (304A, 10μs before current zero). This set of results are obtained using a slight different geometry from that shown in figure 6.13 and 6.14. the dimensions and arcing conditions are similar.

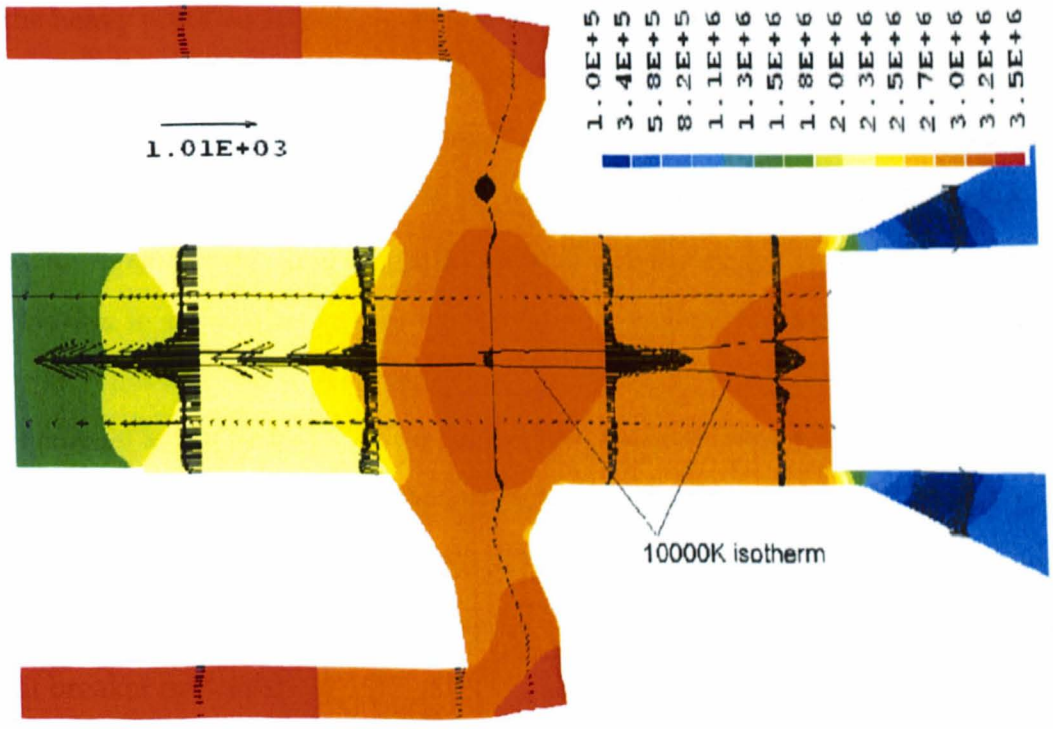

Figure 6.16: Pressure and velocity field shortly before final current zero (304A, 10μs before current zero).

mined by the length of the link-way between the nozzle and the chamber and also the minimum flow cross area. The race between gas exhaustion from the arcing space and the filling process by gas from the heating chamber determines the pressure variation in the former. This pressure fluctuation adversely affects the breaker performance if the pressure reaches the lowest value at current zero. Its very existence could also add uncertainty/scattering to circuit breaker performance thus is best to be avoided. Several factors can affect the evolution of pressure but the most sensitive parameters are the length and cross section of the heating channel.

From the above results it is apparent that large pressure fluctuation can exist in the contact space under certain switching duties. It naturally follows the question that what would be the optimum global flow and thermodynamic environment for reliable thermal interruption and the subsequent dielectric recovery process?

The first requirement would be a pressure that is as high as possible in the contact gap when the current passes its final peak: Firstly a higher pressure would be beneficial to a better convection of energy away from the contact space since it generates a stronger flow field towards the nozzle exits. Secondly, a high pressure would aid the dielectric recovery process since there are more collisions between the free electrons and the heavy particles leading to a high dielectric strength.

Secondly, there exists a question to be answered: Could the large pressure fluctuation be advantageously used for thermal interruption? From results obtained so far, there is no concrete evidence to conclude the answer is yes, to the question since the pressure fluctuation is intrinsically related to the change of arc column which is unavoidable in alternating current interruption. The situation is further complicated by the fact that a circuit breaker needs to perform different switching duties with different current levels, arcing duration and phase angle of contact separation. To benefit the thermal interruption process, the pressure needs always to be at or around its peak under different switching duties. If the answer were no, then it is reasonable to expect that the pressure fluctuation be as small as possible, thus reducing the scattering in circuit breaker performance.

The ambient temperature of the arc is also important since together with pressure it determines the density of the cooling gas. This is shown later when different cases are compared. There is also a requirement on the maximum gas temperature in the

contact gap at current zero since if the gas is excessively hot ($> 2,500$K) the dielectric strength will be substantially reduced [128]. Gas flow velocity is also an important factor since it affects the convective effect and the turbulence through the velocity gradient. The convective cooling can be represented by the term of axial velocity multiplied by density. Since velocity field is coupled to the pressure field, we will thus focus our assessment on pressure, temperature and the convection term as defined here without employing a specific model for the current zero period. The relationship between the critical rate of rise of the recovery voltage and the flow and thermal dynamic environment are quantitatively studied in here due to reasons which will be discussed in the conclusion chapter. In the following sections the design parameters affecting the pressure and temperature evolution are studied and useful information is obtained to help to the optimum the design of such a breaker.

6.3 Influence of Design Parameters

6.3.1 Geometric parameters that may influence the formation of thermal and aerodynamic environment

Thermal interruption performance of an auto-expansion circuit breaker depends on the whole arcing history. This is because the formation of appropriate flow and thermodynamic environment for arc extinction at current zero results from the pressurisation of the heating chamber at the high current phase as discussed in the previous chapter. However it must be made clear that a high pressure in the heating chamber is only a necessary condition, not a sufficient condition. The exact distribution of the pressure, velocity and temperature in the arcing chamber depends on a number of interrelated factors, such as the flow distance from the heating chamber to the contact gap, the geometry and size of the fluid dynamic linkage (heating channel) between the former and the latter and the internal structures present in the heating chamber.

The heating channel for example, is an important factor since its cross section or any internal structure that presents in the flow passage may potentially affect the flow of gas mixture into the arcing nozzle and further affect the thermal and aerodynamic environment build-up near current zero. Secondly the structure in the heating chamber may affect the mixing process of the hotter PTFE vapour and the existing colder

gas. This mixing process basically determines how hot the gas is when it flows into the heating channel. Thirdly, during current zero period sufficient colder gas is needed to fill the arcing space to maintain a smooth change of pressure, thus there needs to be a mechanism to supply gas rapidly to the arcing space when current deceases quickly immediately before current zero. Thus in this chapter new designs of the arcing chamber have also been computationally tested for its ability to smoothen the pressure fluctuation immediately before current zero.

A number of simulations were carried out to study the influence of the design parameters on the pressure transient in the arcing space. The design parameters that were investigated include the volume and structure of the heating chamber, length of the heating channel, and addition of internal structures. It is to be noted that results in Groups 1 to 6 (in the following sections) were obtained using a slightly smaller effective flow area between the moving contact and the main nozzle in comparison to that in the real circuit breaker. This is a result of the approximation made to the moving contact. In reality the tip of the moving contact is rounded whereas in the simulation it is represented by a right angled tip. The effect of increasing this area is examined in cases given in section 6.5.

All pressure results given in this section are the value at Point *D* shown in figure 6.1. However, when a single design parameter is changed, the predicted arc column shape and arc voltage can be different from that in the reference case because of possible modification to the pressure and flow fields and the interactions between the flow field and the arc. As a consequence the absolute pressure maximum may also be different from that of the reference case. The focus is thus paid on its effect in influencing the pressure fluctuation in the period shortly before the final current zero.

6.3.2 Group 1: Dimensions and volume of the heating chamber

The simulation aims at the understanding of how the dimensions and volume of the heating chamber affect the pressure build-up in the contact space near current zero. Six cases are available for comparison with the reference case. The differences in the dimensions and geometry are given in Table 6.1. The symbol EV in the case ID means the total volume of the heating chamber and channel is kept as the same as that in the reference case. DV means the total volume of the heating chamber and heating

Case ID	Relative chamber length (axial dimension) (ratio to that of the reference case)	Relative chamber width (radial dimension) to the reference case	Relative volume to the reference case
REF	1.000	1.000	1.000
Chamber-EV-SL1	0.607	1.000	1.003
Chamber-EV-LL1	1.250	0.762	1.005
Chamber-DV-SL1	0.607	1.000	0.703
Chamber-DV-SL2	0.750	1.000	0.851
Chamber-DV-SL3	0.929	1.000	0.941
Chamber-DV-LL1	1.232	1.000	1.154

Table 6.1: Relative dimensions of the heating chamber used in each test. SL - smaller length of heating chamber; LL - larger length of heating chamber.

channel is different from that in the reference case.

Results show that varying the length of the heating chamber results in differences in the maximum pressure (figure 6.17) in the heating chamber. Examination of the detailed results shows that this is caused by a difference in the predicted arc voltage, which directly determines the total electrical energy input into the computational domain. The pressure variation in the arcing space is given in figure 6.18. The lowest pressure around 31.3ms in each curve is following the same order as the pressure peak in the heating chamber. It is interesting to note that the pressure recovery in the two cases with higher peak pressure in the heating chamber is less than that in the reference case. Taking into account the differences in the peak pressure, changing the dimensions of the heating chamber does not give any clear indication towards optimum design. For information the radial temperature distribution along a line passing Points C and *D* (see figure 6.1 for their locations) at 32.02ms is given in figure 6.19. The temperature of the surrounding gas is well below the dissociation temperature of SF_6. The arc has approximately the same radial size while the gas temperature immediately around the thin arc column has some difference.

Other simulations in this group give results with different chambers length while with the same chamber width. This means the volume is no longer constant. The smallest heating chamber volume produces the highest pressure peak (29.9ms, top curve of figure 6.20) in the arcing space but the pressure at current zero in the arcing space exhibits a more complex pattern. In the larger volume case, corresponding to

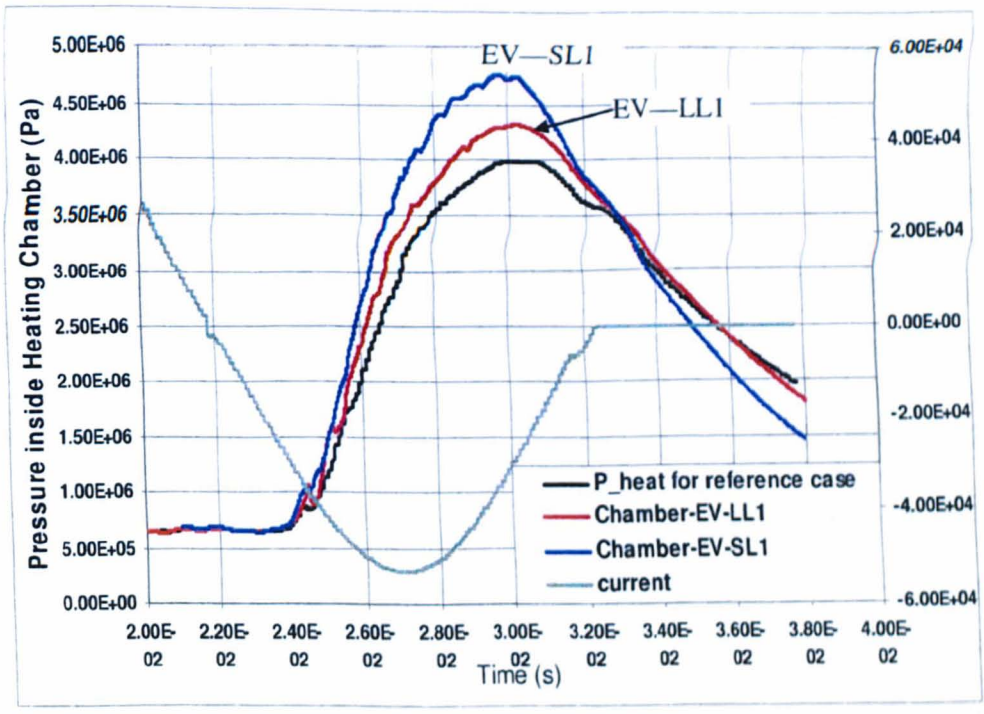

Figure 6.17: Pressurisation of the heating chamber in three cases when the length of the chamber varies.

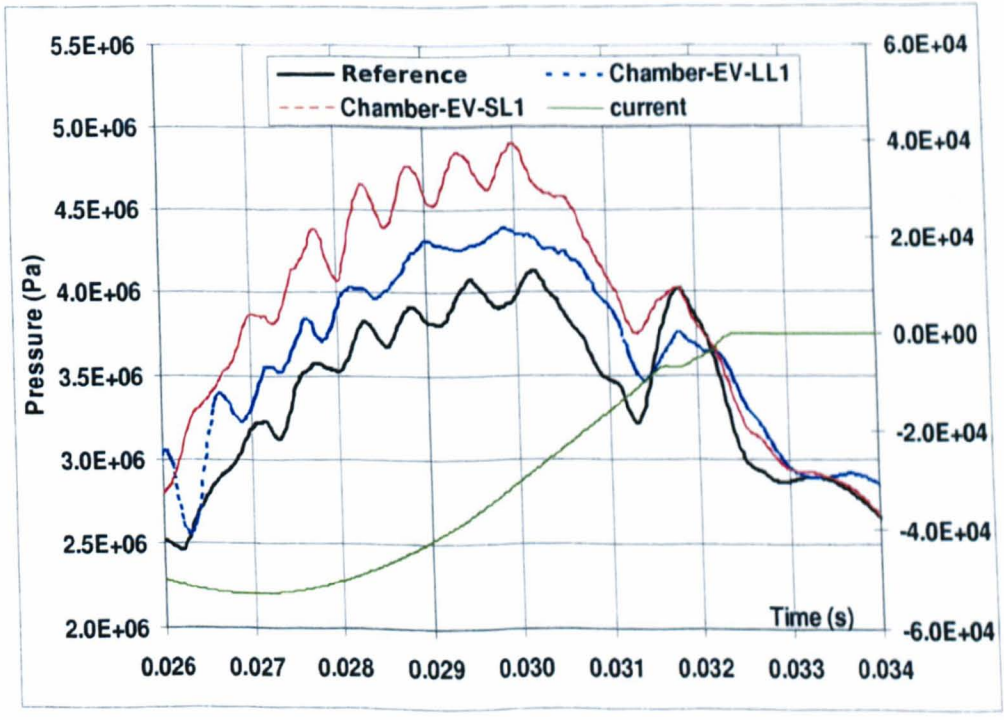

Figure 6.18: Pressure variation at Point D in figure 6.1 for three cases. The volume of the chamber is kept constant.

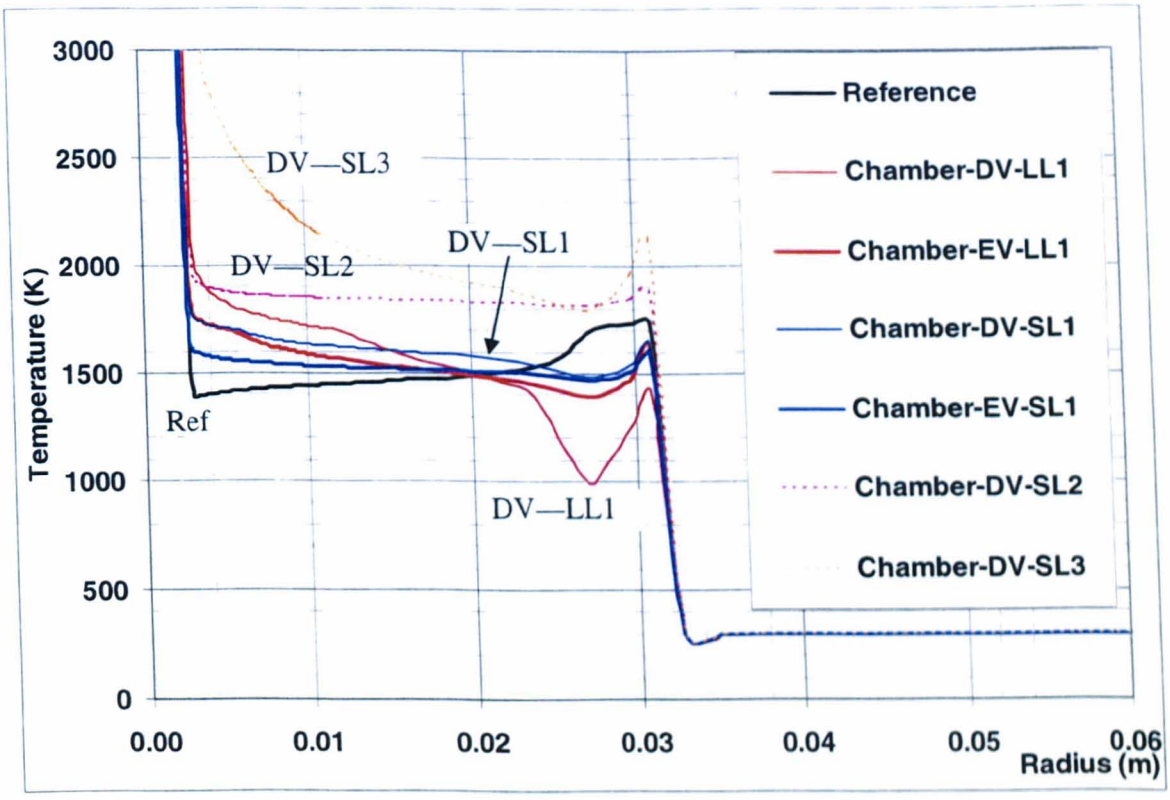

Figure 6.19: Radial temperature distribution along line passing Points C and D in figure 6.1 for three cases, at around 32.02ms.

a longer heating chamber, the pressure peak is delayed by almost 1ms immediately before current zero. Figure 6.20 also indicates that the small pressure oscillation before 31ms behaves differently for different chamber lengths. In the case where the length is slightly smaller than the reference case, the pressure oscillation is most significant. The frequency of the oscillation clearly varies with the chamber length which is due to the reflection of compression waves from the arcing space. Another important point is that, consistent with the observation given in section 6.2, a higher peak pressure in the heating chamber produces a smaller pressure recover peak in the arcing space while a lower pressure peak produces a larger pressure recover peak thus resulting in stronger pressure fluctuation. In other words, the problem associated with pressure fluctuation can be more severe in switching duties where pressure rise in the heating chamber is moderate.

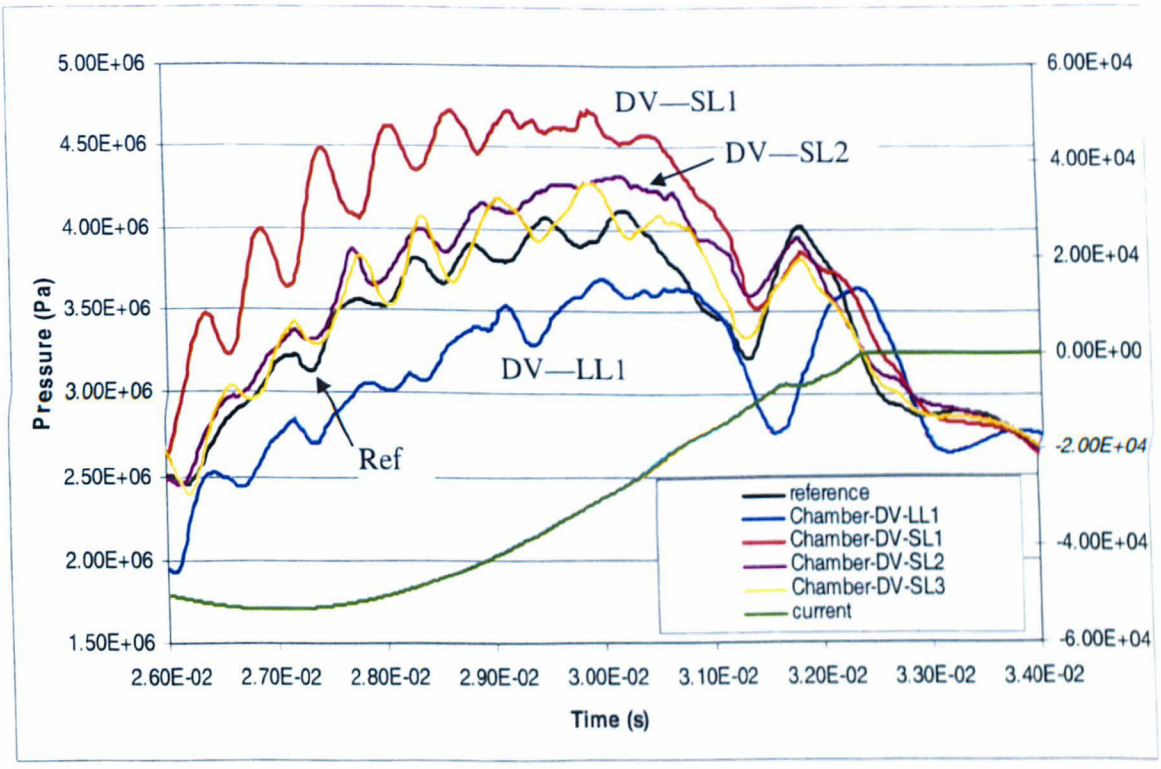

Figure 6.20: Pressure transient in the arcing space.

6.3.3 Group 2: Length of heating channel

This set of simulations is to examine the role of the channel length in forming the pressure and temperature conditions in the contact gap. From this group of simulations we derive the effect of length on the profile of the pressure transient. This information is useful to further understand the non-uniform temperature in the heating channel during the arcing process since there is no simple model to correlate the pressure profile to the length. The geometric details of the simulated cases are given in Table 6.2 and figure 6.21. The original channel length in the reference case is 83mm. It should be noted that when the channel length is adjusted, the volume is also adjusted for cases labeled with EV to maintain approximately a constant total volume of chamber and channel.

The standard length of the heating channel, which is measured from Point A to Point C in 6.1, has much influence on the pressure build-up in the arcing space. This is shown in figure 6.22 and figure 6.23 for all the cases investigated.

The most informative observation from the results is that with a shorter channel length (case EV-SL1) the pressure continues to oscillate after current zero in compar-

Case ID	Relative channel length (horizontal dimension) to reference case	Relative channel width (vertical dimension) to reference case	Relative total volume (chamber + channel) to reference case
REF	1.000	1.000	1.000
Channel-EV-SL1	0.547	1.000	1.003
Channel-DV-LL2	1.000	1.000	1.251
Channel-EV-LL2	1.500	1.000	0.987
Channel-EV-LL3	1.928	1.000	0.975
Channel-DV-LL1	1.347	1.000	1.162

Table 6.2: Dimensions of the Group 2 cases: SL - smaller length of heating channel; LL - larger length of heating channel.

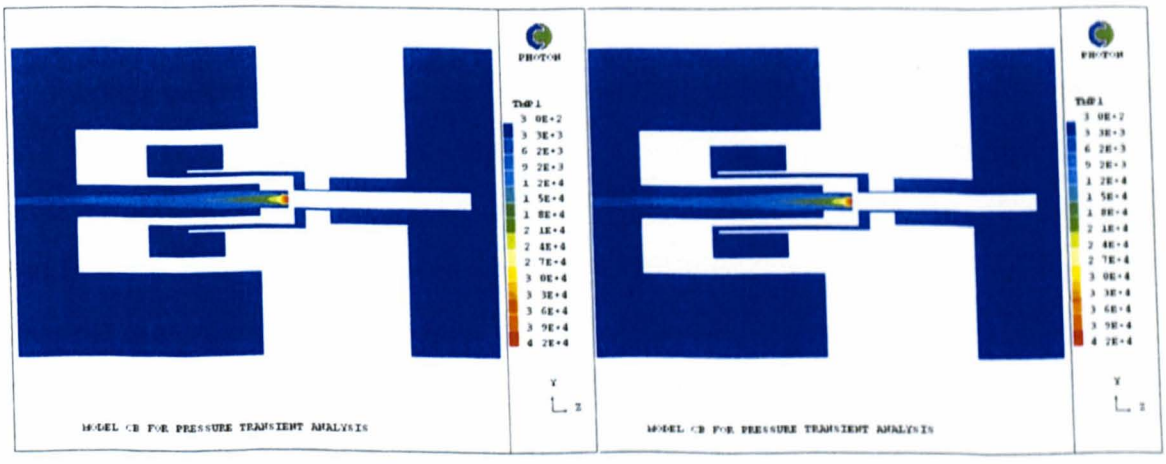

Figure 6.21: Diagrams showing the geometry in Cases Channel-EV-LL2 (left) and Channel-EV-LL3(right). Other cases in Table 6.2 do not have the tube extended into the heating chamber.

ison with the reference case (figure 6.23). It creates the highest pressure at current zero.

With a longer channel length (case DV-LL1, the total volume is also slightly larger than that in the reference case), the pressure continues to drop after 31ms and reaches the lowest value of 25 bar at 31.6ms (also in figure 6.23). The pressure transient behaviour in case DV-LL1 is mainly caused by the difference in channel length, not the difference in the total volume. This can be confirmed by inspecting the results from case DV-LL2 which has the same channel length as in DV-LL1 but with an even larger total volume. In case DV-LL2, the heating chamber volume is slightly bigger, so the peak pressure is lower. If this influencing factor were taken out, the two curves would have approximately the same pressure at 31.6ms.

Results from cases DV-LL1 and DV-LL2 show that with the same channel length the minimum pressure occurs at 31.6ms and the following pressure peak at 32.2ms in both cases. In case DV-LL1 the pressure recovers to a value at current zero that is only 1 bar above that in the reference case. It is also important to note that with a longer channel length the occurrence of the minimum pressure is delayed from 31.2ms in the reference case to 31.6ms. This is clear evidence that with a longer heating channel the response from the heating chamber to provide mass to fill the arcing space for decreasing arc column size is slower.

Further extending the channel into the heating chamber removes the oscillation and results in a smoothly decreasing pressure in the arcing space (case EV-LL3). Results here suggest that removing the pressure fluctuation results in a slowly decaying but lower pressure when thermal interruption takes place. The length of the heating channel is a critical design parameter in shaping and timing the pressure fluctuation. The choice of the appropriate channel length, apart from mechanical design considerations, should be guided by results from computer simulation of different switching duties.

With a short channel length, gas from the heating chamber takes less time to arrive at the arcing space, which is favourable of pressure building up in the arcing space. By contrast in the case of longer channel length, the excessive time taken by the gas flow results in the pressure drop at 31.5ms. This low pressure tends to slow down the axial flow in the hollow contact given that the pressure at the exit of the hollow con-

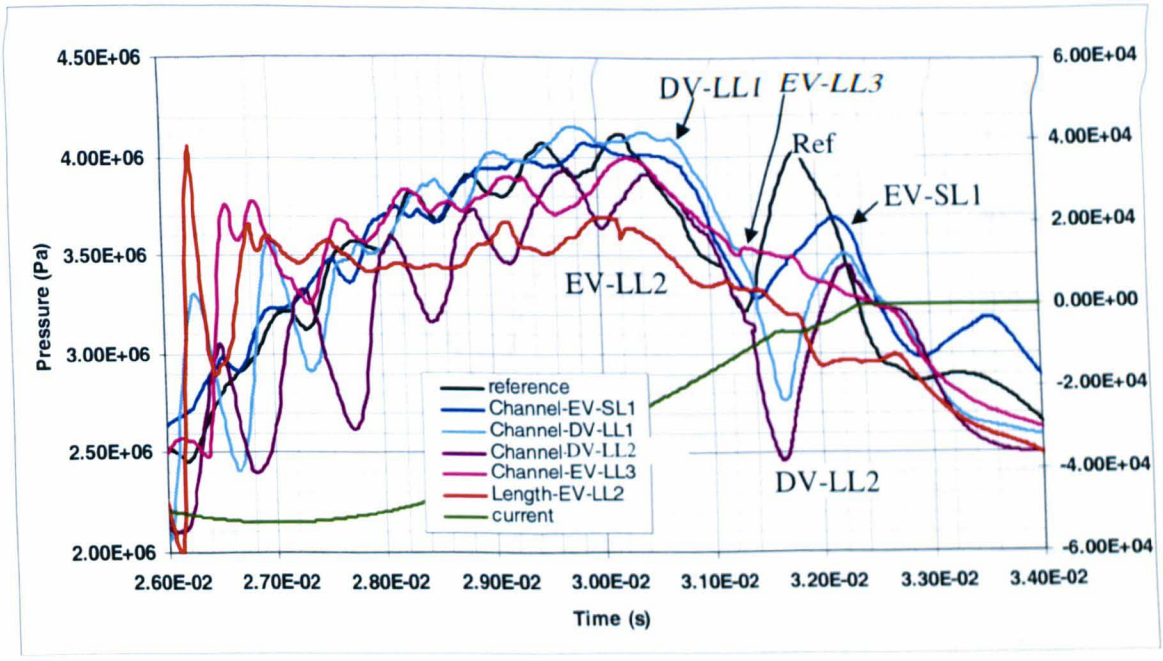

Figure 6.22: Pressure at Point *D* in figure 6.1 for all cases in Group 2.

tact maintains constant. When the gas from the heating channel arrives, the pressure experiences a sharp increase and reaches an instantaneous value at current zero that is higher than that in the reference case.

Figure 6.24 shows the temperature field around the arc for the short channel length case. The white arc column indicates a temperature that is higher than 5000K. It is interesting to note that a cold patch of gas that is initially compressed by the incoming PTFE vapour now flows into the arcing nozzle, setting up a cold gas environment for thermal interruption. The results in figures 6.24 and 6.25 have two important implications. Firstly, an optimised design should aim at regulating the gas compression/mixing process in the heating chamber so that at current zero a patch of cold gas could be displaced into the arcing space for better thermal interruption performance. Secondly, the linking length between the arcing space and the location of pressurisation needs to have an optimised value so that maximum pressure could be achieved at current zero. Although the effective flow area at the exit of the main nozzle is smaller than the real circuit breaker (as mentioned at the beginning of this section), the results still present the typical features of the problem. The combined effect of pressure, temperature and velocity could be represented by the product of velocity and density, as given in figure 6.25. It is apparent that a higher pressure in the arcing space produces

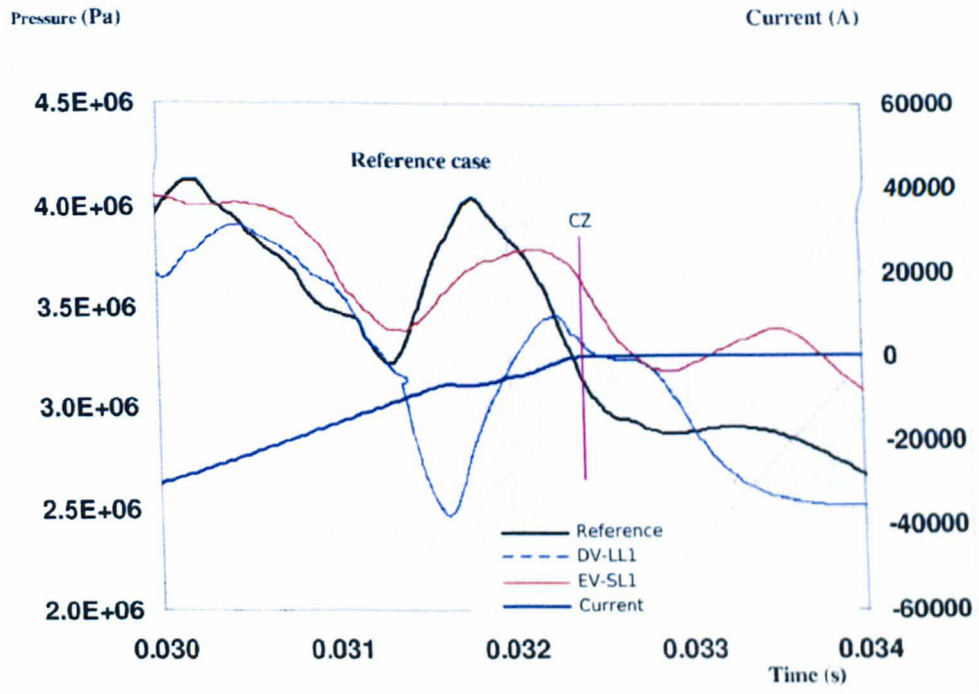

Figure 6.23: Selected cases from figure 6.22 for comparison.

a stronger convective flow.

6.3.4 Group 3: Thickness of heating channel

This set of cases aim at confirmation of the influence of channel cross sections in the pressure build-up in the contact gap. It is known from practice that the cross section of the channel must have a minimum value for expected satisfactory thermal interruption performance. The results here give quantitative evidence as regards how it controls the pressure transient in the arcing space. The details are given in Table 6.3. The original heating channel length in the reference case is 83mm with 5mm radial width.

Results in figure 6.26 indicate that reducing the thickness of the heating channel results in a lower pressure build up in the heating chamber and also a lower pressure at current zero.

With case EV-LT1, the channel has a larger cross section than that in the reference case while with the same chamber and channel total volume as in the latter. This allows a larger amount of mass to flow towards the contact space to compensate for the

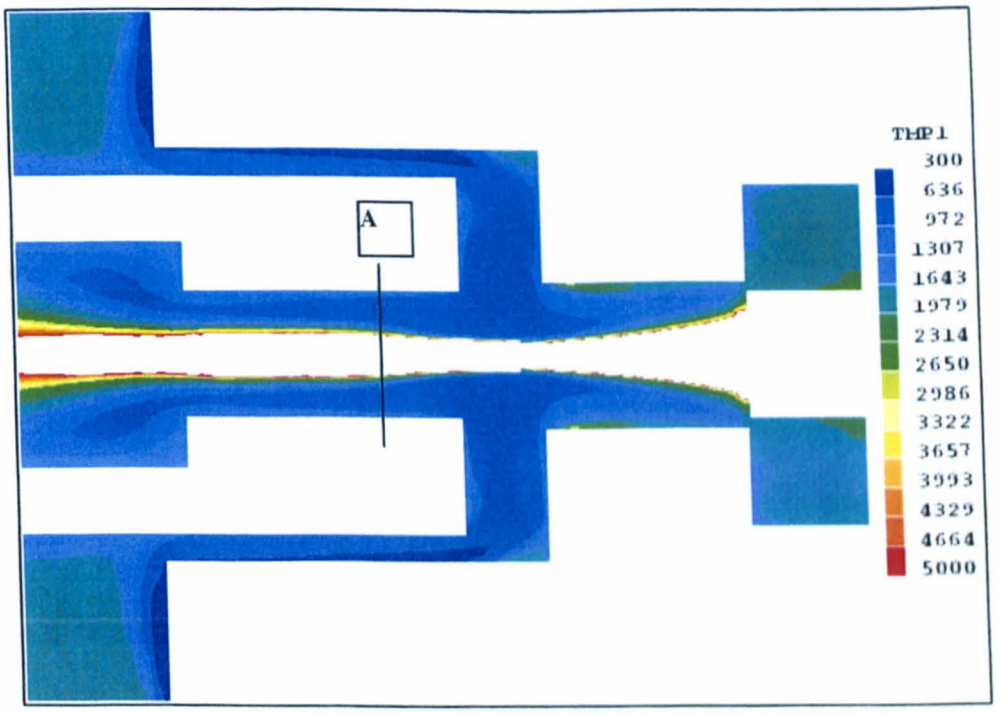

Figure 6.24: Temperature field at 32.17ms with a current of 3.1kA in the case with a shorter heating channel length.

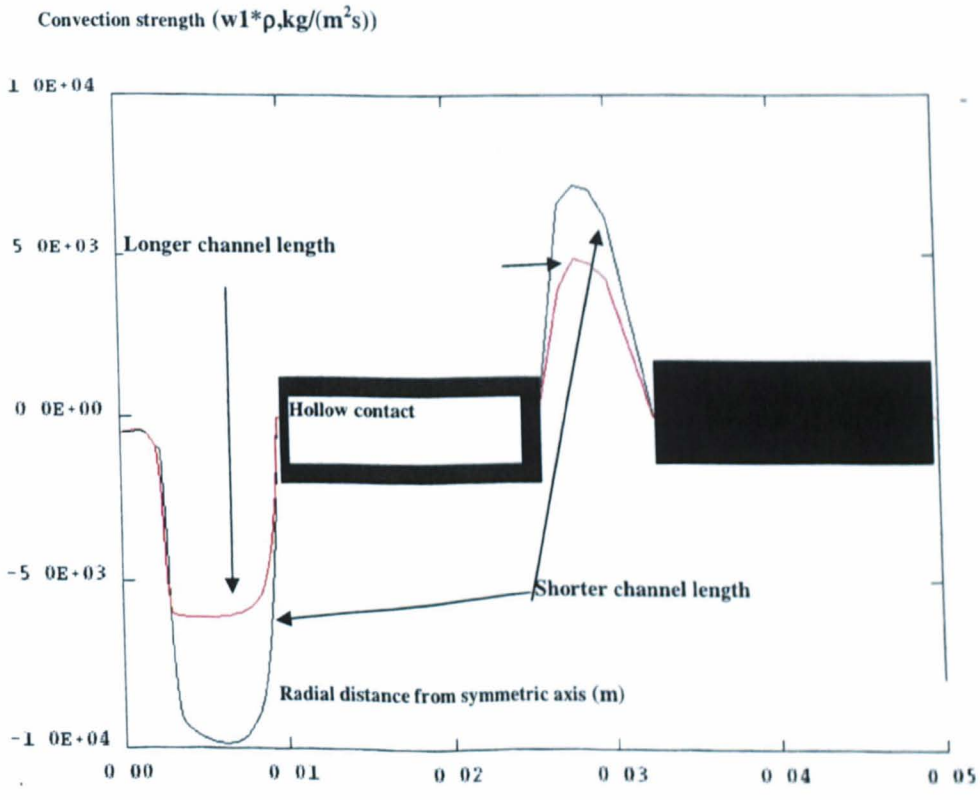

Figure 6.25: Radial profile of the product of density and axial velocity shortly before current zero at the interface of auxiliary nozzle and hollow contact. See line *A* in figure 6.24. Longer channel length is from case DV-LL2 and short channel case is from EV-SL1.

Case ID	Relative channel length (horizontal dimension) to reference case	Relative channel width (vertical dimension) to reference case	Relative total volume (chamber + channel) to reference case
REF	1.000	1.000	1.000
Channel-EV-ST1	1.000	0.400	0.966
Channel-EV-ST2	1.000	0.600	0.983
Channel-EV-LT1	1.000	1.319	1.002
Channel-DV-LT1	1.000	1.319	1.093

Table 6.3: Dimensions of the Group 3 cases: ST - small thickness; LT - large thickness

pressure drop caused by shrinkage in the arc size. As a result, the pressure minimum is higher than that in the reference case. Case DV-LT1 has the same channel dimensions as Case EV-LT1 but its chamber and channel total volume is slightly larger. These two cases have similar results with the latter case having a slightly lower pressure peak due to its larger volume.

Although the results here seem to be fairly straightforward, there are implications for the choice of the cross section of the heating channel. The requirement that the minimum cross section of the heating channel is equal to the minimum flow cross section of the nozzle-contact gap is based on quasi-steady state considerations. As results so far suggest, the formation of pressure field in the contact gap is highly transient shortly before the final current zero. To achieve optimum design, the heating channel cross section may need to be different from that of the nozzle exit. The optimised value should be obtained by computer simulation.

6.3.5 Group 4: Addition of internal structures to heating chamber

The simulation performed in this group attempts to identify the effectiveness of adding internal flow guide structures in order to influence the pressure and temperature environment shortly before current zero. Altogether six cases have been simulated with different internal structures added. The details are shown in figure 6.27 and Table 6.4.

Results with internal structures in the heating chamber are shown in figure 6.28. It can be seen that, with the E-shaped or inverse E-shaped structure, the effective volume of the heating chamber is substantially reduced. The gas in the heating chamber has higher temperature, as shown in figure 6.29) for temperature of gas around the arc which is from the heating chamber at 380μs before current zero, at current 4.8kA. The

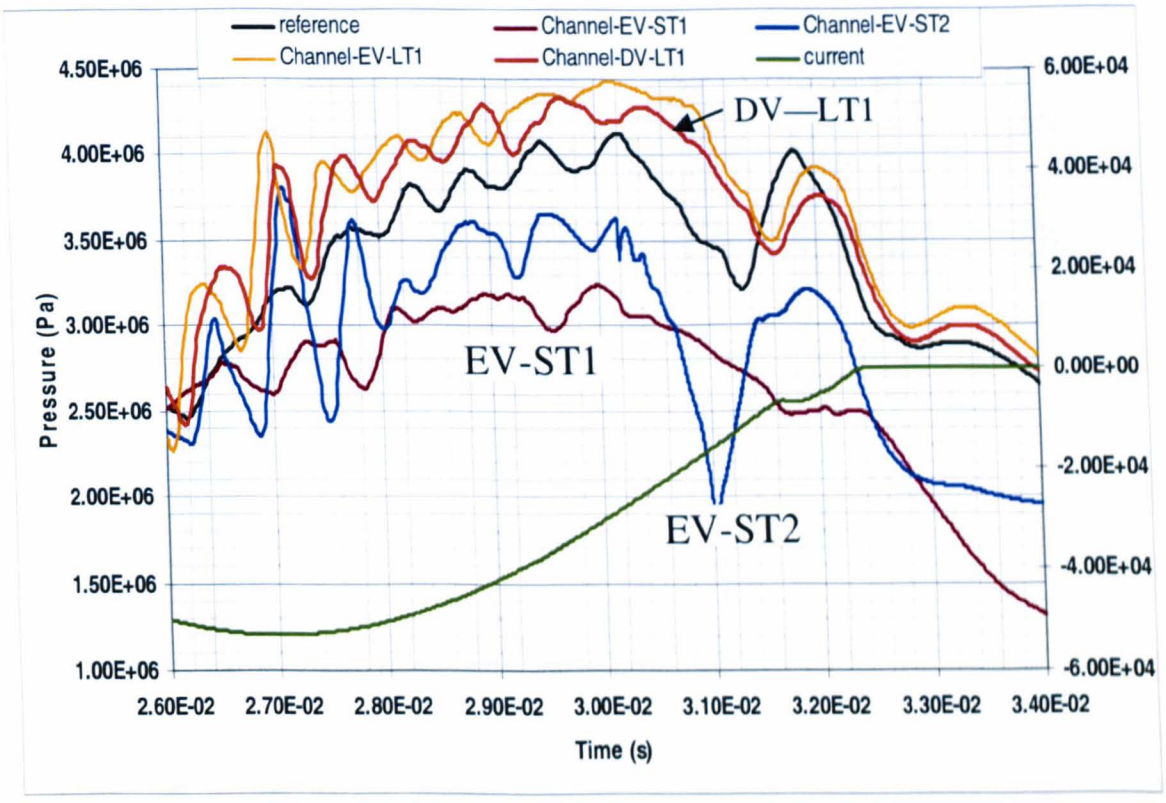

Figure 6.26: Pressure at Point *D* in figure 6.1 for all cases in Group 3.

Case ID	Description of internal structure	Relative total volume (chamber + channel) to reference case
REF	-	1.000
FG-DV-Sshaped	Flow guide with shape similar to "S"	0.770
FG-DV-Eshaped	Flow guide with shape similar to "E"	0.752
FG-DV-InverseE	Flow guide with shape similar to inverted "E" in the horizontal direction	0.758
FG-DV-2Rings	2 rings with same diameter as the outer boundary of the heating channel	0.978
FG-DV-3Rings	3 rings with same diameter as the outer boundary of the heating channel	0.981
FG-DV-4Rings	4 rings with same diameter as the outer boundary of the heating channel	0.978

Table 6.4: Dimensions of the Group 4 cases: FG stands for flow guide; DV is for different volume of heating chamber and channel from the reference case.

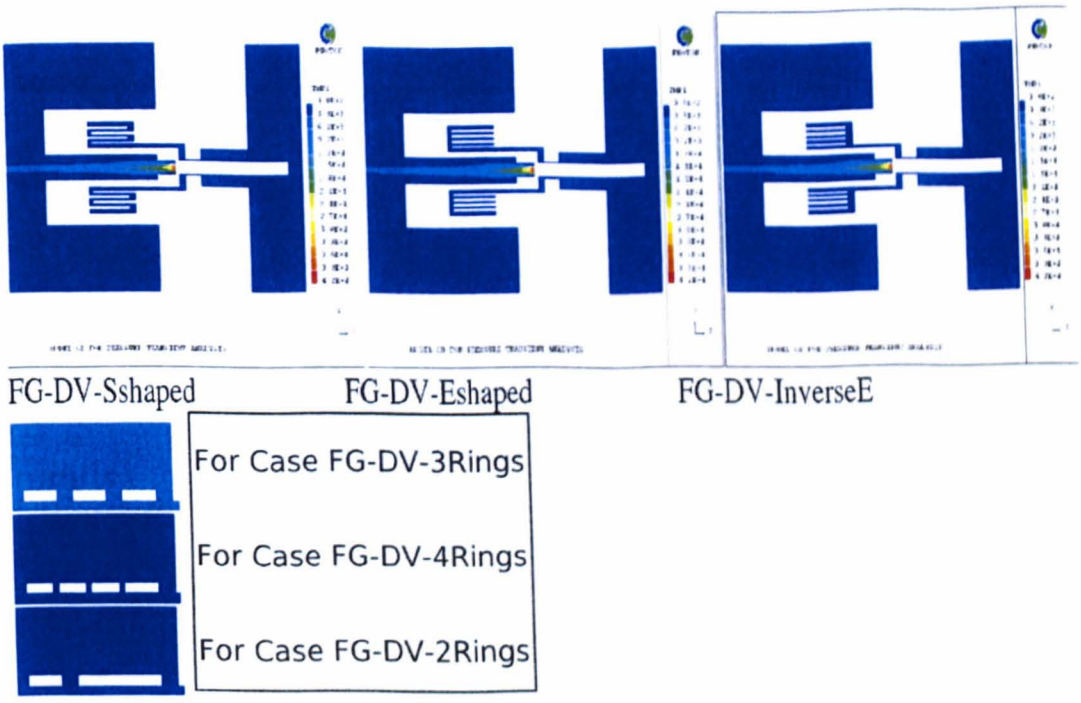

Figure 6.27: Diagram showing the cases with different flow guides in the heating chamber

pressurised chamber cannot sustain a high pressure after flow reversal. As a result, the pressure in the contact space drops continuously to a low level. The different pressure decay rate is due to the difference in the structure. Case DV-Sshaped behaves in a similar way but its higher pressure at 30ms is due to its unique shape (resembling an extended heating channel).

Results in this group also suggest that the annular rings change the flow/mixing pattern and as a consequence more pressure drop in the arcing space is observed and the pressure recovery process is shifted to a later stage. This shift is advantageous to the thermal interruption process because of the high pressure and low temperature (figure 6.29) in the region surrounding the arc. Care however must be exercised when translating the information to circuit breaker design because the conclusion here is drawn on this single simulation. More simulations need to be performed in future to check if the conclusion arrived here can be extended to the arcing process in other switching duties. The results also require experimental verification which is not available at this stage.

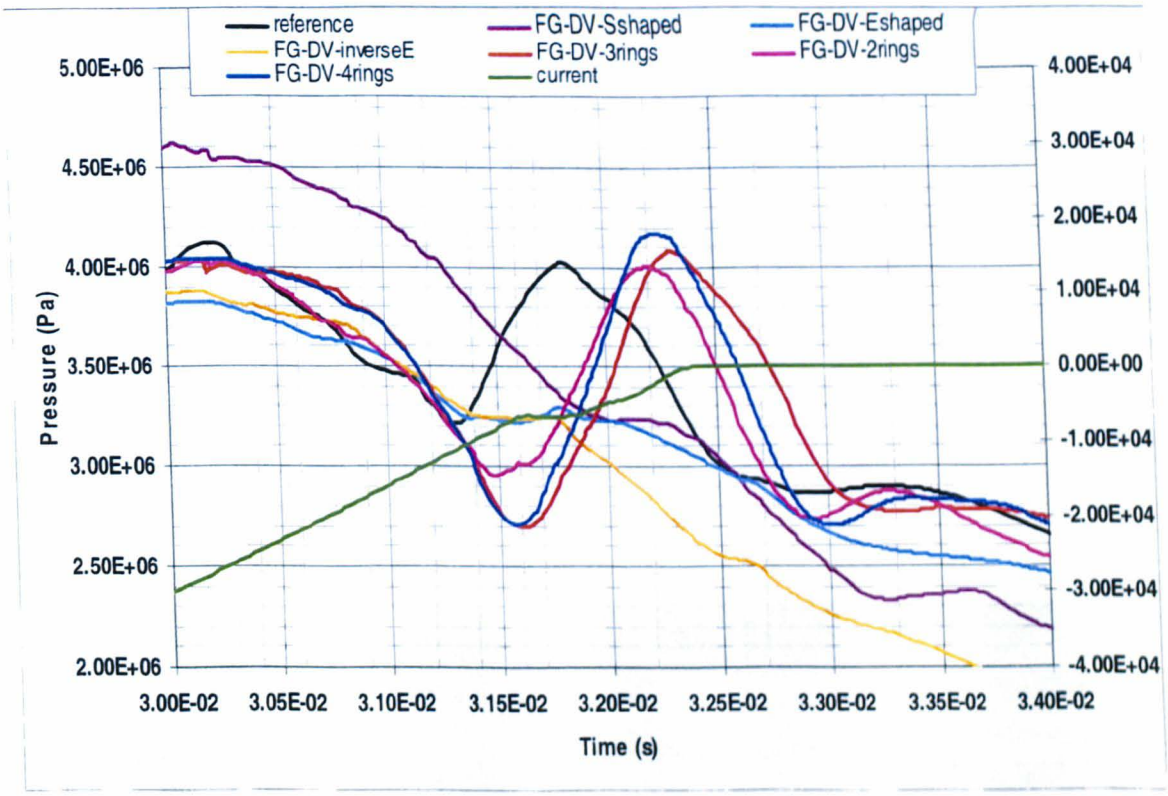

Figure 6.28: Pressure variation at Point D in figure 6.1 when internal structures are added to the heating chamber, at current 4.8kA, 380μs before current zero.

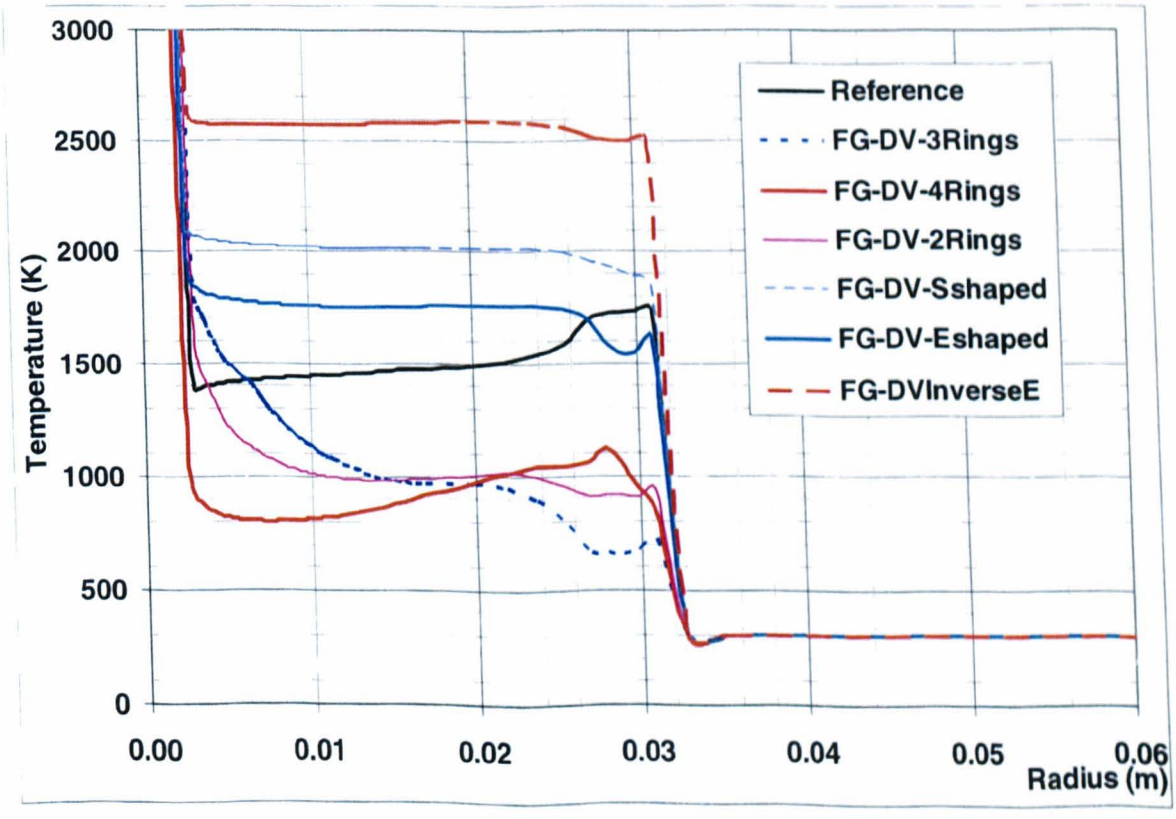

Figure 6.29: Temperature distribution along a line passing points C and D in figure 6.1, at current 4.8kA, 380μs before current zero.

Case ID	Description of internal structure	Relative total volume (chamber + channel) to reference case
REF	-	1.000
CFin-DV-SF1	Flow guide with shape similar to "S"	0.998
CFin-EV-SF2	Flow guide with shape similar to "S"	1.002
CFin-DV-LF1	Flow guide with shape similar to "S"	0.996

Table 6.5: Dimensions of the Group 5 cases. Cfin stands for extra fins in the heating channel, DV for different volume size, whereas EV for equal volume size, SF for short fin length and LF for long fin length.

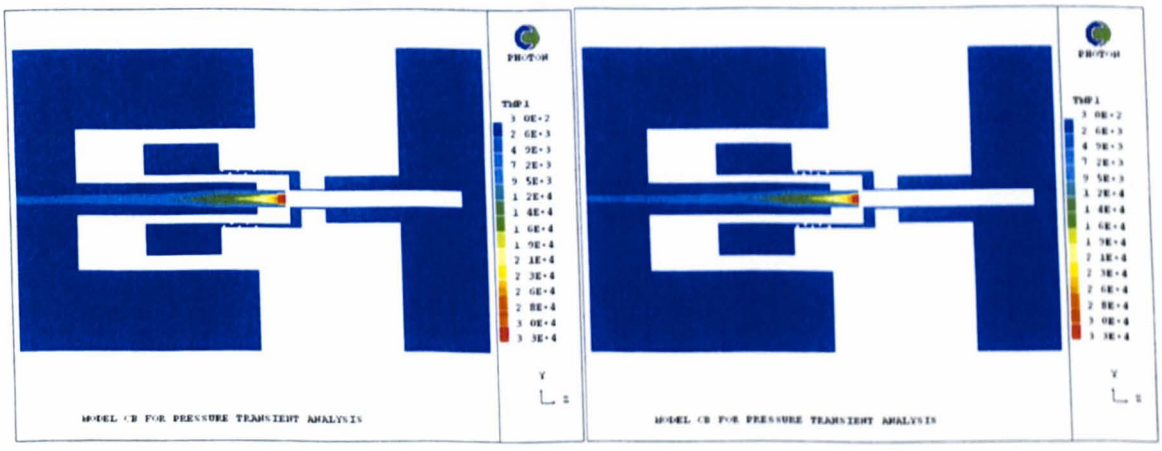

Figure 6.30: Diagram showing the cases with different shape of fins in the heating channel. Left - SF1 and SF2; right - LF1.

6.3.6 Group 5: Addition of internal fins to the heating channel

This set of simulations is carried out with the intention to examine if the pressure transient in the channel as well as in the arcing space can be smoothed by adding blockages to the flow. The simulation is based on ideas proposed by the industrial collaborators. The details are given in Table 6.5 and figure 6.30.

Adding fins to the heating channel effectively reduces the flow cross section thus increases the blocking effect. As a result the peak pressure in the heating chamber is reduced (figure 6.31). This is similar to the case channel-EV-ST1 in figure 6.26 with a thinner channel. The reduction in the cross section prevents adequate mass flow towards the contact space after flow reversal. As a result the pressure in the arcing space drops continuously to less than 25 bar at current zero. With the larger fins in

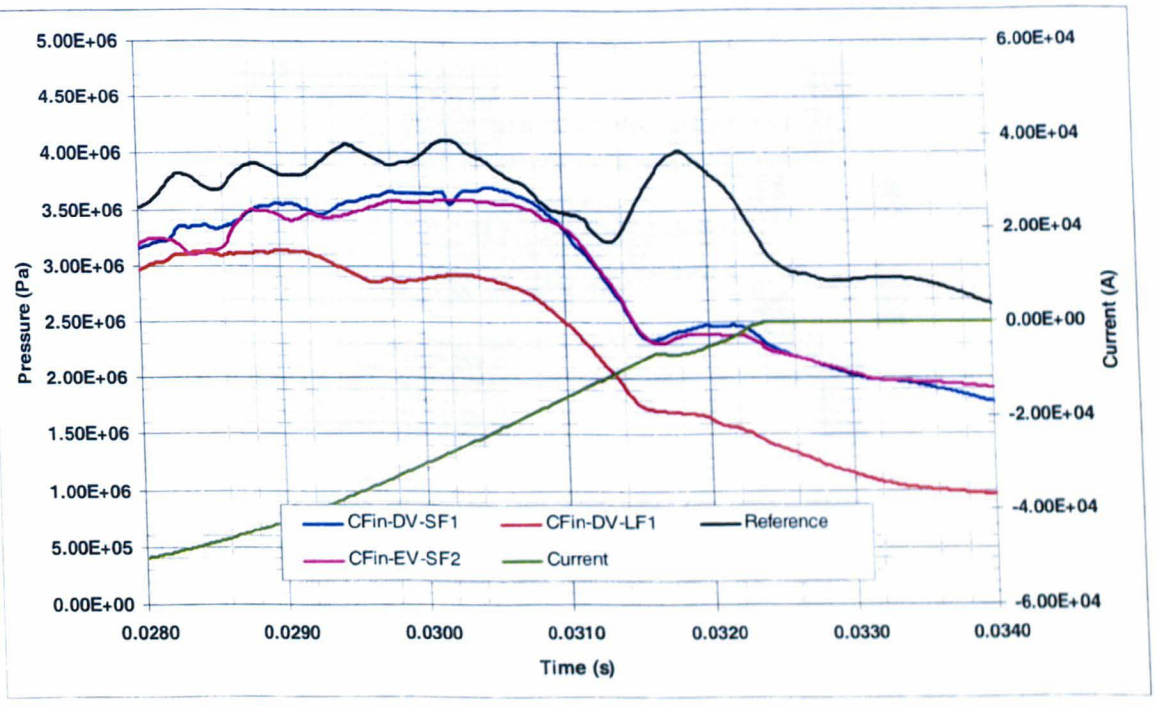

Figure 6.31: Pressure variation at Point D in figure 6.1 when fins are attached to the heating channel surface.

case DV-LF1 the pressure drops to 15 bar at current zero.

6.4 A Proposal to Smoothen the Pressure Fluctuation: Addition of a Buffer Volume

From the above sections it is clear that the pressure fluctuation shortly before current zero is due to two important phenomena in the flow reversal period. Firstly, as current decreases, the arc size shrinks, creating a vacuuming effect to reduce the pressure in the arcing space. Secondly, the relatively cold gas exiting from the heating chamber via the heating channel cannot efficiently supply gas to compensate for this pressure drop. The simulations in this group is used to assess the efficiency of a proposed structure of creating a smooth pressure variation in the arcing space before current zero. The new structure is shown in figure 6.32. With the help of the buffer volume, gas will be supplied to the arcing space more promptly where simulation results show that excessive pressure fluctuations has been avoided due to the cancellation of the resonance by the two different paths travelled by the gas.

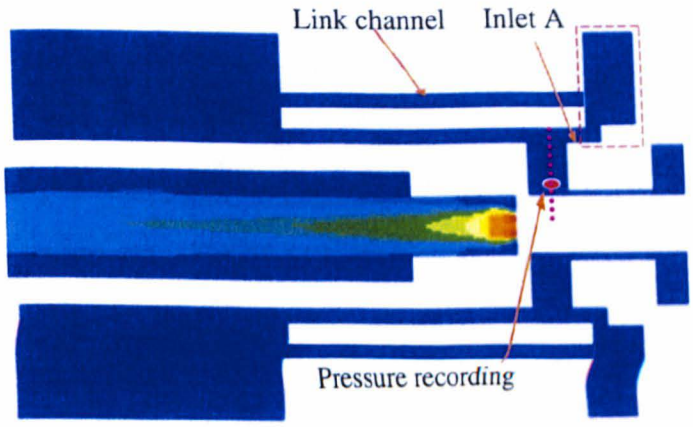

Figure 6.32: Diagram illustrating the idea of a buffer volume.

6.4.1 Typical results with a buffer volume

Results in figure 6.33 show the effects of adding a buffer volume to the arcing chamber. The link volume shown in figure 6.32 is not present in these two cases. Case DV-B1 represents the results with the addition of a buffer volume without changing the dimensions of the remaining part of the arcing chamber. Case EV-B2 reduced the volume of the heating chamber so that the sum of the heating chamber and buffer volume is equal to the chamber volume in the reference case. The most interesting effect is that with the buffer volume the pressure oscillation is shifted to an earlier stage and the thermal interruption process takes place in a period when pressure in the arcing space decays slowly. The temperature distribution of the cases is given in figure 6.34. It is clear that with the buffer the temperature is slightly higher than that in the reference case because part of the hot vapour is stored in the buffer volume. The temperature however is still lower than the dissociation temperature of SF_6.

In the case labelled Linked buffer-EV-blocked, a link channel is added between the original heating chamber and the buffer volume but the inlet A shown in figure 6.32 is blocked for the whole simulation. The peak pressure rise is lower due to the increased volume of the heating chamber. The gas temperature around the arc is higher is due to the fact that the original cold SF_6 gas in the heating chamber is driven into the added link channel thus after flow reversal gas flowing towards the arcing space has a higher temperature. This means closing inlet A makes the pressurisation process much less efficient. This can be easily seen if we compare with the other two cases where inlet A

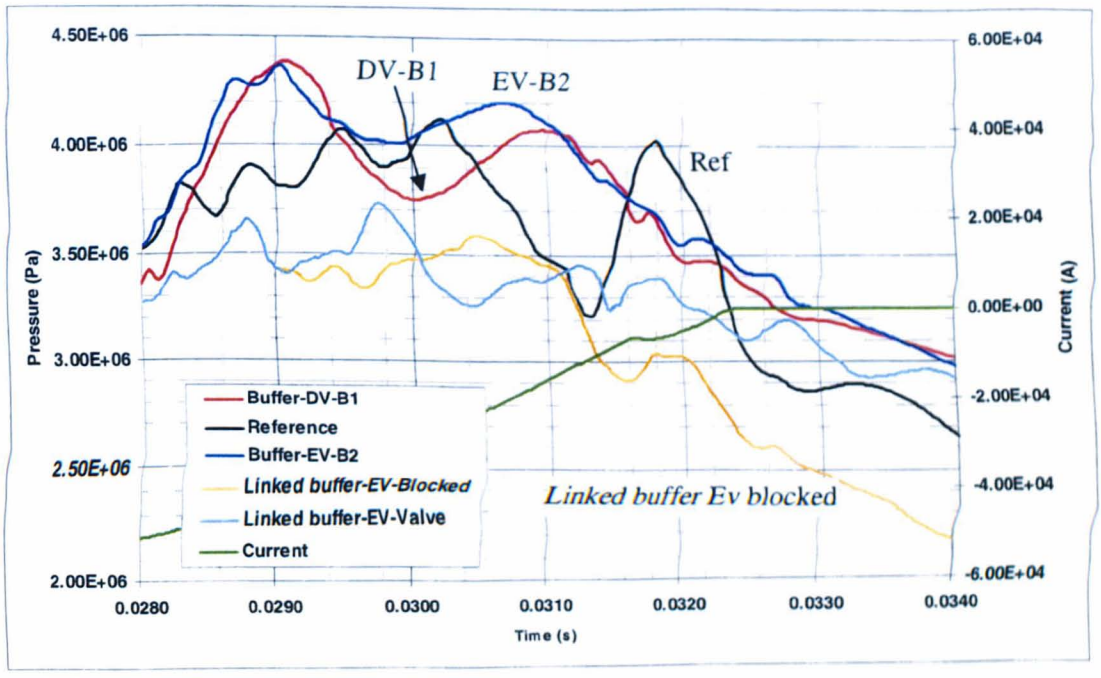

Figure 6.33: Pressure variation at Point D in figure 6.1 when a buffer volume is added to the arcing chamber.

is kept open.

Another case (linked buffer EV-valve in figure 6.33) has also been tried where the inlet A is numerically opened at 29.0ms. It could be seen that the pressure goes up slightly at 29.8ms and then drops. The opened inlet A supplies extra mass to the arcing space. The pressure at current zero is substantially higher than that when inlet A is always blocked but still lower than the cases (DV-B1 and EV-B1) where inlet A is always opened but without the link channel. Another important outcome from this simulation is that with a controlled open of inlet A at appropriate time the cold SF_6 gas can directly fill the contact gap when necessary. As a result, the temperature is very low, typically 500K, as shown in figure 6.34. The gas density in this case is the highest in all the cases in this group. The idea of adding a buffer has some advantages as discussed above although practically there may be difficulty implementing it. The idea also needs experimental confirmation in future when temperature measurement is possible in the heating channel.

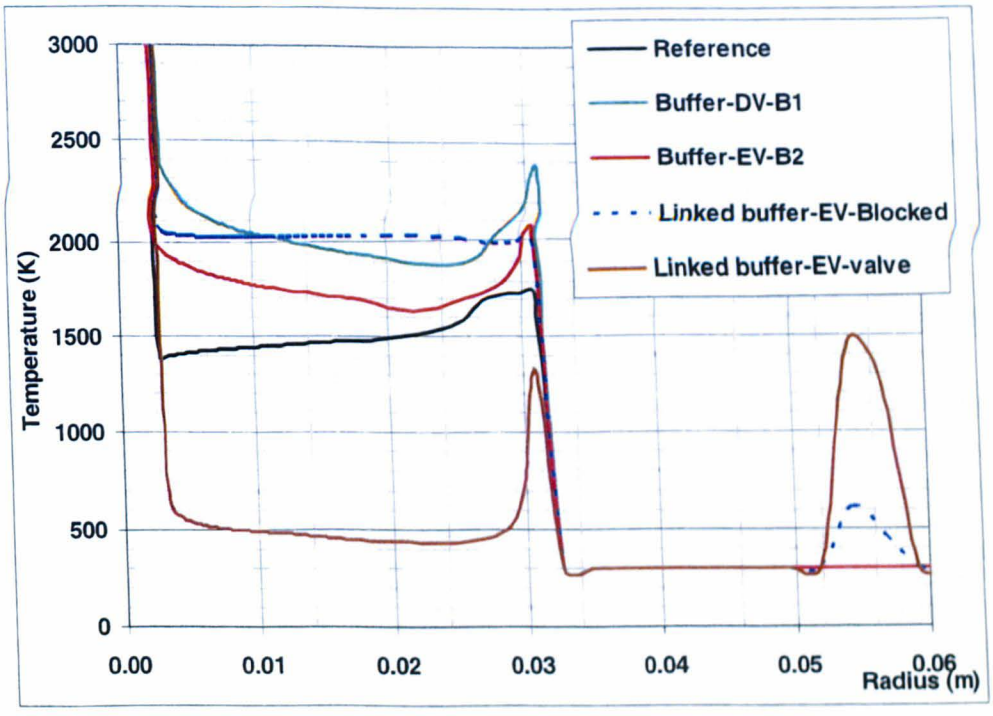

Figure 6.34: Temperature distribution shortly before current zero along a line pass points *C* and *D* in figure 6.1 for the additional buffer volume case.

6.4.2 Pressure fluctuation with the buffer volume for different arc durations

Simulation in Groups 1 to 5 is based on the same current waveform as that in the reference case. ABB has indicated that thermal interruption with shorter arc duration of around 10ms is a more difficult case in switching duties due to the relatively short contact gap. It is thus useful to assess the pressure and temperature variations for a selected case with shorter arcing duration.

A good design should give optimum flow and thermodynamic conditions at current zero for all possible switching duties. Two cases were selected to assess the situation at shorter or longer arc duration. For the case with a buffer volume, results in figure 6.35 show that for shorter (than the reference case) arc duration, the pressure variation (not the pressure amplitude) behaves in a similar way. The only difference is that for the shorter arc duration the pressure at current zero with a buffer volume is about 2 bar lower (compare with the corresponding curve in figure 6.36) than that of the reference geometry, while in the longer arc duration case the pressure at current zero with a buffer volume is 2 bar higher than the reference case (figure 6.37,

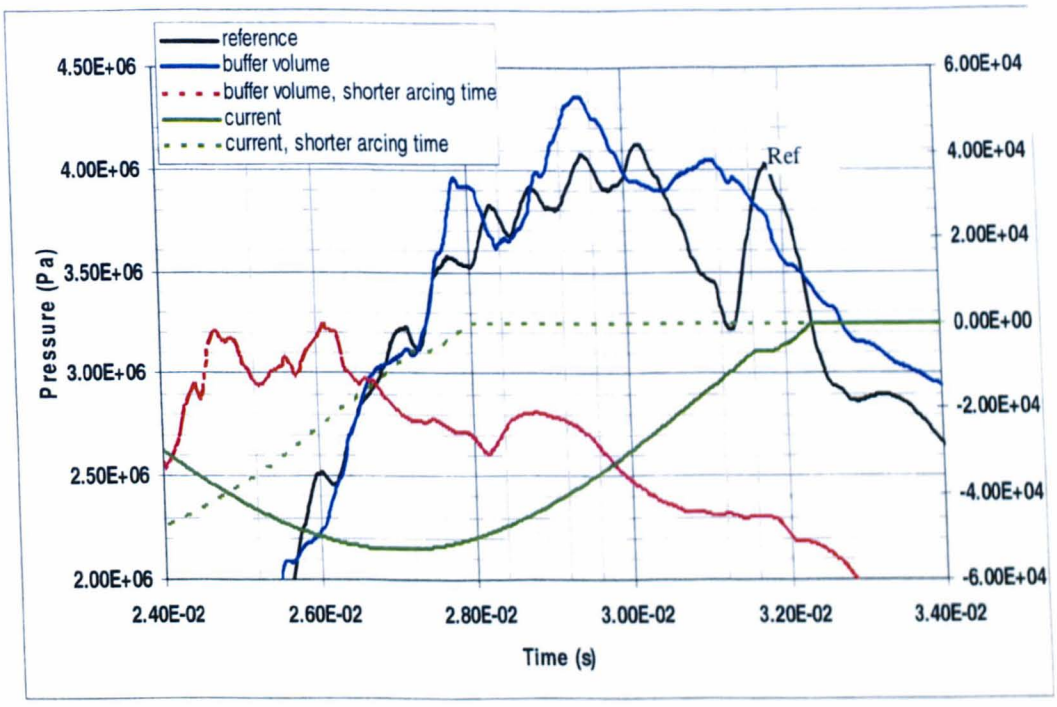

Figure 6.35: Pressure variation at Point *D* in figure 6.1 when a buffer volume is added to the arcing chamber.

the pressure without the buffer volume for longer arc duration is not plotted). The temperature distribution is given in figure 6.38. In all cases the temperature is below 2,000K.

With a longer arcing duration, the peak current is reached after the main nozzle is unblocked. Since gas is exhausted through both the hollow contact and the main nozzle, pressure in the arcing space has a very flat profile from 25ms to 32ms and then it smoothly decays (see curve buffer -DV-B1, long arcing time in figure 6.37). From the above discussion, it is clear than with a buffer volume, the pressure field in the arcing space does not experience sharp drops immediately before the final current zero. This applies to all three cases with different arcing times. The advantage of using such a buffer volume is therefore apparent.

6.5 Sensitivity of Flow Field and Temperature in the Arcing Space on the Shape of the Moving Contact

At the end of section 6.3.1 it was noted that results from Groups 1 to 5 were obtained using a slightly smaller flow cross section between the moving contact and the main

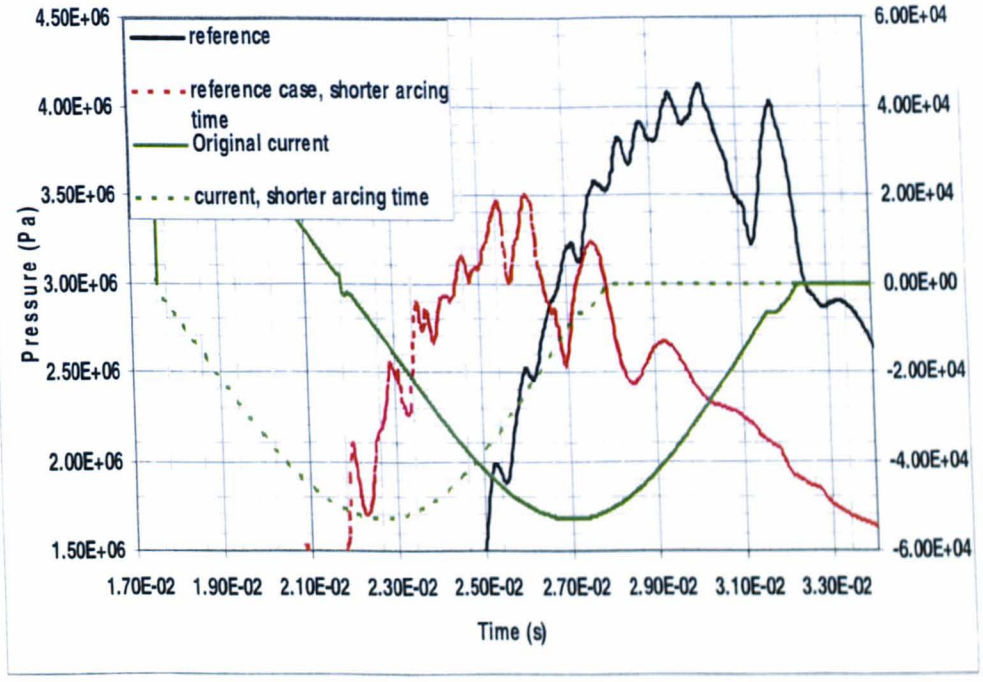

Figure 6.36: Pressure transient at Point *D* in figure 6.1 for the original reference case and that with exactly the same geometry but a shorter arcing duration. In the short arcing duration case the current follows a sinusoidal waveform starting at 17.59ms with a peak current of 53kA.

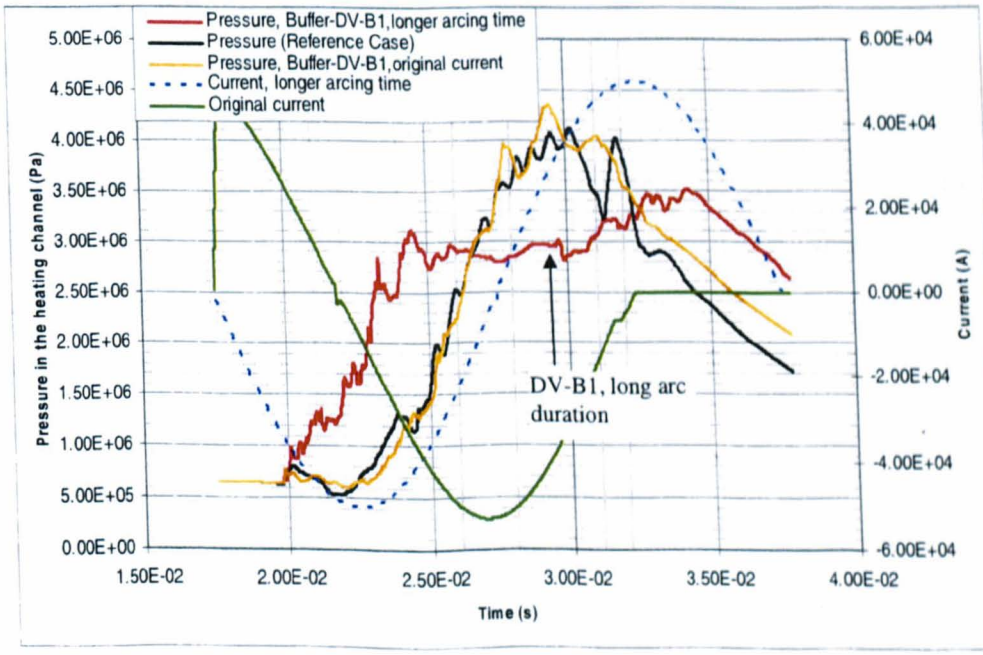

Figure 6.37: Pressure transient at Point *D* in figure 6.1 for the original reference case and that with exactly the same geometry but a longer arcing duration. In the longer arcing duration case the current follows a sinusoidal waveform starting at 17.59ms with a peak current of 53kA.

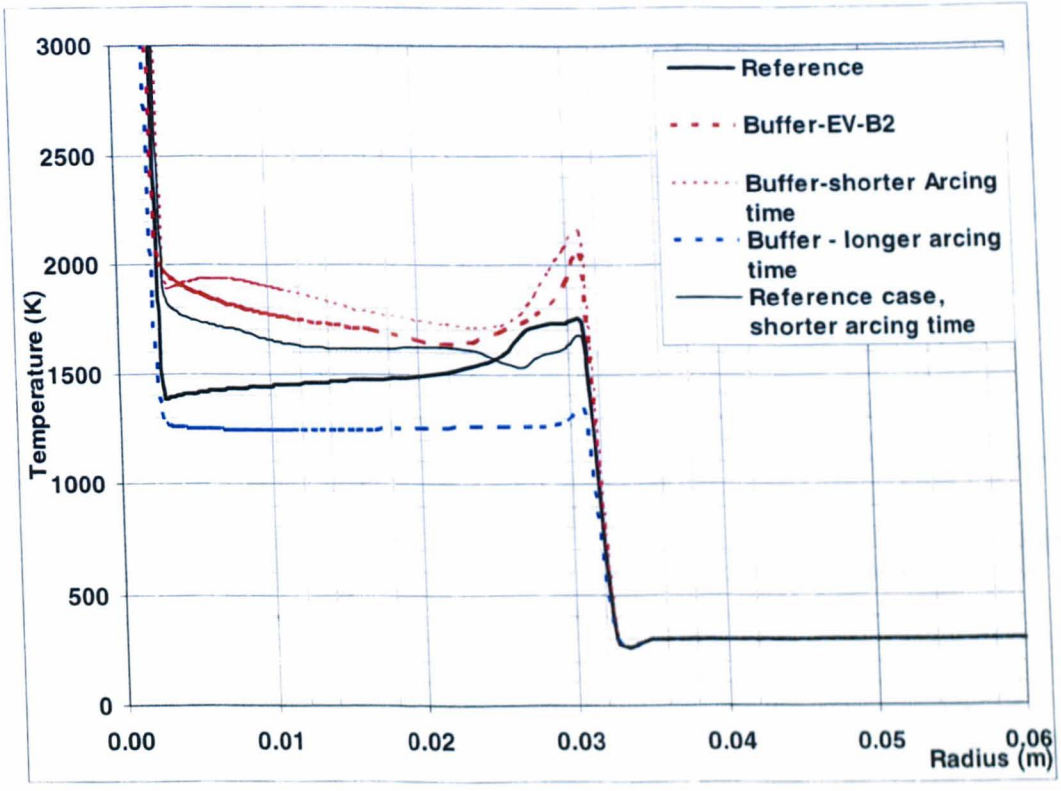

Figure 6.38: Temperature distribution at 32.02ms along a line pass points C and D in figure 6.1 for the cases buffer volume with different arcing durations.

flat nozzle when the moving contact reaches its maximum travel. The nozzles and heating channel have right-angled tip corners (a rectangular shape for the cross section) and the moving solid contact has a flat tip. The effective flow area at current zero between the solid contact and the main nozzle is smaller than that in the real circuit breaker. It is therefore necessary to study the influence of this difference on the pressure transient in the arcing space. In this section simulation on a selected case with an effective flow area equal to that in the real circuit breaker has been carried out. Results in figure 6.39 indicate that increasing the flow area to a value that is equal to that of the real circuit breaker does not make much difference to the pressure transient. This is because for the current waveform and contact travel used, the solid contact starts to clear the main nozzle just 0.4ms before the final current zero. Since the contact continues to move until 35.5ms, it is expected that this difference in flow area will not substantially affect the results in this report hence the conclusions drawn will be valid.

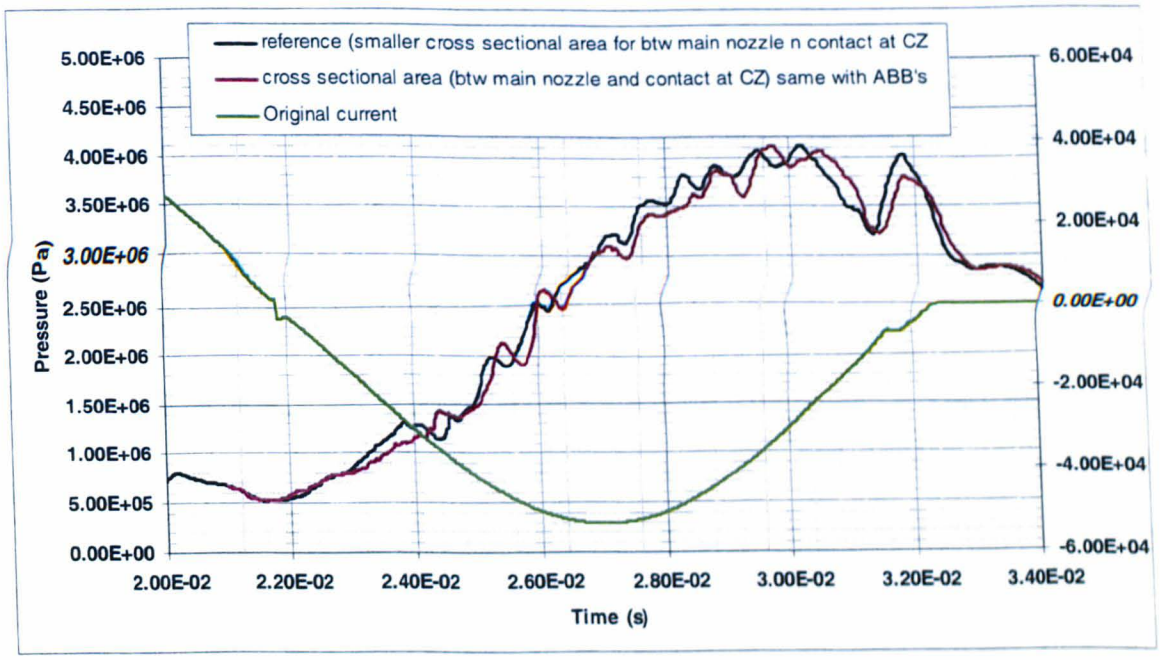

Figure 6.39: Pressure transient at Point D in figure 6.1 for the original reference case and that with a larger effective flow area that is similar to that in the real *170PM40* circuit breaker.

6.6 Main Findings and Discussion of Their Implications

The systematic studies performed in this report lead to some important findings which are of interest to circuit breaker designers and analysts:

1. With the geometry used, pressure oscillation always occurs in cases where the arcing duration is moderate (15ms or less). In these cases the main nozzle is blocked by the solid contact *when the pressurisation* of the heating chamber takes place. The shrinkage of arc column results in a pressure drop in the arcing space which is then compensated by gas flow from the heating chamber. Adding internal structures or changing the heating channel length can substantially affect the profile and timing of this oscillation.

2. Optimum design in terms of the global pressure and temperature environment in the arcing space should aim at an efficient and timely supply of gas into the arcing space when the current decreases rapidly towards its final zero. This could be realised by, for example, using a larger channel thickness or using a buffer volume which is close to the arcing space.

3. In shorter arcing duration cases (10ms), the pressure build-up in the heating chamber is lower and gas is mainly exhausted through the hollow contact. As long as the main nozzle is blocked, strong pressure oscillation exists. Effort on optimum design of this type of auto-expansion circuit breakers should therefore be focused on the short arcing duration switching duties with high peak currents.

4. With long arcing duration the main nozzle is normally cleared when pressurisation in the second current loop takes place. Pressure variation in the arcing space before the final current zero is much smooth. Therefore the problem associated with pressure transient in long arcing duration switching duties is not so critical.

5. Apart from pressure distribution in the arcing space, the temperature of the gas from the heating chamber following flow reversal is an important parameter. Together with pressure field, it determines the gas density which influences the ability to remove energy from the contact space. Measurement of gas temperature in the heating nozzle will give direct evidence on how realistically the modelling results represent the real situation.

6.7 Summary

Computer simulations of the arcing process in a model circuit breaker with different geometry and dimensions were carried out and typical results analysed. Results show that, for moderate or short arcing duration cases (15ms or less) the flow field and distribution of thermodynamic parameters in the arc surrounding region change substantially shortly before the final current zero. This is caused by the finite response time of flow reversal associated with rapid current decrease towards current zero. It has been shown that design parameters can significantly affect the thermodynamic environment. Systematic studies using computer simulation can help identify key influencing design parameters and experiment with new design ideas.

Pressurisation of the heating chamber relies on pumping thermal energy into the heating chamber. The thermal energy is carried by PTFE vapour that is heated up by arc radiation or originated from the arc region. The temperature of the vapour when it

flows into the heating channel largely depends on the arc model used. So far there are no experimental results available for verification of vapour temperature. Therefore temperature measurement of PFFE or PTFE-SF_6 mixture will be a subject of immense interest.

It should be noted that studies on pressure transient only produce information on the global thermal and flow environment in the arcing space for thermal interruption. It does not however produce any quantitative prediction on the thermal interruption capability of the breaker. To make the results in this report more useful to circuit breaker development, a model for the current zero period, which correlates the global environment to the thermal interruption performance is necessary. This is a step that should be taken to make progress in using computer simulation as a design tool for advanced circuit breakers.

Chapter 7

Summary and Future Work

A conclusion is the place where you get tired of thinking.
– Arthur Bloch

7.1 Major Contribution and Achievements

There are two major contributions of the present work in the field of arc modelling. Firstly, the Liverpool arc model was enhanced to simulate the operation of the ABB auto-expansion circuit breaker with complex mechanical mechanisms and simulation results verified by results from no-load pressure measurement and those from short-circuit tests. The second contribution is that it is the first time that a systematic study of the pressure transient phenomenon, which is intrinsic to the operation of auto-expansion circuit breaker, was carried out and the influence of design parameters and arc duration assessed in detail. The mechanisms responsible for the pressure oscillation were identified. Based on the understanding acquired in the present work a novel design of the arcing chamber is proposed which has the advantage of effectively eliminating the pressure oscillation immediately before the current zero.

The present work leads also to the improvement of our understanding of the physical processes involved and to the arc model itself in a number of aspects apart from those mentioned in the above paragraph. For example, the ABB two zone model and the Liverpool model use different values of ablation energy and PTFE vapour temperature while the predicted pressure rise in the heating chamber for the same test case is rather similar. The underlying physical mechanisms leading to this similarity are clearly explained thus avoiding unnecessary misunderstanding or confusion. The radiation model used in the Liverpool arc model was improved to deal with non-

monotonic radial temperature profiles, which leads to considerable improvement in computational stability.

Detailed mass and energy balance in the arcing space and heating chamber has been carried out and contribution from all processes clearly shown in detail. This helps to clarify the dominant processes that are responsible for pressurisation of the heating chamber at high current. The other aspect, which is computationally very important, is the modelling of moving pistons and valves. An appropriate numerical scheme has been developed to ensure mass, momentum and energy are conserved in the process of moving the solid parts and opening or closing the valves. The numerical scheme has been verified using no-load pressure measurement and theoretical isentropic compression theory. This has the important implication that the arc simulation tool developed at Liverpool has reached a stage that the operation of the whole circuit breaker can now be simulated, thus making the tool much more useful in aiding practical circuit breaker design.

7.2 Summary

Computer simulation of the operation of an auto-expansion circuit breaker (also known as the self-blast circuit breaker) has been carried out. Due to the very high power level encountered in such a breaker the arc interacts intensely with its surroundings. The operation of such a breaker is extremely complex and its performance depends on the whole arcing history as well as a number of geometric factors characterising the geometry of the interrupter.

The mathematical model upon which the computer simulation is based encompasses all important physical processes occurring in such a breaker. These processes include convection, turbulent enhanced momentum and energy transport, radiation transport, radiation induced PTFE nozzle inner face ablation, the turbulent diffusion of PTFE ablated vapour and the effects of the Lorentz force produced by the arcing current interacting with its own magnetic field. Thus, the arc and its surrounding gas are described by the time averaged Navier-Stokes equations modified to take into account the Lorentz force and radiation transport. The closure of these equations requires a PTFE mass concentration equation, radiation transfer model, the relevant Maxwell's

equations, and supplementary information in a tabulated form for the equation of state and transport properties. These equations are solved by a commercial CFD package, PHOENICS, for the computational domain, which is an approximate representation of the auto-expansion breaker provided by ABB. PHOENICS has been chosen for the robustness of its equation solver, its easy integration with the user defined subroutines, and its ability to cope with moving boundaries and shock waves. In addition, PHOENICS provides a very good graphic representation of results. The movement of a piston and a contact and the operation of an over pressure valve are considered.

The no-load flow and pressure rise were first investigated and the simulated results were compared with those derived from analytical solutions for simple experimental situations and with the ABB test results. Good agreement has been obtained between the prediction and test results, thus increasing confidence in PHOENICS.

The operation of the ABB breaker under specified arcing current was then simulated for almost the whole arcing period. Emphasis was given to the high current arcing period for which the current was assumed to be no less than 1kA. Thus, the current zero period was excluded. The results indicate that Lorentz force has a profound effect on the flow field as well as the arc shape. The advantage of auto-expansion breaker is the use of arc energy, through radiation induced PTFE nozzle ablation, to create the right flow environment at current zero for arc thermal extinction and dielectric recovery. The pressure built-up in the heating volume relies upon the hot PTFE vapour generated by the auxiliary PTFE nozzle and in the arcing volume between two contacts to mix with the cold SF_6 in the heating volume. When the current decreases toward zero, the temperature within the arc volume decreases rapidly. To maintain the mass conservation in the arc volume gas needs to be supplied into this region from the heating volume as demanded by the rapid increase in gas density due to a decreasing temperature.

It was found that the radiation transport model, especially radiation absorption in the region between the edge of the arc and the inner surface of the nozzle, has a decisive effect on the rate of PTFE ablation, thus affecting the $V - I$ characteristics of the arc, the pressure, velocity and temperature fields within the interrupter. The radiation model employed is a one-dimensional, semi-empirical model, which gives an account of the heating of the entrained PTFE to a temperature equal to that at the

arc edge. When the predicted arc voltage is compared with that of measured, the agreement in the first current loop is very good. However, the predicted arc voltage is in general higher than that measured in the second current loop. For the worst case the discrepancy is up to 25%. The predicted pressure at current zero is within 10% of the test results. On the whole that arc voltage agrees with the test results within 15% of error. Such a prediction is considered as satisfactory. The discrepancy between the prediction and test results is expected in view of the lack of arc plasma properties, especially electrical conductivity, for pressures above 10 bar (which is the pressure range encountered in the second current loop) and the uncertainties in the values of the parameters introduced by the radiation model. The computer simulation based on the arc model presented in this thesis does provide a breaker designer a useful tool for the visualisation of the interaction between various processes occurring in the interrupter and the effects of changing a design parameter.

It has been found that the pressure in the arcing volume changes by a wide margin during arcing. The thermal interruption of an arc and its subsequent dielectric recovery depend on the pressure and temperature fields within the arcing volume between the two contacts at current zero. Pressure fluctuation at current zero results in a scatter of thermal interruption and dielectric recovery performances. Large pressure variation is therefore not desirable. Optimisation of design parameters is necessary in order to avoid pressure variation and to ensure maximum pressure and lowest temperature possible in the arcing volume. Pressure and temperature fields in the arcing volume at current zero depend on the supply of the gas from the heating volume. Thus, optimum design is directly linked with the design of the heating volume and the link channel between the arcing volume and the heating volume. Based on the knowledge and understanding derived from this study a new design has been simulated which produces very promising result in smoothing the pressure fluctuation in the arcing space.

Pressure and temperature fields at current zero depend on the whole arcing history as well as the contact movement which determines the gas exhaust passage. It therefore depends on the switching conditions such as the arcing time. Arcing processes with different arcing time (altogether three cases with different arcing times) were also performed to assess the effect of the new design. In all the cases it has been

shown that with the addition of a buffer volume the pressure smoothly changes in the period approaching the final current zero.

Extensive studies have been carried out to assess the effects on the pressure in the arcing space by changing the design parameters, which include the size and dimension of the heating volume and its internal structure, the size of the channel link (especially its length), and minor structures in the heating channel. Results have shown that the length and cross section of the heating channel have significant influence on the pattern of pressure fluctuation in the arcing space in the period shortly before the final current zero. It is therefore a key design parameter towards reliable performance of the circuit breaker.

In summary, the three objectives stated in chapter 1 have all been achieved by work presented from chapters 2 to 6.

7.3 Future Work

The performance of an auto-expansion circuit breaker depends on a number of interlinked physical processes. Although the arc and its surrounding gas can be described by the simplest model, a turbulent, electrically conducting fluid in LTE, the material properties and the values of some physical parameters in the model depend on the microscopic processes at the atomic and molecular level. At present, there is still a shortage of reliable, experimentally measured collision cross section data for the calculation of transport properties and radiation transport. It is unlikely in the foreseeable future that the required experimentally measured collision cross sections for SF_6 and for a mixture of SF_6 and PTFE will be available for the computation of transport data. It is also not possible to devise a simple experiment to verify the published transport properties. It appears that we will have to live with the uncertainties in the transport data used for an arc simulation and accept that an error of 15% between prediction and test results are acceptable. Even for a commonly used gas such as SF_6 published electrical conductivity from various sources show differs by 15 to 20%. The suggested investigation is therefore based on the currently available basic atomic and molecular data for radiation transport and other transport phenomena occurring in the plasma.

7.3.1 Detailed radiation transport calculation in a mixture of PTFE and SF_6 and the improvement of approximate radiation transport model

The radiation transport model used in this thesis is based mainly on an understanding of radiation transport in nitrogen and in SF_6 with a monotonic radial temperature distribution. A detailed radiation transport calculation needs to be done for the mixture of SF_6 and PTFE vapour in the whole spectrum range by solving the radiation transport equation for a known monotonic radial profile and for a temperature profile similar to that encountered in an auto-expansion breaker. Such a detailed computation can identify the features of radiation transport and the region where radiation is severely absorbed. Detailed knowledge of radiation transport can be used to improve the semi-empirical radiation transport. Such a detailed radiation transport should also be used to calculate the net radiation emission coefficient for SF_6 and PTFE vapour mixture and to provide basic data for more sophisticated, although still approximate, radiation transport model such as the P1 model and the method of partial characteristics.

7.3.2 Extension of the pressure range for transport properties and consideration of contact erosion

For the investigation of the arcing process in an auto-expansion breaker the pressure range often exceeds 10 bar, and the highest pressure for which the transport data are available for SF_6 and PTFE mixture. The mixture is a complex gas and its composition at a given temperature cannot simply be scaled according to pressure. It is necessary to obtain transport properties data within a larger range. Besides that, the importance of contact vapour on circuit breaker may need to be studied if the design of the arcing chamber results in a substantial amount of metal vapour in the arc region. This also requires the thermodynamic and transport properties of the mixture containing the metal vapour.

7.3.3 Extension of computer simulation to cover current zero period: modelling of arc roots and the likely effects of non-equilibrium ionisation and chemical reactions

In the present investigation the hollow contact is modelled using a transparent electrode. This is a good approximation for high current phase during which arc cross section is large enough to block the hole of the hollow electrode. With such a transparent electrode the arc model when applied to the current zero period cannot predict the extinction peak as observed in tests. When current decreases towards zero the rooting of the arc within the hollow electrode becomes important. The approximate arc rooting model adopted for low voltage circuit breakers may be used [129] for auto-expansion breakers.

The design of an auto-expansion breaker usually ensures that the gas in the arcing volume during current zero is pure SF_6. The temperature during current zero varies rapidly with a characteristic time less than one microsecond. For such a short time scale, ionisation and chemical reactions within SF_6 are unlikely to reach ionisation and chemical equilibrium. The composition and the properties of SF_6 could be very different from those of SF_6 in LTE. In addition, the electron temperature could be substantially higher than that of heavy particles due to increased electric field strength and the energy relaxation time between electrons and heavy particles being comparable with that characterising temperature variation. Thus, LTE model will have to be done for the current zero period.

7.3.4 Improvement for PTFE ablation model

There is at present little understanding of the radiation induced ablation process of solid PTFE. With the lack of photo absorption cross section in SF_6 and in the mixture of SF_6 and PTFE vapour as well as the absorption properties of solid PTFE to radiation at different frequencies the improvement of ablation model will have to rely upon experimental results under well defined arcing conditions. The rate of ablation of solid PTFE could then be derived from the test results and be correlated with the range of arcing parameters relevant to the operation of auto-expansion breakers.

7.3.5 Parallel processing and 3D visualisation

Further refinement of the arc model and the inclusion of the processes hither to neglect will inevitably greatly increase the complexity of the computation and the necessity to extend the present two dimensional model to three dimensions. Such a $3D$ computer simulation will have to be based on parallel processing in order to keep computational time within an acceptable limit in a research and development environment. Data compression will have to be used in order to extract features from the vast amount of simulated results. To this end, attempts should be made to apply available $3D$ visualisation tools for the display and analysis of the computational results.

Bibliography

[1] R.W. Libermann and J.J. Lowke. Radiation emission coefficients for sulphur hexafluoride arc plasmas. *J. Quant. Spectrosc. Radiat. Transfer*, 17:253–264, 1976.

[2] J. Slepian. Extinction of an a.c. arc. *Transactions AIEE*, 47:1398–1408, 1928.

[3] J.D. Yan and M.T.C. Fang. Computer simulation of an electric arc in an auto-expansion circuit breaker. *Proceedings of the 6th International Conference on Optimisation of Electrical and Electronic Equipment, Brasov, Bulgaria*, I:40–44, 1998.

[4] J.D. Yan, C.M. Dixon, and M.T.C. Fang. The effects of swirling flow on arc behaviour in a rotary arc circuit breaker. *Proceedings of the 8th International Conference on Optimisation of Electrical and Electronic Equipment*, 1:105–108, 2002.

[5] J.L. Zhang, J.D. Yan, A.B. Murphy, W. Hall, and M.T.C. Fang. Computational investigation of arc behaviour in an auto-expansion circuit breaker contaminated by ablated nozzle vapour. *IEEE Trans. on Plasma Science*, 30:706–719, 2002.

[6] J.L. Zhang, J.D. Yan, and M.T.C. Fang. Prediction of arc behaviour during the current zero period in an auto-expansion circuit breaker. *Proceedings of the XIV International Conference on Gas Discharges and their Applications*, 1:131–134, 2002.

[7] C.H. Flurscheim. *Power Circuit Breaker Theory and Design (IEE Power Engineering Series)*. Peter Peregrinus Ltd, 1982.

[8] Y. Satoru. History of circuit breaker development and research subjects. *Papers of Technical Meeting on History of Electrical Engineering, IEE Japan*, HEE-02:7–12, 2002.

[9] R.T. Lythall. *The J&P Switchgear Book*. Newnes-Butterworths, London, 7th edition, 1972.

[10] T.H. Li. *Physics and Engineering of High Power Switching Devices.* The MIT Press, 1975.

[11] R.W. Blower. *Distribution Switchgear.* Collins, 1986.

[12] K.K. Leung. Replacement of oil-insulated circuit-breakers/switches by vacuumcounterparts. *International Conference on Advances in Power System Control, Operation and Management*, 1:207–210, 1991.

[13] R.W. Sorensen and H.E. Mendenhall. Vacuum switching experiment of california institute of technology. *Trans. AIEEE*, 45:1102–1105, 1926.

[14] M. Homma, M. Sakaki, E. Kaneko, and S. Yanabu. History of vacuum circuit breaker and recent development in japan. *Proceedings. ISDEIV. XXIst International Symposium on Discharges and Electrical Insulation in Vacuum*, 2:378–383, 2004.

[15] J.D. Cobine. Research and development leading to the high power vacuum interrupter - an historical review. *AIEE Winter General Meeting*, pages 62–67, 1962.

[16] M.P. Reece. The vacuum switch and its application to power switching. *JIEE*, 5:275–279, 1963.

[17] S.C. Cooke and R.V. Klint. A new generation of metalclad switchgear using vacuum interrupters. *IEEE Trans.*, PAS-90:1589–1597, 1971.

[18] T.V. Armstrong. The future of vacuum interrupters in distribution switchgear. *IEE Conf. Publ.*, 83:91–97, 1972.

[19] P. Headley. Distribution switchgear with vacuum circuit breakers. *IEE Conf. Publ.*, 83:98–100, 1972.

[20] G.A. Farrall, J.M. Lafferty, and J.D. Cobine. Electrode materials and their stability characteristics in the vacuum arc. *Trans. Am. Inst. Electr. Eng.*, CE-66:253–258, 1963.

[21] R. Frink and J.M. Kozlovic. A magnetic de-ion air breaker for 750 mva 13.8kv. *AIEE Conference Paper*, pages 57–225, 1957.

[22] F.S. Fay, J.A. Thomas, D. Legg, and J.S. Morton. Development of high voltage air-break circuit breakers with insulated-steel-plate arc-chutes. *Proc. IEE*, 106A:381–391, 1959.

[23] T.F. Brandt and P.C. Netzel. New circuit breakers for modern d.c. traction power systems. *ITE Power Equipment Publication SPC-MON-3, 1969.*

[24] E.H. Allison and J.S. Morton. Air break motor switching device in metalclad switchgear. *Pt.1'81, IEE Conf. Pubs.*, 83:76–81, 1972.

[25] J.S. Morton. Coil-less cold cathode arc chutes for high-speed d.c. circuit breakers for use on traction systems. *IEE Proc.*, 127 Pt. B:24–45, 1980.

[26] H. Moissan and P.C. LeBeau. *R. Acad. Sci.*, 130:984–988, 1900.

[27] E.E. Charlton and F.S. Cooper. *Gen. Electr.*, 40:438, 1937.

[28] H.J. Lingal, A.P. Strom, and T.E. Browne. An investigation of the arc-quenching behaviour of sulfur hexafluoride. *AIEE Trans.*, PAS-72:242–246, 1953.

[29] R.L. Champion. Gaseous dielectric 6. *Proc. of Sixth Int'l Symp.*, pages 1–8, 1990.

[30] H.M. Ryan and G.R. Jones. Sf6 switchgear. *Peter Peregrinus, New York*, 1989.

[31] P. Kirchesch and H.G. Thiel. Physical principles and development of a new generation of sf_6 circuit breaker for 145kv. In *Trends in Distribution Switchgear, IEE Conference Publication No.400*, 7-9 November 1994.

[32] C. Lüders, T. Suwanasri, and R. Dommerque. Investigation of an sf6-selfblast circuit breaker. *J. Phys. D: Appl. Phys.*, 39:66–672, 2006.

[33] J.D. Yan, J.L. Zhang, K.Y. Kweon, C.M. Dixon, and M.T.C. Fang. Computer simulation of high voltage circuit breakers. *the XVth International Conference on Gas Discharges and their Applications.XVth International Conference on Gas Discharges and their Applications,Toulouse, France*, pages 1025–1034, 2004.

[34] M.I. Boulos, P. Fauchais, and E. Pfender. *Thermal Plasmas Fundamentals and Applications Volume 1*. Plenum Press, New York, 1994.

[35] I.P. Shkarofsky, T.W. Johnston, and M.O. Bachynski. *The Particle Kinetics of Plasmas*. Addison-Wesley, 1966.

[36] A. Simon. *An Introduction to Thermonuclear Research*. Pergamon Press, 1959.

[37] A.M. Cassie. Arc rupture and circuit severity: A new theory. Technical Report 102, Internationale des Grands Reseaux Electrigues'a Haute Tension (CEGRE), Paris, France, Paris, France, 1939.

[38] O. Mayr. Beitrage zur theorie des statischen und des dynamischen lichtbogens (contribution to the theory of static and dynamic arcs). *Arch. Elect.*, 37, 37:588–608, 1943.

[39] Jr. T.E. Browne. A study of arc behaviour near current zero by means of mathematical models. *AIEE Transactions*, 78 (Part III):141–143, 1948.

[40] Jr. T.E. Browne. An approach to mathematical analysis of a-c arc extinction in circuit breakers. *AIEE Transactions*, 78 (Part III):1508–1517, 1958.

[41] W. Elenbaas. Phillips research report. *Phillips Research Report*, 1(5), 1946.

[42] G. Frind. Time constant of flat arcs cooled by thermal conduction. *IEEE Trans. on Power Apparatus and Systems*, 84:1125–1131, 1965.

[43] R.L. Phillips. The behaviour of dynamic electric arcs. *ARL Report*, pages 64–150, 1964.

[44] B.W. Swanson and R.M. Roidt. Boundary layer analysis of an sf_6 circuit breaker arc. *IEEE Trans. PAS-90*, pages 1086–1903, 1970.

[45] B.W. Swanson, Roidt.R.M., and T.E. Browne. Arc cooling and short line fault interruption. *IEEE Trans. PAS-90*, pages 1094–1102, 1970.

[46] R.M. Swanson, B.W.and Roidt. Some numerical solutions of the boundary layer equations for an sf_6 arc. *Proc. IEEE*, 59:493–501, 1971.

[47] B.W. Swanson and R.M. Roidt. Thermal analysis of an sf_6 circuit breaker arc. *IEEE Trans. PAS-91*, pages 381–389, 1972.

[48] B.W. Swanson, R.M. Roidt, and T.E. Browne. A thermal arc model for shot line fault interruption. *ET-Z-A,Bd.93*, pages 375–380, 1972.

[49] B.W. Swanson. A thermal analysis of short line fault interruption. *IEE Winter Power Meeting, PaperC-47*, 1974.

[50] B.W. Swanson. Nozzle arc interruption in supersonic flow. *IEEE Trans. PAS-96*, 1977.

[51] D.T Topham. The electric arc in a constant pressure axial gas flow. *J. Phys. D*, 4:1114–1125, 1971.

[52] M.T.C. Fang. A review of gas-blast circuit breaker arc modelling. *ULAP-T75, Dept. of Electrical Eng. and Electronics, the University of Liverpool*, 1983.

[53] D.T. Tuma and J.J. Lowke. Prediction of properties of arcs stabilized by forced convection. *J. Appl. Phys.*, 46:3361–3367, 1975.

[54] J.J. Lowke and H.C. Ludwig. A simple model for high current arccs stabilized by forced convection. *Journal Applied Physics*, 46:3352–3360, 1975.

[55] F.R. El-Akkari and D.T. Tuma. Simulation of transient and zero current behaviour of arcs stablized by forced convection. *IEEE Trans. PAS-96*, pages 1784–1788, 1977.

[56] E. Richley and D.T. Tuma. Free recovery of the gas blast arc column. *IEEE Trans. Plasma Science*, PS-8:405–410, 1980.

[57] D.T. Tuma. A comparison of the behaviour of sf_6 and n_2 gas blast arcs around current zero. *IEEE Trans. PAS*, PAS-99:2129–2137, 1980.

[58] E Richley and D.T. Tuma. Mechanisms for temperature decay in the freely recovering gas blast arc. *IEEE Trans. On Plasma Science*, PS-10:2–7, 1982.

[59] W Hermann and E Schade. Radiation energy balance in cylindrical nitrogen arc. *JQSRT*, 12:1257–1263, 1972.

[60] F.R. El-Akkari and D.T. Tuma. Simulation of transient and zero current behaviour of arcs stabilised by forced convection. *IEEE Trans. PAS*, PAS-96:1784–1788, 1977.

[61] W. Hermann, K. Ragaller, and W. Schneider. Theory of high pressure arc in a strong axial gas flow. *Proc. 10th Int. Conf. on Phenomena in Ionised Gases*, pages 199–201, 1971.

[62] L. Niemeyer and K. Ragaller. Development of turbulence by the interaction of gas flow with plasmas. *Z. Naturfosch*, 28a:1281–1289, 1973.

[63] W. Hermann, U. Kogelschatz, L. Niemeyer, K. Ragaler, and E. Schade. Experimental and theoretical study of a stationary high current arc in a supersonic nozzle flow. *J. Phys. D*, 7:1703–1722, 1974.

[64] W. Hermann, U. Kogelschatz, L. Niemeyer, K. Ragaller, and E. Schade. Investigation of the physical phenomena around current zero in hv gas blast circuit breakers. *IEEE Trans. PAS*, PAS-95:1165–1176, 1976.

[65] W. Hermann and K. Ragaller. Theoretical description of the current interruption in high voltage gas blast circuit breakers. *IEEE Trans. PAS*, PAS-96:1546–1555, 1977.

[66] J.F. Zhang, M.T.C. Fang, and D.B. Newland. Theoretical investigation of a 2 ka dc nitrogen arc in a supersonic nozzle. *Journal of Physics D: Applied Physics*, 20(3):368–379, 1987.

[67] M. D. Cowley. Integral methods of analysing electric arcs: I. formulation. *Journal of Physics D: Applied Physics*, 7(16):2218–2231, 1974.

[68] S.K. Chan, M.D. Cowley, and M.T.C. Fang. Integral method of arc analysis: Part iii. *J. Phys. D*, 9:1085–1099, 1976.

[69] S.K. Chan, M.T.C. Fang, and M.D. Cowley. The dc arc in a supersonic flow. *IEEE Trans. Plasma Science*, PS-6:394–405, 1978.

[70] S.K. Chan, M.D. Cowley, and M.T.C. Fang. Integral methods of analysing electric arcs: Iii shape factor correlation for low radiation and laminar flow. *J. Phys. D*, 9:1085–1099, 1976.

[71] V.R. Malghan, M.T.C. Fang, and G.R. Jones. Investigation of quasi-steady state high current arcs in an orifice air flow. *J. Appl. Phys.*, 48:2331–2337, 1977.

[72] M.T.C. Fang and D. Brannen. A current-zero arc model based on forced convection. *IEEE Trans. Plasma Science*, PS-7:217–229, 1980.

[73] M.T.C. Fang, S. Ramakrishnan, and H.K. Messerle. Scaling laws for gas blast circuit breaker arcs during the high current phase. *IEEE Trans. Plasma Science*, PS-8:357–362, 1980.

[74] M.T.C. Fang and D.B. Newland. DC nozzle arcs with mild wall ablation. *J. Phys. D: Appl. Phys.*, 16:793–810, 1983.

[75] W.H. Bu, M.T.C. Fang, and Z.Y. Guo. The behaviour of ablation-dominated dc nozzle arcs. *J. Phys. D: Appl. Phys.*, 23:175–183, 1990.

[76] M.T.C. Fang and W.H. Bu. Investigation of ablation dominated ac nozzle arcs. *IEE Proc.-A*, 138:71–77, 1991.

[77] K.Y. Park and M.T.C. Fang. Mathematical modelling of sf_6 puffer circuit breakers i: High current region. *IEEE Trans On Plasma Sci.*, 24:490–502, 1996.

[78] K.Y. Park, X.J. Guo, R.E. Blundell, M.T.C. Fang, and Y.J. Shin. Mathematical modeling of sf6 puffer circuit breakers.ii. current zero region. *Plasma Science, IEEE Transactions on*, 25(5):967 - 973, 1997.

[79] H. Maecker. Plasmaströmungen im Lichtbogen infolge eigenmagnetischer Kompression. *Zeitschrift fr. Physik*, 114:198–216, 1955.

[80] J.J. Lowke and R.W. Liebermann. Predicted Arc Properties in Sulfur Hexafluoride. *J. Appl. Phys.*, 42:3532–3539, 1971.

[81] J.F. Zhang and M.T.C. Fang. Dynamic Behaviour of High Pressure Arcs Near Flow Stagnation Pionts. *IEEE Trans. Plasma Sience*, 17:524–533, 1989.

[82] K. Ragaller, W. Egli, and K.P. Brand. Dielectric recovery of an axially blown SF6-arc after current zero, Part II theoretical investigation. *IEEE Trans. on Plasma Science*, PS-13:154–162, 1982.

[83] K. Ragaller, W. Egli, and K.P. Brand. Dielectric recovery of an axially blown SF6-arc after current zero, Part I experimental investigation. *IEEE Trans on Plasma Science*, PS-10:141–153, 1982.

[84] D.T. Mitchell, R.R.and Tuma and J.F. Osterle. Transient two dimensional calculations of properties of forced convection stabilised electric arcs. *IEEE Trans. on Plasma Science*, PS-13:207–213, 1985.

[85] J.J. Lowke and H.E. Lee. A numerical study of a two dimensional circuit breaker arc during current interruption. *Proc. of gas discharge and their applications, Oxford*, pages 54–56, 1985.

[86] H. Lee, S. Ramakrishnan, and Strokes. DC Properties of Arcs in High Speed Flow. *IEEE Trans. Plasma Science*, 17:20–23, 1989.

[87] M.T.C. Fang and W.Y. Lin. Current zero behaviour of a gas blast arc, Part I: nitrogen. *IEEE Proc.*, 137, PartA(4):175–183, 1990.

[88] M.T.C. Fang and Q. Zhuang. Current zero behaviour of an sf_6 gas-blast arc. i. laminar flow. *Journal of Physics D: Applied Physics*, 25(8):1197–1204, 1992.

[89] M.T.C. Fang, Q Zhuang, and X.J. Guo. Current-zero behaviour of an sf_6 gas-blast arc. ii. turbulent flow. *Journal of Physics D: Applied Physics*, 27(1):74–83, 1994.

[90] J.D. Yan, K.I. Nuttall, and M.T.C. Fang. A comparative study of turbulence models for sf_6 arcs in a supersonic nozzle. *Journal of Physics D: Applied Physics*, 32(12):1401–1406, 1999.

[91] R.E. Blundell and M.T.C. Fang. A simplified turbulent arc model for the current zero period of a sf6 gas-blast circuit breaker. *Journal of Physics D: Appl. Phys.*, 31:561–568, 1998.

[92] R.E. Blundell and M.T.C. Fang. The similarity and scaling of radiating arcs burning in a turbulent, axially accelerating gas flow. *J. Phys. D: Appl. Phys.*, 30:628–635, 1997.

[93] M.T.C. Fang, S. Kwan, and S. Hall. Arc-shock interaction inside a supersonic nozzle. *IEEE Trans. on Plasma Science*, 24:85–86, 1996.

[94] R.E. Blundell, M.T.C. Fang, and A. Vourdas. Stability of a dc sf6 arc in an axially accelerating flow. *IEEE Trans. Plasma Sci*, 25:852–859, 1997.

[95] R.E. Blundell, M.T.C. Fang, and J.D. Yan. The stability of argon arcs in axially accelerating flow. *Proceedings of the XXIII International Conference on Phenomena in Ionized Gases, Contributed Papers, Centre de Phys, Plasmas et leurs Applications de Toulouse, Toulouse, France*, 2:150–151, 1997.

[96] M. Claessens, K. Moller, and H.G. Thiel. A computational fluid dynamics simulation of high- and low-current arcs in selfblast circuit breakers. *J. Phys. D: Appl. Phys.*, 30:1899–1907, 1997.

[97] J.D. Yan, M.T.C. Fang, and W. Hall. The development of pc based cad tools for auto-expansion circuit breaker design. *Power Delivery, IEEE Transactions on*, 14(1):176–181, 1999.

[98] Yan JD Zhang JL and Fang MTC. Investigation of the effects of pressure ratios on arc behaviour in a supersonic nozzle. *IEEE Trans. on Plasma Science*, 28:1725–1734, 2000.

[99] J.C. Lee and Y.J. Kim. Calculation of the interruption process of a self-blast circuit breaker. *IEEE Trans. on Magnetics*, 41:1592–1595, 2006.

[100] A. Martin, Reggio M. Trepanier, J.Y., and Y. Guo. Transient ablation regime in circuit breakers. *Plasma Sci. Technol.*, 9:653–656, 2007.

[101] L.S. Frost and R.W. Liebermann. Composition and transport properties of sf6 and their use in a simplified enthalpy flow arc model. *Proceedings of the IEEE*, 59(4):474–485, April 1971.

[102] R.D. Garzon. *High Voltage Circuit Breakers: Design and Applications*. New York, USA: Marcel Dekker Incorporated, 2002.

[103] C.M. Dixon, J.D. Yan, and M.T.C. Fang. A comparison of three radiation models for the calculation of nozzle arcs. *Journal of Physics D: Appl. Phys.*, 37(23):3309–3318, 2004.

[104] S.D. Eby, J.Y. Trepanier, and X.D. Zhang. Modelling of radiative transfer in sf6 circuit-breaker arcs with the p-1 approximation. *J. Phys. D: Appl. Phys.*, 31:1578–1588, 1998.

[105] V Aubrecht and J.J. Lowke. Calculations of radiation transfer in sf6 plasmas using the method of partial characteristics. *J. Phys. D: Appl. Phys.*, 27:2066–2073, 1994.

[106] V.G. Sevast'yanenko. Radiation transfer in a real spectrum: Integration over frequency. *J. Eng. Phys.*, 36:138–148, 1979.

[107] V.G. Sevast'yanenko. Radiation transfer in a real spectrum: Integration with respect to the frequency andangles. *J. Eng. Phys.*, 38:137–139, 1980.

[108] M.T.C. Fang and D.B. Newland. Effects of nozzle wall ablation on gas-blast circuit breaker arcs. *Proc. 7th Int. Conf. on Gas Discharges and their Applications (London, UK)*, pages 36–39, 1982.

[109] C.B. Ruchti and L. Niemyer. Ablation controlled arcs. *IEEE Trans. on Plasma Science*, PS-14:423–434, 1986.

[110] A.B. Murphy and P Kovitya. Mathematical model and laser-scattering temperature measurements of a direct-current plasma torch discharging into air. *J. Appl. Phys.*, 73:4759–4769, 1993.

[111] CHAM. *PHOENICS*. Bakery House, 40 High Street, Wimbledon Village, London, SW19 5AU, United Kingdom.

[112] D. Dufournet. Evolution of the sf_6 thermal blast interruption in high voltage up to 245kv. *GEC Alsthom Technical Review*, 6:47–58, 1991.

[113] D. Godin, J.Y. Trpanier, M. Reggio, X.D. Zhang, and R. Camarero. Modelling and simulation of nozzle ablation in high-voltage circuit breakers. *Journal of Physics D: Appl. Phys.*, 33(20):2583–2590, 2000.

[114] M. de Hesselle and J.Y. Trepanier. Comparison of cfd tools for sf_6 self-blast circuit breaker development. *IEEE Trans. on Power Delivery*, 18(2):468–474, 2003.

[115] M. Schwinne, M.C. Tang, R. Dommerque, C. Kahlen, and A. Schnettler. Influence of the electrode vapour contamination on the interrupting limit of sf_6 circuit breakers. part ii: Cfd-simulations. *XVIth Symposium on Physics of Switching Arc, Brno, Czech Republic*, 2005.

[116] M. Seeger, L. Niemeyer, T. Christen, M. Schwinne, and R. Dommerque. An integral arc model for ablation controlled arcs based on cfd simulations. *J. Phys. D: Appl. Phys.*, 29:2180–2191, 2006.

[117] S.V. Pantankar, editor. *Numerical Heat Transfer and Fluid Flow.* Hemisphere, New York, 1984.

[118] B. Chervy, H. Riad, and A. Gleizes. Calculation of the interruption capability of sf -cf and sf -c f mixtures-part i: Plasma properties. *IEEE Trans. Plasma Sci.*, 24:198–217, 1996.

[119] P. Kovitya. Thermodynamic and transport properties of ablated vapors of ptfe, alumina, perspex and pvc in the temperature range 5,000-30,000 k. *IEEE Trans. Plasma Sci.*, PS-12:38–42, 1984.

[120] ABB. Private communication.

[121] M.T.C. Fang, J.D. Yan, S. Kwan, and W. Hall. The application of commercial cfd packages for the simulation of gas blast arcs. *Proceedings of the XIIth International Symposium on Physics of Switching, Invited Paper, Bruno, Czech Republic*, 2:13–22, 1996.

[122] J.D. Yan and M.T.C. Fang. Visualisation of arcing process in an auto-expansion circuit breaker. *IEEE Trans. on Plasma Science*, 27:40–41, 1999.

[123] J.D. Yan, J.L. Zhang, A.B. Murphy, W. Hall, and M.T.C. Fang. Arc behaviour in the mixture of sf6 and ptfe vapour in an auto-expansion circuit breaker. *Proceedings of the XIII International Conference on Gas Discharges and their Applications, Glasgow, UK*, 1:58–61, 2000.

[124] M.T.C. Fang, J.D Yan, J.L. Zhang, C.M. Dixon, and W. Hall. Computer simulation as a design aid for circuit breakers. *Proceedings of the XIV Symposium on Physics of Switching Arc, Invited Paper, Brno, Czech Republic*, II:260–271, 2001.

[125] J.L. Zhang, Murphy A.B. Yan, J.D., and M.T.C. Fang. Effects of wall ablation on the arc behaviour in an auto-expansion circuit breaker. *Proceedings of the XIV Symposium of Switching Arc, Brno, Czech Republic*, pages 181–184, 2001.

[126] K.Y. Kweon, J.D. Yan, W.P. Song, and M.T.C. Fang. Swirling flow and its influence on high current dc arcs. *Proceedings of the XIV International Conference on Gas Discharges and their Applications*, 1:67–70, 2002.

[127] J.D. Yan, T.M. Wong, and M.T.C. Fang. Computational investigation of pressure transient in auto-expansion circuit breakers and its implication to the thermal interruption process. Technical report, Report to ABB, from the Electrical Engineering and Electronics, The University of Liverpool., 2006.

[128] J.D. Yan, M.T.C. Fang, and Q.S. Liu. Dielectric breakdown of a residual sf_6 plasma at 3000 k under diatomic equilibrium. *Dielectrics and Electrical Insulation, IEEE Transactions on [see also Electrical Insulation, IEEE Transactions on]*, 4(1):114–119, 1997.

[129] M. Lindmayer. Arc motion and pressure formation in low voltage switchgear. *IEEE Trans on Components, Packing, and Manufacturing Technology*, Part A 21 (1):33–38, 1998.